

Thermal performance enhancement in heat exchangers using active and passive techniques: a detailed review

Suvanjan Bhattacharyya¹ · Devendra Kumar Vishwakarma¹ · Adithya Srinivasan¹ · Manoj K. Soni¹ · Varun Goel² · Mohsen Sharifpur^{3,4} · Mohammad Hossein Ahmadi⁵ · Alibek Issakhov⁶ · Josua Meyer³

Abstract

The objective of this article is to study the work carried out in heat transfer augmentation using active and passive techniques. A comprehensive summary of the work is highlighted to showcase the strength of these techniques in terms of enhancement in heat transfer. In this work, research studies done in the area of electrohydrodynamic, magnetic field, corona wind, vortex generators, tape and coil inserts, roughness, and modified duct were reviewed and an attempt has been made to make a common platform on which the performance enhancement has been compared and presented. It was found out that passive methods are comparatively more investigated than active methods due to their safe and sound operation along with no additional requirement of power. Result shows that duct modification is an effective and efficient way for heat transfer enhancement (HTE). Based on the literature studied, more emphasis must be focussed on the usage of HTE methods in combination to get the advantages of both the methods and they should complement each other in the best possible way. On comparing the active and passive way of THE, results with active methods are more appreciable. However, passive techniques gain more momentum due to ease of operation and low cost of equipment. Use of passive augmentation techniques, i.e. vortex generators, artificial roughness, etc., changes flow pattern significantly that helps in the heat transfer augmentation. Although understanding of fluid flow behaviour is very essential and helps in the cause of the heat transfer augmentation that will further help in using compound techniques, altering the duct's surface using ribs, dimples, roughness, etc., shows the thermal performance enhancement of more than 200% when the results were compared with the plain channel. The modified duct may be combined with any other passive augmentation technique which will further lead to performance enhancement.

Keywords Active and passive techniques · Heat transfer enhancement · Swirl devices · Vortex generators · Duct modification

Abbreviations

DR	Depth ratio = Depth of V-cut/width of tape
WR	Width ratio = Width of V-cut/width of tape
EHD	Electrohydrodynamic
HE	Heat exchanger

HT	Heat transfer
HTC	Heat transfer coefficient
HTE	Heat transfer enhancement
HTT	Helically twisted tape
PEC	Performance evaluation criteria

✉ Suvanjan Bhattacharyya
suvanjan.bhattacharyya@pilani.bits-pilani.ac.in

Mohsen Sharifpur
mohsen.sharifpur@up.ac.za

Mohammad Hossein Ahmadi
mohammadhossein.ahmadi@gmail.com

¹ Department of Mechanical Engineering, Birla Institute of Technology and Science Pilani, Pilani Campus, Vidya Vihar, Pilani, Rajasthan 333 031, India

² Department of Mechanical Engineering, National Institute of Technology Hamirpur, Hamirpur, Himachal Pradesh 177 005, India

³ Clean Energy Research Group, Department of Mechanical and Aeronautical Engineering, University of Pretoria, Hatfield, Pretoria, South Africa

⁴ Department of Medical Research, China Medical University Hospital, China Medical University, Taichung, Taiwan

⁵ Faculty of Mechanical Engineering, Shahrood University of Technology, Shahrood, Iran

⁶ Faculty of Mechanics and Mathematics, Department of Mathematical and Computer Modelling, Al-Farabi Kazakh National University, Almaty, Kazakhstan

TI	Turbulence intensity
TSC	Twisted square channel
TST	Twisted square tube
TT	Twisted tape
TTT	Twisted tri-lobed tube
TOT	Twisted oval tube
TEF	Thermal performance enhancement factor
SAH	Solar air heater
SCPP	Solar chimney power plant
VG	Vortex generator
CFD	Common flow down
CFU	Common flow up
CRWP	Combined rectangular winglet pair

Symbols

f	Friction factor
j	Coburn j -factor
Re	Reynolds number
Nu	Nusselt number
d/W	Diameter ratio
d	Perforation diameter
s/W	Perforation ratio
s	Perforation pitch, mm
P/D or p/D	Helical pitch ratio
H or P or p	Pitch or pitch length, mm
D	Inner diameter of tube, mm
Y or y/W	Twist ratio
y	Length of one twist, mm
W or W_d	Width of tape, mm
w	Width of V- or U-cut, mm
d_e	Depth of V- or U-cut, mm
e	Relative fin height, mm
R_B	Relative fin height ratio
R_P	Relative fin pitch ratio
e or d	Diameter of coil wire, mm
B_R	Blockage ratio
P_R	Relative pitch ratio
Pr	Prandtl number
d_i	Inner diameter of conical ring turbulator
D_c	Outer diameter of conical ring turbulator

Introduction

Energy consumption in the last few decades increased drastically. This is because of the increase in world population, industrialization, urbanization, etc. With increased consumption of energy, the need for efficient equipment is also increased. Besides this, our non-renewable resources are also exhausted because of excessive exploitation. The extraction and burning of these fuels are disastrous to the health of the earth's atmosphere. This made us think about a new source of energy that is safe and available in

abundance, i.e. renewable energy (solar power, geothermal energy, hydropower, wind energy, etc.). Though this energy is available to us free of cost and anybody can access it, there is a need to develop equipment that is compact in design, portable, economical, and of utmost efficiency. Researchers and scientists around the world are working round the clock to develop such equipment.

A heat exchanger (HE) is one such device. HEs are used for transferring energy from one fluid to another. HEs are used in power generation industries, refrigeration, and air conditioning plants, automobile industries, chemical industries, waste heat recovery systems, etc., throughout the world. The effort was made by the researchers to improve the performance, size reduction, better design, and thermal transport of the heat exchangers. From a very compact size to a very large size, heat exchangers of different sizes as per the requirement are designed to obtain better thermal performance [1–4].

With increasing demand, the need for more efficient heat exchangers is also increasing. The performance of HEs depends upon the fluid properties and flow rate [5]. The performance of HEs can be further increased with the help of a magnetic field, electric field, different types of inserts, nano-fluids, hybrid fluids, etc. [6–8]. The methods used for augmentation of heat transfer (HT) can be broadly categorized as active, passive, and combined/combinational techniques.

In active techniques of heat transfer enhancement (HTE), external power is required. The external power is in the form of electric field, magnetic field, mechanical aids, vibrations, etc. [9]. The use of external power disturbs the boundary layer and produces secondary flow which allows the mixing of the fluid and promotes heat transfer. While passive methods involve the enhancement of surface area for heat exchange, this involves different types of extended surfaces in the form of wavy fins [10], offset fins [11], louvred fins [12–16], sinusoidal plate [17–19], dimpled tube [20], etc. Besides these different kinds of tapes [21–25], surface roughness [26, 27] and swirl/vortex generators [28–30] are also used. While in combined techniques, more than one method of HTE was employed to get a high rate of HT [31–33].

Need of the study

Heat transfer augmentation can be achieved in several ways. Several manuscripts are available in the open literature which reviewed the methods of HTE. However, most of the studies are reported either on turbulators inserts or tube modifications or enhanced fluids to augment heat transfer and that brings the idea to the authors of the present work to concise all the research related to HTE in a single work for the researchers those who are working in these area. Besides, as per the knowledge of the authors, no review work on the

HTE using tube/duct modifications is available in the open literature. Hence, we include a subsection on duct modification in the present review study. Therefore, in this assessment, an effort has been made to summarize various research works related to HTE using active and passive methods of HTE. The summarization of the present work is broadly categorized into two main sections—active techniques and passive techniques. While the main emphasis of this review is to investigate the various research works related to the passive techniques, a summary of work related to active techniques is also presented briefly. The section dealing with passive techniques is subdivided into swirl devices, artificial roughness, and modified duct.

Active techniques

As we already discussed, active methods of HTE use external power. This external power is in the form of the magnetic field, electric field, mechanical aids, pulsations, vibrations, etc. The active method of HTE is broadly categorized into two: (i) active method without motion in channel wall and (ii) active method with motion in the channel [34]. Electrohydrodynamic (EHD) [35], magnetohydrodynamic (MHD) [36–38], jets, and spray fall in the first category, while acoustic waves, ultrasound, synthetic jets, vibrations or pulsations, etc., fall in the second category. A lot of research work is available to access the work done on active methods of HTE.

Dhanalakshmi et al. [39] had conducted experiments to investigate the influence of acoustic waves on HTE in a miniaturized furnace. They utilized a low-frequency and high-intensity ultrasound as a potential HT enhancer. The study revealed that sonification plays a significant role in the augmentation of up to 40% near stagnant flow at low Reynolds number (Re) below 500, while at high flow velocities, the role of sonification diminished. Staats and Brisson [40] experimentally reveal the augmentation of convective thermal transport using different designs of integrated centrifugal fans in the heat sink. The study revealed that the integration of a heat pump close to the surface of HT decreases thermal resistance per unit pumping power. It was also observed that HT mainly depends on the rotational speed of the fan and flow rate of air, while the change in geometry of fans shows a negligible impact on thermal performance.

Pour and Esmailzadeh [41] experimentally reported the effect of installing an electrohydrodynamic (EHD) actuator on convective HT in the flow through a rectangular duct with a cylindrical heat source. The results obtained from the sets of experiments revealed that the installation of EHD actuator augments the HT in both laminar/viscous and turbulent flow at a low Reynolds number. The intensity of the electric field

affects the whole process. The installation of a secondary electrode enhances the electric field in the region and hence is more effective for all Re . Diao et al. [42] experimentally investigated electric field application on HT rate on the rectangular micro-grooved evaporation plate. It was found from the experiments that on applying an electric field, the heat transfer coefficient (HTC) gets increased by 45% which implicates the enhancement in HT rate. The bubble growth and nucleation density were significantly influenced due to the electric field. Both bubble growth and nucleation density decrease due to the application of the electric field.

Moghanlou et al. [43] had performed an experimental study to investigate the impact of EHD on the rate of HT and pressure drop in minichannel for the range of Re between 6.5 and 32. Four square channels with heating at the bottom and a high voltage wire were installed at the top of the test section. The electric wire produces EHD effect in the test section. Enhancement in HT and pressure drop was observed with all the value of Re . It was also revealed that EHD performed well at lower Re , while with an increase in mass flow rate, the effect of EHD on HTE decreases.

Nasirivatan et al. [44] conducted experiments to investigate influence of corona wind on the thermal performance of chimney. Two experimental set-ups were used for the study. It was observed that EHD effect increases the augmentation of HT, while corona wind enhances the HT and fluid flow most effectively if electrodes are placed at 25 mm distance. Iron absorber performs better in comparison with aluminium absorber for solar chimney power plant (SCPP) setup. The performance of the absorber plate was significantly improved with increasing number of electrodes. The phenomenon of HTE due to a sound wave in the nucleate boiling regime was explained by Ang et al. [45]. The experimentation revealed that enhancement in thermal transport occurs at low-, moderate-, and high-frequency sound waves. It was observed that at low frequency, the thermal enhancement is mainly due to detachment of bubble from the heated surface, which promotes thermal mixing in the fluid, while at moderate frequency, the heat transport is due to rapid bursting of the bubble at the fluid–air interface. It was also revealed that further enhancement in the frequency of sound waves leads to atomization, which further increases the HT.

Another way of analysing the HTE is through simulating the experiments in the computers using various software applications such as ANSYS, COMSOL, and OpenFOAM. The simulation studies provide almost similar results to experimental works with fewer efforts. Various authors throughout the globe are studying HT augmentation using active techniques through numerical modelling techniques.

Izadpanah et al. [46] computationally investigated the augmentation of HT and pressure drop in a channel in which non-Newtonian fluid is flowing. The channel is fitted with a

blade inside it. Four simulations have been run with different operating conditions. Four cases of the simulation are developed as (i) no blade in the channel, (ii) stationary blade in the channel, (iii) oscillatory blade in the channel, and (iv) rotating blade in the channel. It was reported from the study that enhancement in HT was observed in all the cases with the blade in comparison with without blade. With the presence of a stationary blade in channel, 58% enhancement in heat transport was observed, although oscillating and rotating blade shows the highest HT rate. Bezaatpour and Goharkhah [47] numerically analysed the effect of magnetic field on the thermal performance of double-pipe mini HE. The magnetic field disturbs the boundary layer and promotes the mixing of fluid which results in the improvement in HT in the HE. This technique proved to be very beneficial as HT increases by more than 300% with a very slight increase in pressure drop.

The efficient cooling of electronic items is a heated topic in the field of HTE. Nowadays, we can observe that all the electronic items are becoming compact, and hence the cooling of such equipment is becoming a tough task. To provide their contribution in this field, Ramadan et al. [48] numerically reported the cooling in laptops. The electric field is used to improve the HT rate in the laptop cooling system. Plate fin heat sink with EHD blower is used for the analysis. Optimized geometrical parameters were obtained for better heat transfer. It was reported that the EHD cooling system performs significantly better in comparison with the traditional cooling system. In addition to this, Bao et al. [49] numerically revealed the application of alternating magnetic fields for the augmentation of convective thermal transport in liquid oxygen-based compact heat exchangers. The paramagnetic properties of liquid oxygen have been used to increase the HT due to convection in miniature heat exchangers. It was revealed from the study that alternating magnetic field breaks the vortices produced in the flow field, which results in the development of secondary flow and rapid mixing of cold fluid with hot fluid and enhances the heat transport. With only a single steel bar, 86% enhancement in local Nu is observed at $Re = 500$ without any pressure drop comparative to without enhancement flow.

Wang et al. [50] investigated the effect of EHD on the rate of HT in a double-walled rectangular channel. A pair of electrodes is placed in the channel. Four different ground configurations have been used to improve the HT characteristics. The configuration in which one electrode strikes on the upper wall while the second on the lower wall was found to be the most beneficial arrangement with 166% improvement in HT in the upper wall and 242% increase in the lower wall. Table 1 gives a summary of researches related to active techniques discussed in this section.

Passive techniques

Passive techniques, as we had already mentioned, do not require any external power. In this section, we will discuss the various passive methods of HT augmentation. Passive techniques involved the use of vortex generators, different kinds of tape inserts, roughness, nanofluids, channel modifications, etc. Researchers are preferring passive techniques over active techniques due to low cost, safe and sound operation, appreciable enhancement in the thermal performance, easy availability of accessories needed, etc. Lots of review papers with detailed overview are already available on the passive techniques of HTE using vortex generators, swirl device, inserts, surface roughness, nanofluids, etc. [51–55]. This section of the paper is broadly divided into three subsections, namely swirl devices, artificial roughness, and modified duct.

Swirl devices

Swirl devices are one of the most popular passive methods of HTE. They create vortices in the flow domain by setting up various secondary flows which disturb the boundary layer and ensure the better fusion of the core flow and outer flow and boundary layer. They also reduce the hydraulic diameter and increase the turbulence intensity. All of this contributes to increased HT and pressure drop.

Twisted tapes

Twisted tapes (TT) are metallic strips that are twisted and placed in the heat exchanger to enhance HT with a corresponding increase in the pressure. They act as turbulators which increases the disturbance in the flow field as a result of which fluid mixing enhances which led to higher heat transfer. The geometry of the tapes introduces the swirling in the flow field. This facilitates the mixing of fluid in the core region with that of fluid at the wall surface [56–58]. The geometrical parameters such as twist ratio, length of tape inserts, and modification over tape inserts plays vital roles in determining the performance of thermal devices equipped with tape inserts [58–61]. Other important parameter is clearance between the channel and tape insert. This parameter should be chosen very carefully as both low and higher clearance led to performance drop. Also, insertion of twisted tape inside the channel led to an increase in the heat transfer surface area. This will also increase the pressure drop in the channel due to higher flow resistance.

Twisted tape inserts with nanofluids The studies in the field of nanofluids have gained momentum recently. The authors are investigating various nanofluids for different operating conditions in different flow regimes, and the

Table 1 Summary of important researches on HTE using active technique

Author's name	Year of publication	Method used	Short description	Key results
Dhanalakshmi et al. [39]	2012	Acoustic	Effect of acoustic waves on HTE in a miniaturized furnace	Sonification plays a significant role in augmentation of up to 40% near stagnant flow at low Re below 500, while at high flow velocities the role of sonification diminished
Staats and Brisson [40]	2015	Centrifugal fans	Augmentation of convective thermal transport using different designs of integrated centrifugal fans in heat sink	Integration of heat pump close to surface of HT decreased the thermal resistance per unit pumping power HT mainly depends on the rotational speed of fan and flow rate of air
Pour and Esmaeilzadeh [41]	2011	EHD	Effect of installing electrohydrodynamic (EHD) actuator on convective HT flow through a rectangular duct with cylindrical heat source	At low Re, EHD actuator enhances Ht in both laminar and turbulent regime The installation of a secondary electrode is more effective for all Re
Diao et al. [42]	2014	Electric field	Electric field application on HT rate on the rectangular micro-grooved evaporation plate	The HT coefficient gets increased by 45% which implicates the enhancement in HT rate Bubble growth and nucleation density decrease due to the application of electric field
Moghanlou et al. [43]	2014	EHD	Effect of EHD on HT and pressure drop in minichannel for range of Re between 6.5 and 32	Enhancement in HT and pressure drop was observed with all the Re EHD performed well at lower Re, while with an increase in mass flow rate, the effect of EHD on HTE decreases
Nasirivatan et al. [44]	2015	Corona wind and EHD	Effect of corona wind on thermal performance of chimney	EHD effect increases the augmentation of heat transfer Corona wind enhances the HT and fluid flow most effectively if electrodes are placed at 25 mm distance
Ang et al. [45]	2016	Sound Wave	HTE due to sound wave in nucleate boiling regime	Enhancement in thermal transport at low, moderate and high-frequency sound wave Enhancement in frequency of sound wave lead to atomization which further improve the heat transfer
Izadpanah et al. [46]	2017	Rotating and oscillating Blades	HT and pressure drop in a channel in which non-Newtonian fluid is flowing	58% enhancement in heat transport was observed with stationary blade Oscillating and rotating blade shows the highest heat transfer rate
Bezaatpour and Goharkhah [47]	2020	Magnetic field	Effect of magnetic field on the convective HT in a double-pipe mini heat exchanger	HT increases by more than 300% with a very slight increase in pressure drop
Ramadan et al. [48]	2018	EHD Blower	Cooling in laptops	Optimized geometrical parameters were obtained EHD cooling system performs significantly better
Bao et al. [49]	2016	Magnetic field	Application of alternating magnetic field for augmentation of convective thermal transport in liquid oxygen-based compact heat exchangers	86% enhancement in local Nu is observed at Re = 500 without any pressure drop

Table 1 (continued)

Author's name	Year of publication	Method used	Short description	Key results
Wang et al. [50]	2017	EHD	Effect of electrohydrodynamics (EHD) on the rate of HT in a double-walled rectangular channel	166% improvement in HT in the upper wall and 242% increase in lower wall

results are very appreciable [62–68]. Sharifpur et al. [62] reported on the optimal concentration of TiO_2 nanoparticles in water for heat transfer enhancement under free convection condition. Giwa et al. [63, 64] carried out experiments to evaluate the various thermophysical properties on hybrid nanofluid by varying the temperature, base fluid, mass percentage of nanoparticles, magnetic field intensity, etc. Mahdavi et al. [65] reported on nanoparticles motion and deposition in inclined channel. The thermophysical properties of nanofluid play important roles in the augmentation of heat transfer and pressure drop [69–71]. Recently, nanofluid along with tape inserts has been investigated by several authors with the objective of higher heat transfer rate. Esmaeilzadeh et al. [72] conducted an experimental study on the HT characteristics of twisted tape inserts in $\gamma\text{-Al}_2\text{O}_3$ /water nanofluid flowing in a circular tube in a laminar flow regime ($150 \leq \text{Re} \leq 1600$). The twist ratio of the tape was kept constant, while the thickness was varied through three values: 0.5, 1, and 2 mm, and the volume concentration varied through two values: 0.5% and 1%. An increase in HTE and friction factor (f) was observed with an increase in the thickness of the twisted tape. The best results were found to occur with the highest thickness (3 mm) and 1% volume concentration, while an increase in the friction factor (f) was also observed. He et al. [73] numerically studied HT effects of twisted tape in CuO –water nanofluid in different concentrations using single- and two-phase mixture models. The study was conducted in a turbulent flow regime with Re varied between 3000 and 36,000 for two scenarios: single twisted tape and two twisted tapes. The two-phase model was shown to be more reliable than the single-phase one due to the existence of the strong velocity gradients in the flow field. The results showed that a higher concentration and higher Re number produced the best performances in both cases. Azmi et al. [74] conducted a similar numerical study but with SiO_2 nanofluid and varied the volume concentration and twist ratio. A maximum enhancement of 94% increase in heat transfer coefficient (HTC) and 160% increase in friction factor (f) were found for the configuration of twist ratio of 5.0, Re 19046, and 3% volumetric concentration. Sundar et al. [75] experimentally studied the effectiveness of twisted tape inserts in solar flat plate collectors with Al_2O_3 nanofluids flow. The thermal performance factor was found to increase with decreasing twist ratio. It was observed that for a Re of 13,000 and volume concentration of 0.3%, the twisted tape inserts enhanced the HT from 21% (due to nanofluid) to 49.75% with the pressure drop increase of 25%.

Helically twisted tape inserts Eiamsa-ard and Promvonge [76] experimentally investigated the HTE of helically twisted tape (HTT) for three different configurations in a concentric heat exchanger in the Re range of 2300–8800. The maximum increase in Nusselt number of 160% was observed for HTT

with the centre rod, but a large penalty in terms of pressure drop was observed. Ibrahim [77] experimentally studied the augmentation of HT due to helical screw tape inserts in laminar flow. The effect of variation of spacer length and twist ratio was studied, and correlations of the parameters with Nu and friction factor (f) were presented. For a fixed Re, it was found that f and Nu increase with a decrease in twist ratio and spacer length for flat tubes. Nanan et al. [78] experimentally studied the impact of perforated helically TT on HT and f under uniform heat flux conditions. The experiments were carried out with three different diameter ratios (d/W) of 0.2, 0.4, and 0.6 and three different perforation ratios (s/W) of 1, 1.5, and 2, while the helical pitch ratio (P/D) and twist ratio ($Y=y/W$) were fixed at 2 and 3, respectively. A maximum thermal performance factor of 1.2 was reported for the configuration of diameter ratio (d/W) = 0.2 and perforation ratio of 2.0 for Re = 6000.

Multiple twisted tape inserts Bhuiya et al. [79] experimentally investigated the effects of double counter twisted tapes on HT. Four different twist ratios ($Y = y/W = 1.95, 3.85, 5.92, 7.75$) were studied in the turbulent flow regime of Re = 6950–50,050. It was found that Nu, f , and thermal performance enhancement factor (TEF) increased with decreasing twist ratio. The performance of multiple twisted tapes of different arrangements inserted in TiO₂-water nanofluid was studied numerically and experimentally [80]. The increase in the number of twisted tapes led to increased thermal performance due to increased contact area, residence time, swirl intensity, reduced hydraulic diameter, and increased fluid mixing. The highest thermal performance factor of 1.59 was shown by quadruple counter tapes with a nanofluid concentration of 0.21% by volume.

Bhuiya et al. [81] made an experimental study of HT characteristics of tubes with perforated double counter twisted tape inserts in turbulent flow regimes. The double counter twisted tapes led to the separation of flow into two streams creating a counter swirl which increased the overall residence time of the fluid on the twisted tapes. The HTE increased with decreasing porosity, while the f increased. Abolarin et al. [82] studied the HT and pressure drop characteristics of alternating clockwise and counterclockwise twisted tape (CCCTT) inserted in a tube under constant heat flux. Twelve strips of twist ratio, $Y = 5$, were joined longitudinally with alternating clockwise and counterclockwise arrangements with various connection angles. The connection angle and heat flux were found to be a major influencing factor regarding the onset of transition. It was found that with increasing connection angle, the HT was enhanced due to increased mixing, while transitional flow occurred at lower Re. An increase in heat flux on the other hand was found to delay the transition.

Twisted tape with cuts Murugesan et al. [83] experimentally studied the effect of V-cut TT insert on HT and flow

characteristics. The experiments were performed for three different twist ratios (Y) and different combinations of depth ratio (DR) and width ratios (WR). The tube with V-cut TT was found to have better HT characteristics than plain TT, and this was attributed to additional turbulence and vorticity in the vicinity of the tube wall due to the V-cuts. The mean thermal performance factor of V-cut TT is higher than that of plain TT by 1.65%. They also experimentally studied the effect of square-cut TT on turbulent HT [84]. Similar to the previous experiment, square-cut TT performed significantly better than plain TT for similar reasons—increased turbulence and vorticity near the tube wall region due to square cuts. The highest thermal performance factors were observed for the twist ratio of 2.0 and ranged between 1.19 and 1.27. Abed et al. [85] numerically studied the effects of V-cut TT on HTE using the finite volume method, specifically the realizable κ - ϵ (RKE) model. The average Nu was found to decrease with increasing twist ratio, and this was attributed to stronger vortex flow generated by a lower twist ratio. Chu et al. [86] experimentally investigated the thermo-hydraulic performance of tubes with various V-cut configurations. The effect of the gap between the twisted tape and the tube wall was also studied. Various V-cut configurations were tested in the transient flow regime. The obtuse V-cut configuration was shown to achieve the highest Nu. The obtuse V-cut produced a comprehensive thermal performance of 1.18–1.23.

Twisted tape with attachments Eiamsa-ard and Promvonge [87] experimentally studied the HTE due to a double-sided delta wing insert on a straight tape. The enhancement mechanism is very similar to that of vortex generators—relying on vortices and swirling flow to ensure disruption of the boundary layer and enhanced mixing. It was found that the F-wing showed a higher Nu, pressure drop, and thermal performance than B-wing due to stronger turbulence intensity and flow blockage. Lin et al. [88] numerically studied the use of twisted tape with parallelogram winglet vortex generators (VG) as an effective means of reducing the contact area between the fluid and the twisted, thereby reducing f . The major advantage is that both the parallelogram winglet VG and the twisted tape itself contribute to strengthening the local secondary flow which in turn greatly enhances HT at lower pressure drop penalties.

Promvonge et al. [89] experimentally studied the HTE due to the combined effect of winglet VGs (on the wall) and twisted tape inserts in a square duct. The twist ratio ($Y = y/W$), winglet type, winglet height ratio (R_b), and winglet pitch-to-tape width ratio (R_p) are varied for a constant angle of attack. The combined effect of both VGs and twisted taped increased turbulence intensity and mixing, which led to consistent thermal performance increase over just a twisted tape. The thermal performance of quadruple twisted tapes with V-fin VGs in a square duct in a turbulent flow regime was experimentally studied [90]. The V-finned

quadruple twisted tape is obtained by incorporating 30 degrees V-fins to the edges of twisted tapes with a twist ratio $Y=4$. The effect of the following geometric parameters was studied: relative fin height ($R_B=e/W$) and relative fin pitch ($R_P=P/W$). It was found that the Nusselt number increased with the increment of R_B and a decrement in R_P . Furthermore, the V-finned twisted tapes performed better than just the quadruple twisted tapes, with an improvement in the TEF of 2–16%.

Tapered twisted tape Piriyarungrod et al. [91] experimentally studied the effect of tapered twisted tapes on HTE and pressure drop characteristics in a turbulent flow regime. The effect of taper angle and corresponding twist ratio (Y) was studied. An increase in taper angle reduced the HTE as the swirl intensity was found to decrease, which resulted in poorer mixing between wall and core regions. Thus, the conventional twisted performs better than the tapered twisted tape, although they both performed significantly better than just a plain tube. Mushatet et al. [92] experimentally and numerically studied the effects of new tapered configurations of TT, namely increased tapered TT on HTC under constant heat flux conditions. The study focussed on understanding the effects of varying the starting width and tapered region length in the turbulent flow regime. The Nu of the increased tapered TT increased with decreasing starting width and decreasing length of the tapered region.

Novel twisted tape inserts Zhang et al. [93] did a thermal performance evaluation of a novel type of twisted tape: self-rotating TT with an experimental study. The self-rotating TT was compared with stationary TT in the turbulent flow regime while varying the twist ratio Y . Self-rotating TT performed better than stationary TT, and it was found that the Nu, f , and TEF increased with decreasing twist ratio. He et al. [94] experimentally studied the mechanism of HT in circular tubes with inserted cross-hollow TT under uniform heat flux condition. The cross-hollow twisted tapes were found to have a higher Nu than a plain tube without inserts but an increased pressure drop. There was a little variation in the thermal performance factor (TEF) between the three configurations for the same Re number. But the TEF was found to be close to 1 only for low Re flow and decreased significantly for increased Re numbers, indicating that it might be advantageous to use only in laminar flow conditions. Figure 1 shows the different configurations of tape inserts reviewed in the above section. Refer Table 2 for the summary of research discussed in this section.

In comparison with the other instances (refer Fig. 2), the twisted tape inserts with winglets were found to have the best thermal efficiency. Surprisingly, of all the twisted tape inserts studied, the twisted tape insert with v-winglets had the highest thermal performance factor.

Coil inserts

Coil inserts are the passive technique of HTE. This technique involves inserting a coiled wire into the tube and is very popularly used in many HT applications such as heat extraction process equipment, air conditioning and refrigeration equipment, chemical reactors, and food processing industries. A metallic wire is tightly wrapped around a rod to create wire coil inserts of desired dimensions. As the coil spring is pushed up, the wires generate a helical roughness. Two factors that impact the performance of these devices are wire coil pitch and cross section shapes. Large solar collectors linked in tandem to supply warm water for large household end-users are better suited to wire coil inserts.

Sharifi et al. [95] made a computational study of the HT and pressure drop characteristics of helical wire inserts, as shown in Fig. 3a in a double-pipe heat exchanger for laminar flow. The pitch length (P) and diameter (D) of the coils were varied. The helical wires reduced the hydraulic diameter and impeded the flow movement on the surface of the tube wall. This led to an increase in both Nu and f . There was intense swirl motion generated by the helical coils, which increased with an increasing Re number which further led to an increase in Nu. Reddy and Rao [96] experimentally studied the HT characteristics of ethylene glycol water-based TiO_2 nanofluid and evaluated the effectiveness of the additional helical coil wire inserts. The volume concentration of the nanofluid and the pitch-to-diameter ratio (P/d) of the helical coils were varied, and the experiment was conducted in the turbulent flow regime. The nanofluid with 0.02% concentration was found to provide the highest enhancement of 7.85–10.73% for the Re range of 4000–15,000.

San et al. [97] experimentally studied flow and HT characteristics of coiled wire inserts (refer Fig. 3b) in circular tubes with both air and water as working fluids in a turbulent flow regime. The ratio of wire coil diameter to inner tube diameter (d/D) and coil pitch tube diameter (P/D) was varied in between the range of 0.0725–0.134 and 1.304–2.319, respectively. Contrary to the previous finding by Sharifi et al., both Nu and f increased slightly with d/D value, while it increased strongly with a decrease in P/D . This trend held for both water and air. The best performance was shown by the configuration of $d/D=0.101$ and $P/D=1.739$ for water and $d/D=0.101$ and $P/D=2.319$ for air. Keklikciogulu et al. [98] conducted an experimental investigation on the thermo-hydraulic performance of coiled wires with an equilateral triangular cross section which was installed with a small separation from the inner wall of the tube (refer Fig. 3c). The separation length was varied to investigate the effect of disturbance on the laminar sub-boundary layer. The separation of $s=1$ mm was found to be better than $s=2$ mm as the coiled wire insert destroyed the laminar boundary layer

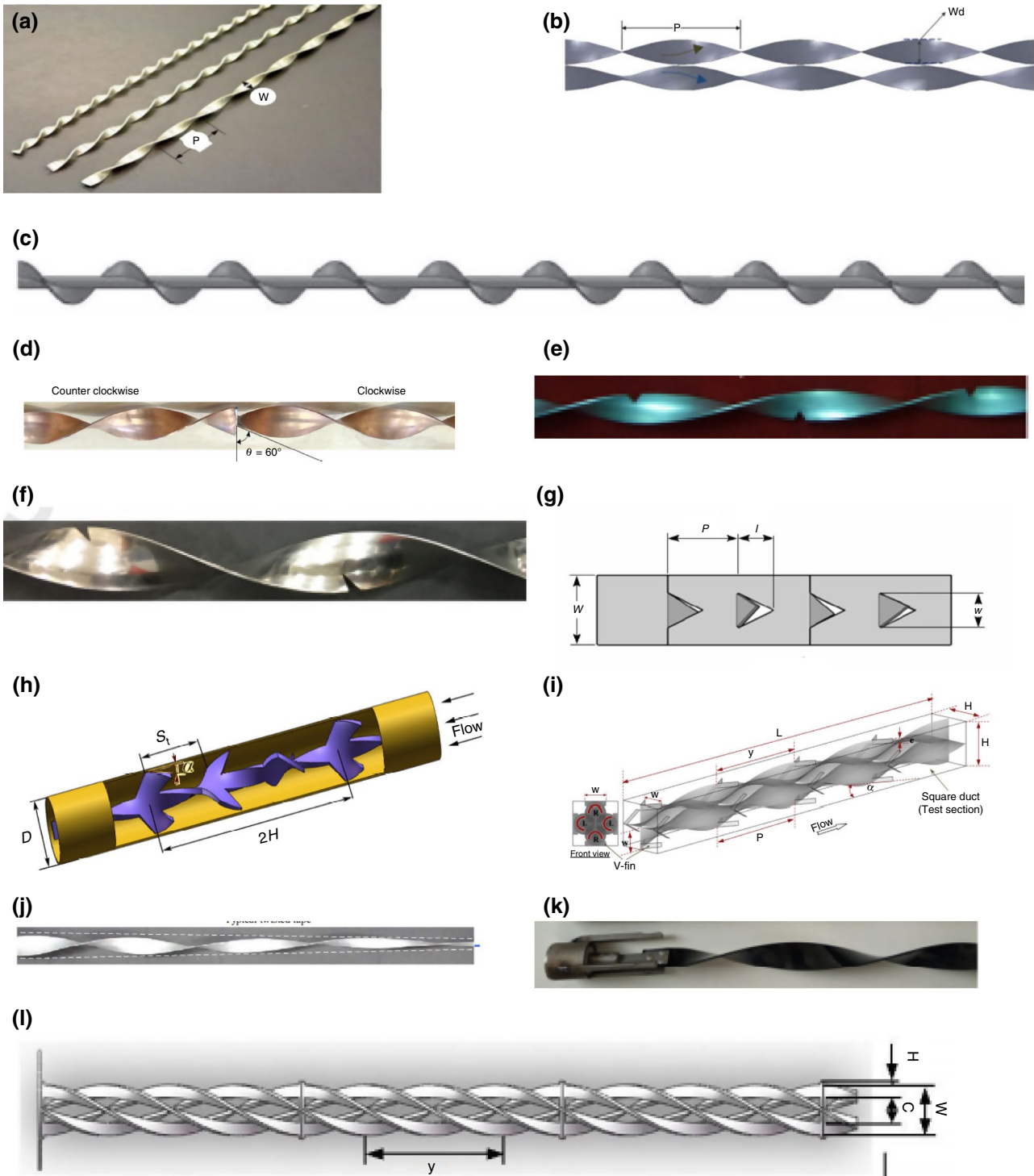


Fig. 1 Different types of tape inserts [56, 77, 79, 82, 83, 86–88, 90, 91, 93, 94]

effectively in the previous case leading to enhanced heat transfer.

Hamid et al. [99] experimentally studied the effect of wire coil inserts on HTE in $\text{TiO}_2\text{-SiO}_2$ nanofluid flow in transition and turbulent flow regimes. The volume concentration

and the geometric characteristics of the coiled wire like P/D ratios were varied. The HT performance increased with the volumetric concentration up to 2.5% after which it deteriorated due to the nanofluid exceeding the critical viscosity condition. Saedina et al. [100] carried out an experimental

Table 2 Summary of experimental investigations in swirl flow devices

Author and year	Configuration	Flow regime	Parameters	Important results
Kumar and Prasad [57]	Typical twisted in solar water heater	Laminar and turbulent	Pitch-to-diameter ratio (P/D) range is 3–12	Twisted tape inserts perform better than plane channel
Esmailzadeh [72]	Twisted tape in $\gamma\text{-Al}_2\text{O}_3$ /water nanofluid	Laminar	Twist ratio 3.21 Volume concentration 0.5%, 1% Tape thickness 0.5, 1, 2 mm	Nusselt number increased by 18–70% and pressure drop by 87–132% The highest enhancement was achieved at the highest thickness and volume concentration
Sundar [75]	Twisted tape in Al_2O_3 nanofluid	Turbulent	Volume concentration Height of tape-to-diameter ratio (H/D)	The twisted tape insert provided an additional thermal performance enhancement over the nanofluid flow
Eiamsa-ard and Promvongse [76]	Helically twisted tape (HTT) in concentric heat exchanger	Turbulent	With and without centre rod	With rod configuration provided high HT than the without rod configuration
Ibrahim [77]	Helical screw tape inserts	Turbulent	Regularly spaced helical tape with free spacing ratio (L_s/L_h) = 0.5, 1.0, 1.5, and 2.0 Spacer length = 0, 100, 200, 300, 400 mm Twist ratio = 2.17, 3.33, 4.3, 5	The configuration with space ratio $s = 0.5$ gave the best results at low Re
Nanan [78]	Perforated helically twisted tapes (P-HTT)	Turbulent	Diameter ratio (d/w) = 0.2, 0.4, 0.6 Perforation ratio (s/w) = 1, 1.5, 2 Twist ratio = 2	The Nusselt number and friction factor increased with a decrease in twist ratio and spacer length P-HTT performed worse than HTT
Bhuiya [79]	Double counter twisted tapes	Turbulent	Twist ratio = 1.95, 3.85, 5.92, 7.75	Maximum PEC = 1.2 for $d/w = 0.2, s/w = 2$ and $Re = 6000$ Nusselt number and friction factor values increased by 60–240% and 91–286%, respectively
Eiamsa-ard and Kiatkitipong [80]	Multiple twisted tape in TiO_2 -water nanofluid	Turbulent	Various configurations: ST, Co-DT, C-DT, Co-TT, Co-QTs (Fig)	The TEF was always greater than 1 Counter current tapes significantly outperformed all other configurations for every tape number
Bhuiya [81]	Perforated double counter twisted tape	Turbulent	Nanofluid concentration Porosity (R_p) = 1.2, 4.6, 10.4, and 18.6%	The highest PEC is 1.59 shown by the configuration of CC-QTs with nanofluid concentration of 0.21% The PEC increased with decreasing value of porosity except 1.2%
Abolarin [82]	Alternating clockwise and counterclockwise twisted tape (CCCTT)	Transition	Twist ratio: $Y = 5$ Varying connection angle in CCCTT: 0, 30, 60 degrees	The Nusselt number and friction increased by 80–290% and 111–335%, respectively CCCTT outperformed CTT in transitional flow while performing as good as CTT in laminar flow regime Increase in connection led to increased Nusselt number and quicker onset of transitional flow

Table 2 (continued)

Author and year	Configuration	Flow regime	Parameters	Important results
Murugesan [83]	V-cut twisted tape (VTT)	Turbulent	Twist ratio (Y) = 2.0, 4.4, 6.0	VTT outperformed plain twisted tape with a mean thermal performance of VTT 1.25% higher than PTT
Murugesan [84]	Square-cut twisted tape (STT)	Turbulent	Depth ratio, width ratio = 0.34, 0.43; 0.34, 0.34; 0.43, 0.34 Twist ratio (Y) = 2.0, 4.4, 6.0	Nu and friction factor increased with increasing DR and decreasing WR STT had a better performance over PTT The thermal performance of STT is 2–6% better than PTT
Chu [86]	Various V-cut twisted tapes	Transient	Configurations: U-cut, V-cut, obtuse V-cut, isocoles V-cut	All configurations performed better than a plain twisted tape The obtuse V-cut was the best and produced a CTP of 1.18–1.23
Eiamsa-ard [87]	Double-sided delta wing insert	Turbulent	Wing-width ratio (Ew) Wing-pitch ratio (Ep) Forward/backward wing configuration Regular and alternate axes arrangement	F-wing performed better than B-wing The HT increased with a decrease in Ep and increase in Ew
Promvongse [90]	Quadruple twisted tape with V-fins	Turbulent	Twist ratio = 4 Relative fin height (ϵ/w) = 0.16, 0.21, 0.32, 0.42 Relative fin Pitch (P/w) = 4, 8, 12, 16 Fin attack angle = 30 degrees Taper angle	The Nusselt number increased with increment in Rb and decrement in Rp
Priyaranrod [91]	Tapered twisted tape	Turbulent	Twist ratio	V-finned twisted tapes performed better than quadruple twisted tapes by a factor of 2–16% Increase in taper angle resulted in a decrease in PEC Tapered twisted tape performed worse than a conventional twisted tape
Mushatet [92]	Increased tapered twisted tape	Turbulent	Starting width (W) Tapered region length (l) Various configurations Twist ratio Y = 2.2, 3, 4, 6	The Nusselt number increased with decreasing starting width and length of tapered region
Zhang [93]	Self-rotating twisted tape (SRTT)	Turbulent	SRTT vs stationary twisted tape (STT) comparison	SRTT performed better than STT in terms of thermal performance factor Decreasing Y caused high rotational speed and better performance

Table 2 (continued)

Author and year	Configuration	Flow regime	Parameters	Important results
He [94]	Cross-hollow twisted tapes	Turbulent	Hollow width (w) 6–10 mm	Cross-hollow twisted tapes have a higher Nusselt number and friction factor compared to a normal twisted tape $W=8$ had the lowest pressure drop, while $w=6$ had the highest pressure drop PEC close to 1 at low Re flows only

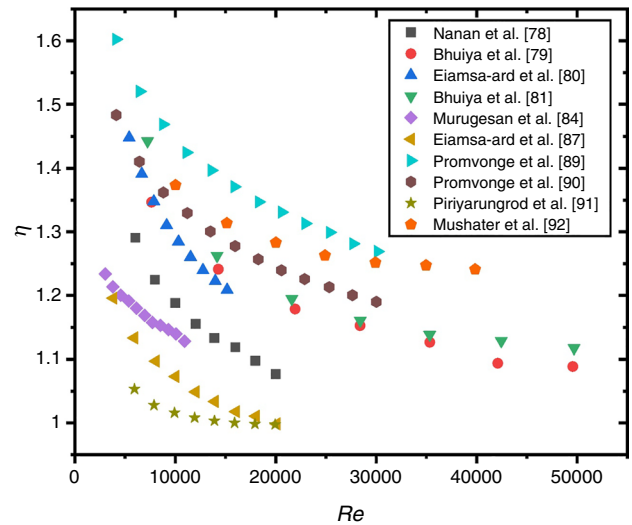


Fig. 2 A comparison of thermal performance factor for different types of tape inserts

investigation on HT effects of horizontally coiled wire inserted in CuO/base oil laminar nanofluid flow (refer Fig. 3d). They found that the coiled wires provide a significant increase in thermal performance over just nanofluid with a maximum HTE of 40.2% with a significant increase in f also. Table 3 gives the summary of research works discussed in this section.

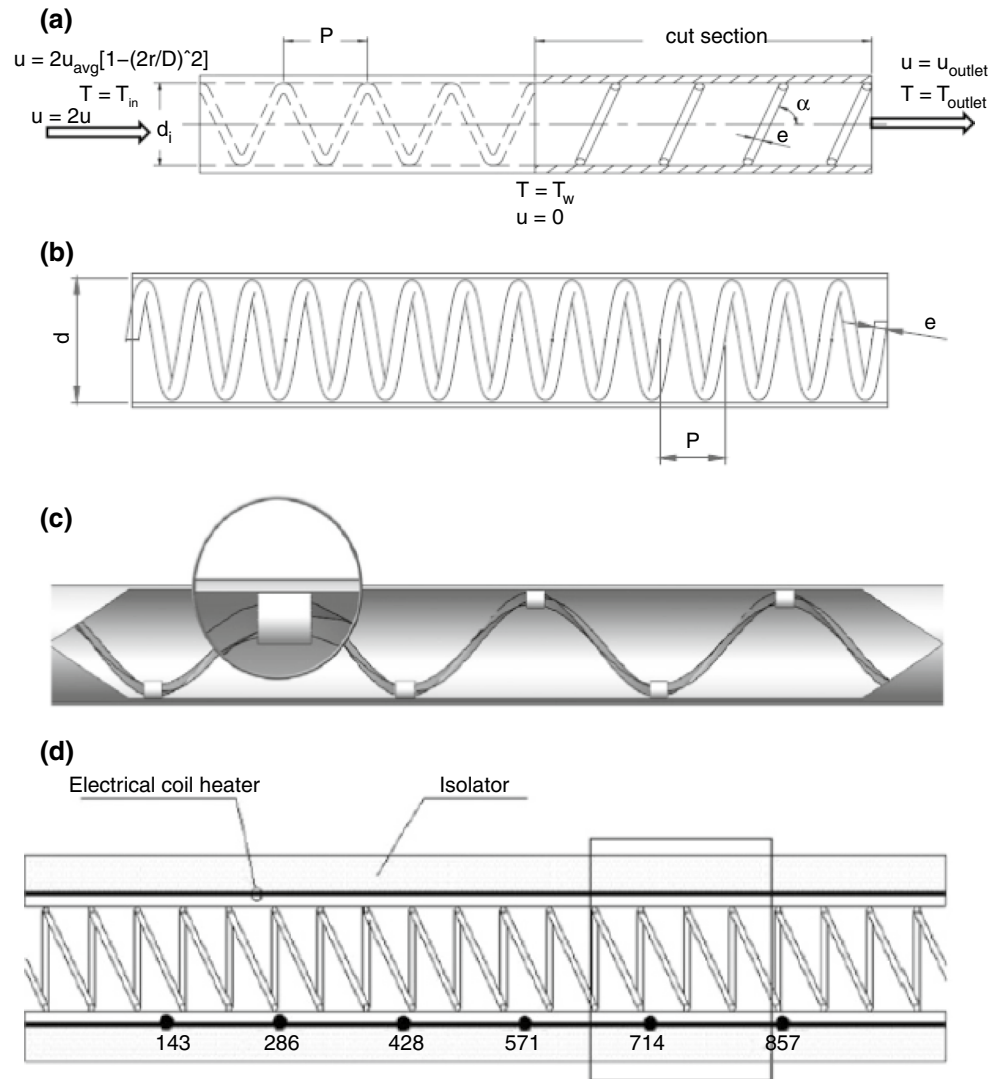
A significant enhancement in the thermal and flow performance has been observed with the use of wire coil inserts (see Fig. 4). The wire coils enhance the swirling motion in the flow field which ultimately results in the heat transfer enhancement. However, at higher mass flow rate, the ability of wire coil to enhance the heat transfer reduces.

Ring-shaped inserts

One of the passive approaches that has been studied by numerous researchers is the use of ring insert on the inner surface of circular tubes. Flow eddies may occur as a result of such turbulation devices being purposefully positioned inside the flow field. Eddy currents have an effect on the thermal boundary layer and can enhance the convective heat transfer coefficient.

Conical ring inserts Anvari et al. [101] conducted a study of the HT behaviour of a round tube with modified conical ring inserts with both experimental and numerical methods. The study was carried out with two configurations of conical ring: converging array (CR) and diverging array (DR). On the comparison between the simulation results and experimental ones, the simulation result estimated the Nusselt number values well but overestimated the pressure drop values. They reported that the DR array performed better than the CR array, although both had thermal performance

Fig. 3 Different wire coil configurations used in the investigations [95, 97–100]



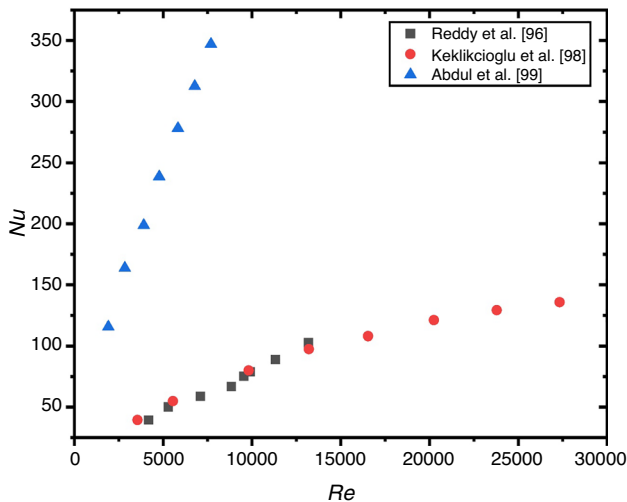
factor less than unity. A numerical study of HT characteristics of conical ring turbulators in a turbulent flow regime was conducted by Ibrahim et al. [102]. Nu and f were found to decrease with an increase in pitch ratio and diameter ratio values, and this was attributed to reducing turbulence intensity.

Circular ring-shaped inserts Kongkaitpaiboon et al. [103] presented an experimental investigation of HTE of a smooth tube fitted with circular ring turbulators (CRT) in a turbulent flow regime. The geometric parameters of the CRT, like diameter ratio ($DR = d_i/D_c$) and pitch ratio ($P_R = P/D_c$), were varied, and their effect on the flow characteristics was investigated. Nu and f were found to increase with decreasing pitch ratio due to increasing turbulent flow intensity and higher contact surface area, leading to dissipation of the dynamic pressure head in the system. An experimental study of HT characteristics of a perforated circular ring (PCR) fitted in the air to water heat exchanger was conducted by Sheikholeslami et al. [104]. The experiments were carried

out by varying the pitch ratios (P_R) and the number of perforated holes (N) in a turbulent flow regime. Like the circular ring (CR), the thermal performance factor PCR_s also decrease with the Re . The PCR_s showed a lower HTE than their CR counterparts but also showed a significant decrease in f . Nu and f decreased with an increase in N , while they decreased with an increase in PR similar to CR. Acir et al. [105] conducted an experimental study to see the effect of perforated circular ring turbulators (CR) on solar air heaters. The experiment was conducted by varying the pitch ratio (P_R) and the number of holes. The results showed that the PCR significantly enhanced the performance of solar air heater. The highest HT augmentation of 229% was achieved with $P_R = 2$, $N = 2$ in comparison with the plain tube. The highest thermal performance factor observed was 1.83 for the same configuration. All the geometries of ring turbulators are summarized in Fig. 5. Table 4 gives the summary related to this section.

Table 3 Summary of investigation on the wire coil inserts

Author and year	Configuration	Flow regime	Parameters	Important results
Reddy and Rao [77]	Helical wire in TiO ₂ nanofluid	Turbulent	Volume concentration 0.0004%–0.02% Pitch-to-diameter (P/d) ratio	Helical wire was found to provide increased performance over the nanofluid enhancement P/d = 2.5 provided the best performance
San [78]	Coiled wire inserts in circular tubes	Turbulent	Wire coil diameter-to-tube inner diameter (e/D) = 0.0725–0.134 Coil pitch-to-inner diameter ratio (p/d) = 1.304–2.319	Nusselt number increased slightly with e/D but strongly increased with a decrease in p/D for both water and air
Keklikioglu [79]	Coiled wire with equilateral triangular cross section	Turbulent	Constant side length of triangle = 6 mm P/D = 1, 2, 3 Separation length from wall(s) = 1, 2 mm	S = 1 mm performed better than s = 2 mm Highest PEC of 1.82 was observed for P/D = 1 and s = 1
Hamid [80]	Wire coil inserts in TiO ₂ –SiO ₂ nanofluid	Turbulent	Volume concentration P/D ratios	The PEC increased up to a volume concentration of 2.5% and then deteriorated Nusselt number and friction factor increased with a decrease in P/D ratios All configurations had a PEC greater than 1
Moghaddam [82]	Coiled wire inserts in R-600a	NA	Pitch of wire coils = 10, 20, 30 mm Wire diameters = 0.5, 1, 1.5 mm Vapour quality Mass flow rate	Coiled wire inserts provided a significant increase in performance of the condenser Coiled wire inserts delayed the change of annular flow to intermittent flow

**Fig. 4** Comparison of Nusselt number with different wire coils

It has been concluded that ring inserts significantly improve the heat transfer rate between the fluid and the channel walls. The inserts with holes show better flow

performance over other inserts. The holes in the inserts further enhance mixing of fluid by promoting the eddies formation in the wake region. These eddies' formation improves the heat transfer with a slight increase in the pressure drop.

Vortex generators

Vortex generators (VG) are described as protrusions from the heat transfer surface that produce swirling flow around an axis, resulting in the creation of vortices. VG-induced vortices are divided into two types: transverse vortices and longitudinal vortices. Vortex generators are used to create longitudinal vortices that lead to the development of a secondary flow structure which in turn enhances heat transfer. Vortex generators (VGs) improve heat transfer performance by disturbing and degrading the boundary layer, intensifying the turbulent flow, and thereby lowering the thickness of the boundary layer. Fiebig et al. [106] postulate three mechanisms for the observed HTE:

1. The extended surface of the vortex generators promotes the growth of new thermal boundary layers that increases local heat transfer coefficient (HTC).

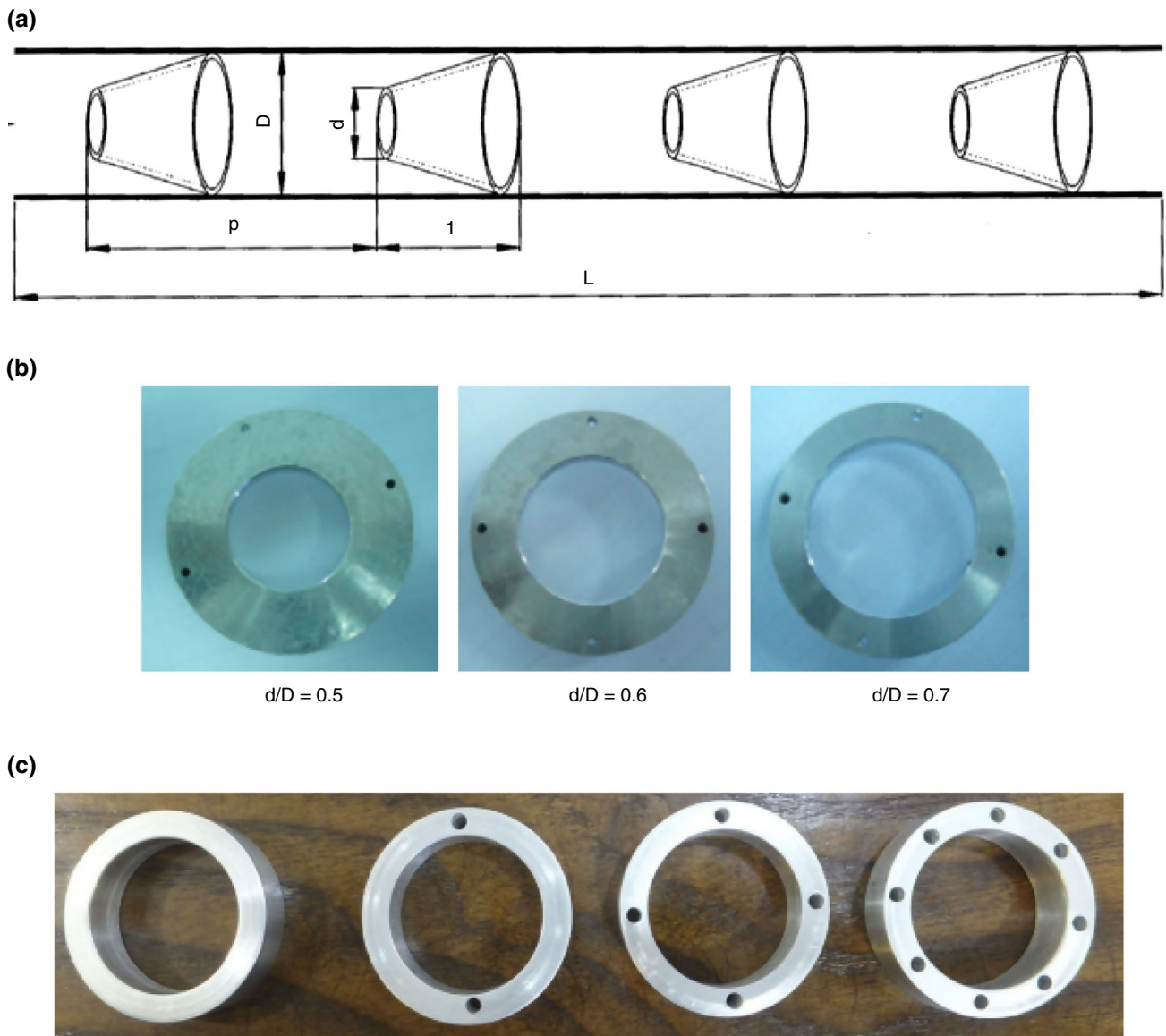


Fig. 5 Ring turbulators [102–104]

2. Vortex generators create swirls in the core flow through flow separation from the extended surfaces. This is the major mechanism of heat transfer. It was shown that the HTE produced by longitudinal vortices (with axis in the direction of the flow) is significantly higher than that of lateral vortices [106, 107]. This creates the major secondary flow structure that disrupts the boundary layer and encourages strong mixing with the core flow. It was also observed that the surface with the VGs had a significant increase in local heat transfer coefficient (HTC) compared to opposite surface, which had a relatively lower increase.
3. The vortex generators also destabilize the flow and significantly reduce the critical Re number for the flow,

thereby increasing the turbulence (or TI) in the flow, which increases the global heat transfer coefficient (HTC) in the channel.

Various types of VG devices like cans, wings, winglets, and obstacles have been investigated, but the most popular device has been wings, winglets, and their variations.

Gentry [108] carried out experiments using delta wing vortex generators, which showed that the local heat transfer coefficient (HTC) in the secondary flow region increased by 300%, while the average heat transfer coefficient (HTC) increased by 55% and pressure drop by 100%. Fiebig et al. [107] experimentally studied the flow characteristics with multiple shapes of rectangular and delta wing and winglet

Table 4 Summary of ring-shaped inserts

Author and year	Configuration	Flow regime	Parameters	Important results
Anvari [101]	Modified conical ring inserts	Turbulent	Arrangements: converging array (CR), diverging array (DR)	DR performed better than CR, but both of them had enhancement efficiencies below unity
Ibrahim [102] (Computational)	Conical ring turbulators	Turbulent	Arrangements: converging array (CR), diverging array (DR), converging-diverging array (CR-DR) Diameter ratio (d/D) Pitch ratios	Nu increased with a decrease in PR and diameter ratio values DR was the best arrangement Conical rings in comparison with other passive methods had lower PEC but the highest increase in Nu
Kongkaiatpaiboon [103]	Circular ring	Turbulent	Diameter ratio (DR)=0.5, 0.6, 0.7 Pitch ratio (PR)=6, 8, 12	Nusselt number increases with decreasing pitch ratio HT increases with a decrease in diameter ratio
Sheikholeslami [104]	Perforated circular rings (PCR)	Turbulent	Number of perforated holes (N)=0, 2, 4, 8 Pitch ratio=1.82, 2.92, 5.83	PCR had a higher PEC than circular rings, but a lower Nusselt number The Nu decreased with an increase in N and PR

vortex generators and concluded that the delta winglet was the most effective per unit area of VG in terms of HTE. Various parameters such as the angle of attack, height of vortex generators, and their placement were varied. Xu et al. [109] experimentally studied the effect of winglet vortex generators in a circular tube. Multiple configurations created from varying attack angles (0, 15, 30, 45 degrees), blockage ratios (B_R) (0.1, 0.2, 0.3), relative pitch ratios (P_R) (4.8, 2.4, 1.6), and VGs per row (N) (4, 8, 12) were studied. The maximum Nusselt number increase was 98%, and TPE was 1.45 which was observed for the configuration of $P_R=2.4$, zero degrees angle of attack, and B_R of 0.1.

Zhang et al. [28] numerically investigated the mechanism of HTE for the case of the rectangular channel with the laminar flow by comparing the augmentation with and without longitudinal VG. It was found that longitudinal vortices, as shown in Fig. 18, greatly helped in increasing the local transverse heat flux Q_y which in turn resulted in the increase in Q_x (longitudinal) and, most importantly, Q_z (HT to core flow) through the complex coupling, which ultimately resulted in an increase in overall heat transfer. It was also ascertained that the height of VGs and their angle of attack were the main parameters influencing the velocity contribution which influences the Q_y which in turn influences Q_z . Wu et al. [110] numerically studied the effect of longitudinal vortex generators on laminar convective HT in the rectangular channel and found that the enhancement effects of LVGs were well explained by the field synergy principle. It was also found that the local HTE of punched VGs was greater than the non-punched ones. They also reported that the thickness of

the VG (rectangular winglet) did not affect the global HT significantly and that the optimum angle of attack was 45° . Wu et al. [111] conducted a parametric (numerical) study on the same configuration and studied the effect of the location of LVG in channel, size, and shape of LVG. It was found that the overall Nusselt number decreases with the increase in distance from the inlet and that the pressure drop remained the same. An increase in the area of LVG increased both the average Nusselt number and pressure drop, while for a fixed area and angle of attack, it was determined that an increase in the length of an LVG resulted in a better performance to an increase in height.

Sinha et al. [112] numerically studied the HTE with different arrangements, namely common flow up in series (CFU-CFU), common flow down in series (CFD-CFD), combined (CFU-CFU), inline rows of winglet, and staggered rows of winglet (SRW), as shown in Fig. 19. All configurations produced various combinations of counter-rotating vortexes pair with a central flow at the central longitudinal plane. It was shown that the CFU-CFU configuration was best in terms of HT and quality factors. Lemouedda et al. [113] conducted a study to optimize the angle of attack and arrangement of delta winglets using the strategy of Pareto optimality through a process that consisted of computational analysis, genetic analysis, and appropriate approximation techniques. They concluded that common flow down arrangement performed better in an inline set-up, while CFU (common flow up) arrangement performed better in a staggered set-up, while overall, the staggered CFU arrangement gave the best results.

Oneissi et al. [114] conducted a numerical study of a novel delta winglet pair vortex generator in laminar and turbulent flow regimes and reported an enhancement in heat transfer along with reduction in the friction factor when the results are compared with conventional delta winglet. Min et al. [115] numerically simulated the combined rectangular winglet pair (CRWP) configuration as shown in Fig. 21 and studied its effects on HTE in a turbulent flow regime. The CRWP possesses a unique geometry that consists of a rectangular wing mounted with an accessory wing. The study was conducted by varying various geometric parameters like the angle of attack of both the main VG and accessory wing, placement of the accessory wing, and length of the accessory wing. The main attack angle of the VG had the highest influence on thermal performance, followed by the accessory VGs and attack angle, length, and the placement of the VG. It was found that CRWP had an increase in Nusselt number and friction factor (f) by 2.1–20.7% and 4.7–104.1%, respectively, over the rectangular winglet pair (RWP). The higher performance was attributed to an increased number of vortices generated by CRWP over RWP at the lower core and the ability of the accessory wings to generate vortices that swirl downward to effectively disturb the boundary layer. Gupta et al. [116] numerically investigated the performance of punched winglet for heat exchanger surface as a vortex generator in a fin and tube heat exchanger in a turbulent flow regime. They evaluated different combinations (CFD, CFU, punched, with hole) and varied the angle of attack of VGs. The punched winglet produced an increment of up to 34% in HT augmentation. They found that the punched rectangular winglet outperformed the regular rectangular winglet in all configurations except CFD at upstream locations. The CFD configuration in upstream location was shown to have the best performance. Ahmed et al. [117] numerically investigated the HTE due to VGs (DWP, RWP) on laminar nanofluid flow in a triangular duct. The effect of the type of different nanoparticles with 25 nm average diameters and the concentration of nanoparticle (1–6%) were studied, keeping the angle of attaching constant at 15° . The height and breadth of VG are constant. The nanofluids produced no increase in f but provided a slight increase in the average Nu. Xu et al. [118] numerically studied a novel VG called half-cylinder VG and its effect on the HT characteristics of flow in a rectangular channel in a turbulent flow regime. The half-cylinder VG was compared to five other VGs of the same surface area. The length, radius, and spacing of the half-cylinder VGs were varied, and its effect was studied. The half-cylinder VG performed the best in comparison with the other VGs and was claimed to a new VG with low resistance and high efficiency. The Colburn factor and f increased with an increase in length up to a certain maximum, and the thermal performance peaked at $A/B=0.5$. An increase in HT was also observed with an increase in radius

and decrease in spacing. Ali et al. [119] studied the effect of self-sustained oscillating flexible VG on the HT and mixing enhancement in a circular through a 3-D numerical simulation. Five arrays of four equally spaced trapezoidal vortex generators are inserted into the circular tube with an angle of attack 45° to the water, and two sets of experiments were performed: one with the traditional non-deformable rigid trapezoidal VG and the other with flexible trapezoidal VG which deforms due to the fluid forces. The FVG configuration showed an improvement of 118% compared to the 97% observed in RVG because of self-sustained oscillations of VGs and the improved mixing performance.

The curved trapezoidal winglet pair (CTWP) was experimentally compared to RWP, trapezoidal winglet pair (TWP), and DWP based on Colburn j -factor and friction factor (f) [120]. It was found that DWP was the best in the laminar and transitional region, but CTWP outperformed the others in the fully turbulent regions. CTWP was shown to have the best performance with low angles of attack (0°). Experimental investigation of the plane and curved winglet (rectangular, trapezoidal, and delta) VGs carried with and without punched holes in turbulent and laminar flow regimes was conducted [121]. The effect of hole positioning and hole diameter on HT was studied. It was observed that curved winglets performed better in all flow regions due to their streamlined configuration. The punched holes served to decrease f , and the positioning of the punched holes closer to the wall was shown to have a lower flow resistance and a higher performance. This occurred because the jet from the lower hole increases agitation in the low-velocity area (near the wall) but rarely disturbs the main longitudinal vortex that was generated. The curved delta winglet pair (CDWP) had the best HT performance among the configurations that were tested. The holes on the winglets significantly reduced the loss in pressure drop, but the optimal diameter depended on the area of the VG.

Chamoli et al. [122] experimentally tested perforated VG, as shown in Fig. 24 in a circular tube in a turbulent flow regime of $Re=3000$ – $21,000$. The experiment was conducted with four different perforation indexes $PI=4, 8, 12, 16\%$, three relative pitch lengths of $p/p_a=2, 4, 6$, while the angle of attack and height to inner tube diameter (e/D) was kept constant at 45 degrees and 0.25 , respectively. As is common in VGs, the TEF decreases with Re . The HT decreased with an increase in p/p_a ratio as a higher value of p/p_a led to a weakened jet impingement on the wall which in turn meant ineffective mixing of the fluid. It was found that the TEF increases with PI and a maximum TEF of 1.65 was achieved with the configuration of $PI=16\%$, $p/p_a=2$, and $Re=3000$. On comparison with other passive enhancement techniques (perforated conical rings, triple twisted tape, and others), PVG provides the same HT performance at lower pressure, leading to an overall higher TEF in comparison. Promvong

et al. [123] experimentally studied the thermo-hydraulic performance of V-shaped winglet VG, where V-shaped rectangular and delta winglets (V-RW and V-DW) were mounted periodically on both sides of a straight tube. The effect was of relative winglet pitch ratios ($P_R = P/D = 0.5, 1.0, 1.5, 2.0$) and blockage ratios ($B_R = b/D = 0.1, 0.15, 0.2$) was studied at a fixed angle of attack of 45° in the Re range of 4130–25,900. V-RW had a higher HT rate and pressure drop compared to V-DW, while a risen PR resulted in a decrease in HT rate and pressure loss. The optimal configuration was found to be V-DW with $B_R = 0.15$ and $P_R = 1.0$ which resulted in a TEF in the range of 1.82–2.0. Various configurations of vortex generators are shown in Fig. 6. Table 5 presents the summary of the researches discussed in this section.

Winglet vortex generators are the most common of the different geometries of vortex generators because they generate longitudinal recirculating flows while interrupting the main flow. Furthermore, winglet vortex generators have the smallest pressure loss penalty. For thermal systems, the construction of winglet vortex generators with a greater attack angle is recommended. The pressure loss associated with vortex generators can be reduced by employing winglets with punched holes, which function as airflow bypass. Overall, vortex generators were effective in solar systems because they had the ability to generate substantial amounts of heat transfer by creating powerful longitudinal recirculating flows.

Artificial roughness

The rate of HT is significantly influenced due to roughness in the channel. Roughness acts as a turbulence promoter that directly enhances the thermal transport in the fluid field by disturbing the laminar sub-layer in the boundary layer and increases the mixing of the fluid. Besides this, roughness also increases the friction coefficient. Due to this, it is preferred to use a small height of roughness in comparison with duct height. Various types of roughness have been investigated by many authors, and their effects on thermal and flow characteristics of the fluid have been discussed below.

Katoh et al. [124] conducted an experimental study for the thermal and flow behaviour in the presence of random roughness in the channel. The main aim of this study is to obtain a relationship between HT and friction factor (f) augmentation. It was revealed from the experimental work that whenever the molecular Prandtl number (Pr) is less than a turbulent Prandtl number (Pr), then the efficiency of HT is less than unity. This is because of high skin friction (f) in comparison with heat transfer, while the opposite trend was observed when molecular Pr is more than turbulent because eddy viscosity has more effect on HT than f . Nilpueng et al. [125] experimentally revealed the effect of chevron angle

and surface roughness on the plate-type heat exchanger. Sandblasting is used for generating surface roughness over the cold plate. It was revealed from the study that an increase in the surface roughness and Re increases the heat transport and pressure loss while increasing the chevron angle shows the opposite behaviour. It was also reported that at 30° chevron angle, the highest roughness and lowest Reynolds number are the optimum conditions for the best thermal performance of the heat exchanger.

Alammar et al. [126] conducted experiments to investigate the effect of internal surface roughness on the HTE in a closed thermosyphon. Electrical discharge machining (EDM) has been employed for generating roughness on the surface of thermosyphon. It was revealed from the results obtained from the study that roughness enhances the thermal performance of thermosyphon by decreasing the surface for evaporation and increasing the heat transfer coefficient (HTC). It was reported that the thermal resistance could be decreased by 42% at 3 kPa and by 13% at 30 kPa, while the heat transfer coefficient (HTC) was increased by 115% and 68% at 3 and 30 kPa, respectively. Sagar et al. [127] investigated the thermal characteristics of roughened porous fins. Three different roughness values (250, 300, and 400 μm) have been used for the study. It was revealed that increasing the roughness increases the HT rate for the same area and volume. Zhang et al. [128] numerically reported the reduction in HT due to surface roughness in turbulent convective flow. Results indicated that hot–cold fluid in the flow field gets trapped in the roughened surface, and this led to the enhanced thickness of the thermal boundary layer, which results in the reduction in heat flow. Table 6 shows the summary of research work on arbitrary surface roughness.

Ting et al. [129] investigated the convective HT in the square cavity. The cavity is filled with Al_2O_3 –water nanofluid. The roughness in the form of waviness is present in the bottom wall of the cavity. The vertical walls of the cavity are kept insulated, while the horizontal walls are maintained at a constant temperature. It was concluded that larger amplitude of the roughness results in lower heat transport and higher entropy production and Bejan number (Be), while increasing the concentration of nanoparticles results in increased entropy, HT, and Bejan number (Be). Patil et al. [130–132] also investigated the impact of surface roughness and nanoparticles under the influence of magnetic fields and reported enhancement in thermal transfer. This section is summarized in Table 6.

Solar energy is a renewable form of energy available to all of us at no cost. As a clean form of energy, solar energy is the new advanced technique studied all over the world for its fullest extraction at low cost with high efficiency. Solar radiation that falls on the earth's surface is called insolation. This section deals with researches related to the effect

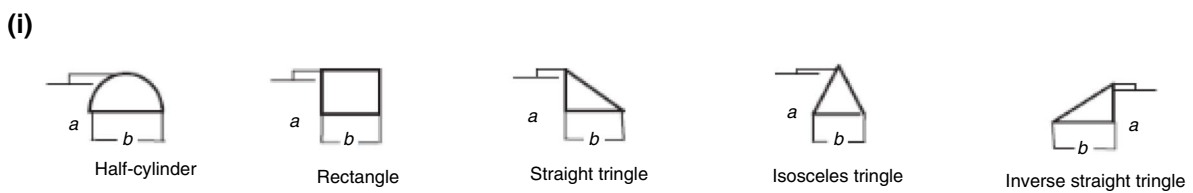
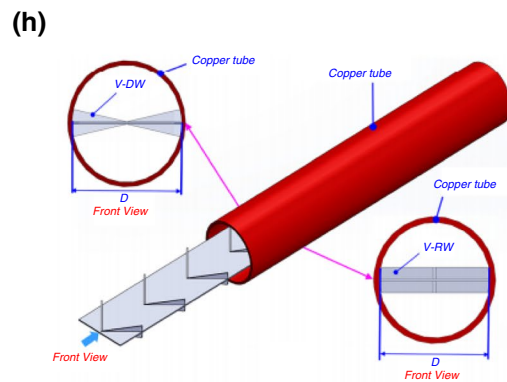
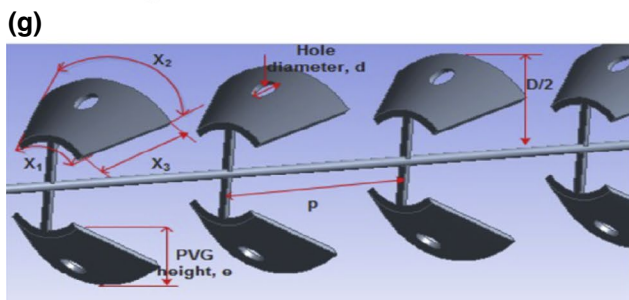
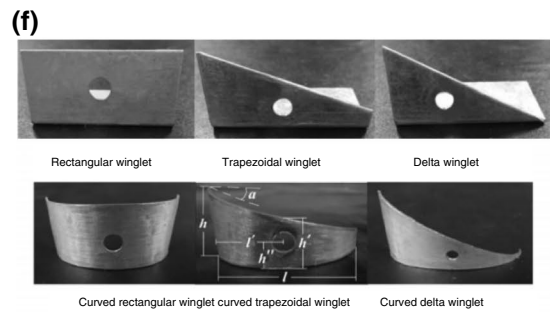
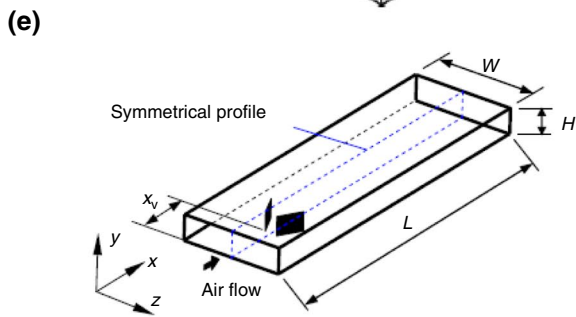
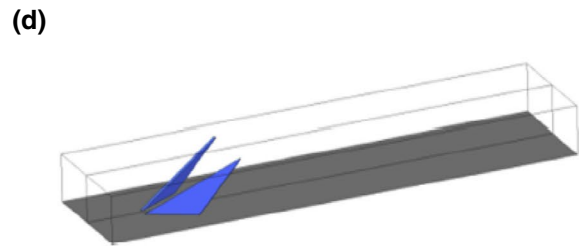
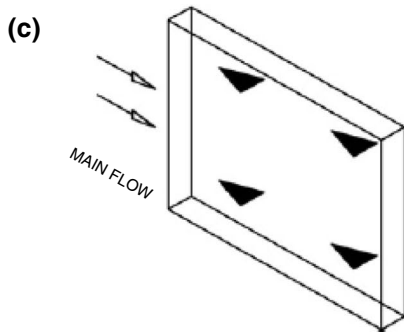
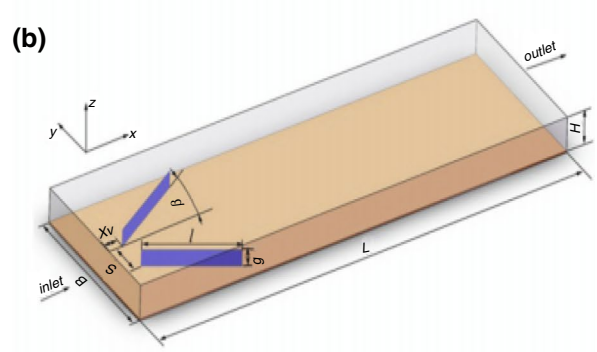
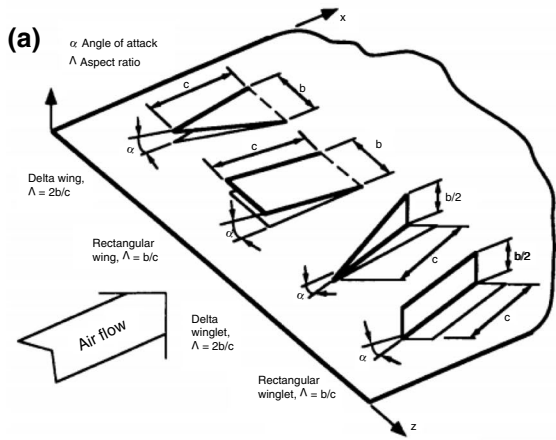


Fig. 6 Various vortex generators [28, 108, 112, 114, 115, 118, 121–123]

Table 5 Summary of experimental studies in vortex generators

Author	Configuration	Flow regime	Parameters	Important results
Gentry [108]	Delta wing vortex generators	Laminar	Aspect ratio—0.5, 1, 1.5, 2 Angle of attack 10°, 25°, 40°, 55°	The heat transfer coefficient (HTC) increased by 55% and pressure drop by 100%
Xu [109]	Delta winglet vortex generators	Turbulent	Attack angles 0, 15, 30, 45 degrees Blockage ratios 0.1, 0.2, 0.3 Relative Pitch Ratios 4.8, 2.4, 1.6	Thermal performance enhancement (TPE) decreases with increasing pitch ratio, attack angle, Re, and blockage ratio A maximum TPE of 1.45 was observed
Zhang et al. [28]	Longitudinal VG	Laminar	Height of VG—2 mm Angle of attack – 30°	Increase in overall heat transfer
Wu et al. [110]	Longitudinal VG	Laminar	Re—800 to 3000 Angle of attack 15°, 30°, 45°, 60°, and 90°	The local HTE of punched VGs was greater than the not-punched ones Thickness of the VG (rectangular winglet) did not affect the global HT significantly
Wu et al. [111]	Longitudinal VG	Laminar	Re—800 to 3000 Angle of attack 15°, 30°, 45°, 60°, and 90°	Overall Nusselt number decreases with an increase in distance from the inlet and that pressure drop remained the same An increase in the area of LVG increased both the average Nusselt number and pressure drop
Oneissi et al. [114]	Delta winglet pair vortex generator	Laminar and turbulent	Re—270, 540, 1080, and 2800–30,000	Enhancement in heat transfer along with a reduction in the friction factor
Xu et al. [118]	Half-cylinder VG	Turbulent	Re—8900–29,900	Increase in HT was observed with an increase in radius and decrease in spacing
Zhou [120]	Curved trapezoidal winglet (CTWP)	All flow regimes	Attack angle 0, 15 degrees Inclination angle Spacing between CTWP in arrangements	Regular delta winglet pair was better than the curved counterparts in laminar and transitional regions, while curved trapezoidal winglet outperformed the regular VGs in turbulent flow

of surface roughness on the thermal and flow behaviour in solar devices.

Kumar et al. [133] experimentally investigate the solar plate with S-shape arc cut roughness for HT and pressure loss. Air is taken as working fluid with Re varied between 2400 and 20,000. Various other parameters used in the experiments are pitch (4–16), height (0.022–0.054), arc angle (30–75°), and width (1–4). It was revealed that roughness on the surface of the solar absorber plate enhances the performance of the solar air heater (SAH). It was found that maximum enhancement in thermal transport was observed at a width of 3, pitch of 8, arc angle of 60°, and height of 0.043. It was also revealed that increasing the Re results in high Nu

and low friction factor (f). Das et al. [134] experimentally revealed the impact of surface roughness on the thermal efficiency of the solar air collector. The roughness is provided in the form of a sand coating on the surface of the absorber plate. The solar simulator has been used to perform the test run with a radiation level of 400, 600, and 800 W/m² and a mass flow rate of 0.01–0.02 kg/s/m². It was revealed that the thermal efficiency of SAC with a roughened absorber plate improves efficiency by 17% with a higher absorption rate in comparison with the plane absorber plate. Bharadwaj et al. [135] experimentally investigated the SAH with inclined triangular ribs roughened surface and reported an enhancement in both thermal transport and friction factor (f).

Table 6 Summary of artificial roughness

Author's name	Year of publication	Short description	Key results
Kato et al. [124]	2000	Experimental study for the thermal and flow behaviour in the presence of random roughness	If molecular Prandtl number (Pr) is less than turbulent Prandtl number (Pr), then the efficiency of HT is less than unity and the opposite trend was observed when molecular Prandtl (Pr) is more than turbulent because eddy viscosity has more effect on HT than friction factor
Nilpueng et al. [125]	2018	Effect of chevron angle and surface roughness on the plate-type heat exchanger	30° chevron angle, highest roughness, and lowest Reynolds number are the optimum conditions for the best thermal performance of heat exchanger
Alammar et al. [126]	2018	Effect of internal surface roughness on the HTE in a closed thermosyphon	Thermal resistance can be decreased by 42% at 3 kPa and by 13% at 30 kPa, while HTC was increased by 115% and 68% at 3 kPa and 30 kPa, respectively
Sagar et al. [127]	2017	Thermal characteristics of roughened porous fins	Increasing the roughness increases the HT rate for the same area and volume
Zhang et al. [128]	2018	Reduction in HT due to surface roughness in turbulent convective flow	Hot cold fluid inflow field get trapped in the roughened surface, and this led to the enhanced thickness of the thermal boundary layer which results in a reduction in heat flow

Prakash and Saini [136] investigated spherical and inclined rib protrusion in SAH as roughness. The range of various parameters considered are Re (2000–20,000); relative roughness pitch (15–30); relative rib length (0.4–1.0); and relative rib pitch (0.2–0.8). An increment in thermal transport, as well as friction factor (f), has been observed. Maithani et al. [137] investigated spherical roughness with different sizes and spacing for Re range between 4500 and 16,500. Enhancement in HT and pressure loss was observed for all the configurations, while maximum efficiency was observed for parameters $D_s/D_H = 0.195$, $X_s/D_s = 4.04$, and $Y_s/D_s = 4.62$ at Re = 10,500. Sethi et al. [138] experimentally investigated the dimpled absorber plate in SAH for HT and friction factor (f). It was revealed that increasing the Re led to an increase in Nu and f . A similar study with similar geometry and results was conducted by Yadav et al. [139].

Ghritlahre et al. [140] experimentally revealed the effect of inward and outward arc shape roughness on the thermal and flow behaviour of SAH and reported that the inward arc shape plate performs better over the outward arc plate. The thermal efficiency of the inward arc plate is 6.9% higher than the outward arc plate. Gill et al. [141] experimentally investigated the novel roughness in the form of broken arc roughness with staggered rib pieces, as shown in Fig. 7 for thermal performance in SAH. Re is varied from 2000 to 16,000. Enhancement in Nu and f is observed as compared with smooth plate SAH, while maximum thermal performance is observed with a staggered rib of size 4. Jain et al. [142] experimentally investigated staggered arc ribs on the absorber plate for the thermal and flow performance of SAH. The results revealed augmentation in heat transfer, pressure

drop, and thermal and flow performance. Multiple arc roughness with the gap, as shown in Fig. 8, has been discussed experimentally [143]. The study is focussed on variation in Nu and f . The results obtained from the analysis show a significant increment in Nu, as well as in f . The summary of the parameters used in various studies in this section is given in Table 7.

It may be inferred that there is a significant increase in heat transmission with low friction cost. If the ribs protrude beyond the viscous sub-layer, the heat transfer rate increases, while friction losses increase dramatically. When the roughness height is somewhat greater than the transition sub-layer thickness, optimal thermal hydraulic performance conditions are achieved.

Modified ducts

Duct or channel modification is one of the less popular, however, very efficient ways of HTE. In laminar and turbulent flow conditions, duct shape is one of the most significant variables influencing heat transmission. In this method of HT augmentation, instead of using any kind of vortex generator, swirl device or inserts, etc., the modifications are done in the channel or duct itself. The modifications are in the form of corrugation [144–148], protrusion, spiral twist, etc. This channel or duct modification enables secondary flow and swirl flow inside the duct which results in the enhancement of thermal transport. The modifications on the surface of the channel act as a turbulence promoter which enhances disturbance in the boundary layers and allows better fusion of fluid which enables the high heat transfer.

Fig. 7 Novel design of arc shape roughness. **a** Relative staggered rib size (r/g)=1, **b** relative staggered rib size (r/g)=2, **c** relative staggered rib size (r/g)=3, **d** relative staggered rib size (r/g)=4, **e** relative staggered rib size (r/g)=5, and **f** relative staggered rib size (r/g)=6 [141]

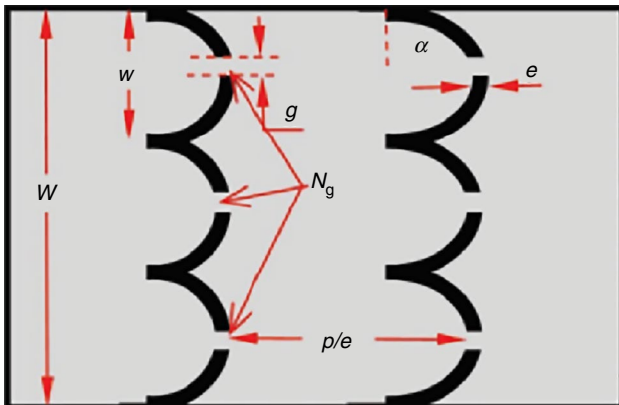
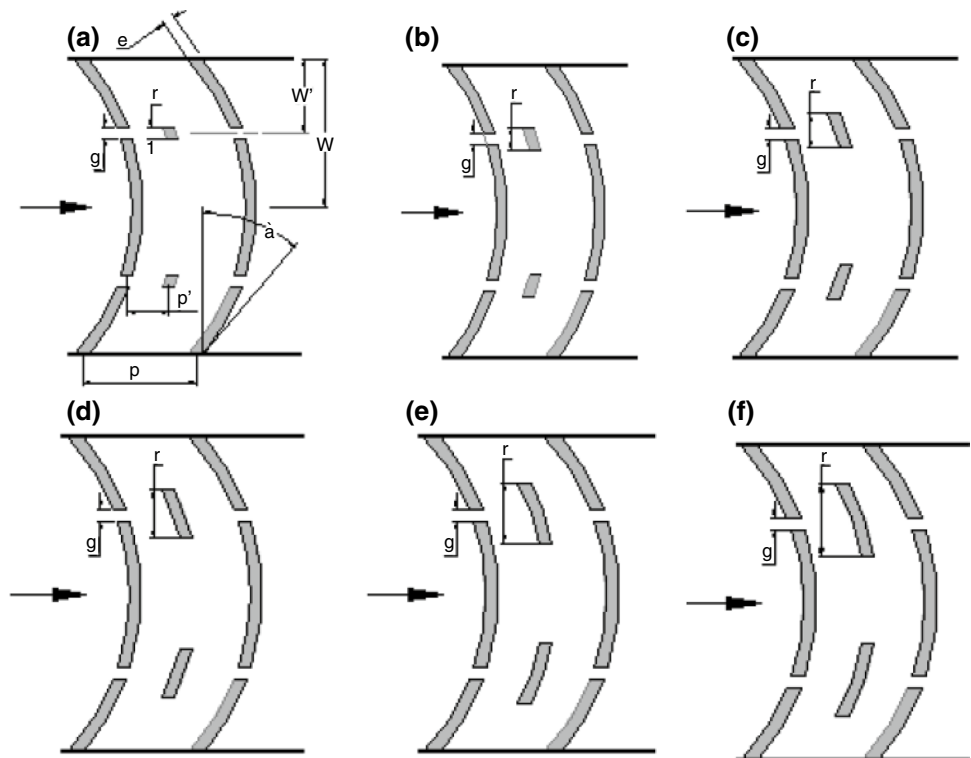


Fig. 8 Arc shape roughness [143]

Ducts with helical corrugations

Corrugated channels are widely employed in industrial heat exchangers as one of the passive flow control strategies for increasing heat transfer rate. The goal of this approach is to disrupt and rebuild the flow boundary layer as it passes through the channel. Fluid recirculation and swirl flow are heat transfer enhancement methods provided by corrugations.

Rainieri et al. [149] reported the effect of the helically coiled twisted corrugated tube for mixed convective heat transport using experiments. For the experimental test run,

ethylene glycol was used as a working fluid with Re varied from 70 to 1200 and dean no. varied between 12 and 290. Three twist ratios were used, while the tube corrugation remains the same for all configurations. The Nu was reported to be 25 for the helically twisted wall, while the pressure drop was 2.5. Bozzoli et al. [150] experimentally assess six corrugated tubes with different pitch and depth of corrugation for HT rate in food processing. The corrugation is in the form of the cross-helix. The purpose of this investigation is to evaluate the optimized geometry for maximum thermal transport. Ethylene glycol and water are used as working fluid with Re ranges between 50 and 14,000. The results revealed enhancement in both HT and friction factor (f), while optimal geometry for double-helix corrugation is found to be pitch, $l=13$ mm, depth, $e=0.8$ mm, and envelope dia., $D_{env}=14$.

Wang et al. [151, 152] numerically investigated outward corrugated tubes, as shown in Fig. 31, and inward corrugated tubes for thermo-hydraulic behaviour. Both works result in enhanced HT and friction factor (f). HT and pressure drop in turbulent flow regime in various helically corrugated circular tubes have been investigated by Pethkool et al. [153]. And the data obtained from the investigation have been compared with the data obtained for the smooth tube. The parameters used for the investigation are pitch, rib height, pitch-to-diameter ratio, rib height-to-diameter ratio, helix angle, etc. A maximum of 123% to 232% of enhancement in HT rate has been obtained for the corrugated tube when compared

Table 7 Parameters used in various investigations in solar heaters

Author's name	Year of publication	Heat flux	Mass flow rate	Range of Reynolds number	Aspect ratio	Relative roughness height	Relative roughness pitch	Relative roughness width	Arc angle
Kumar et al. [133]	2017	0–1200 W/m ²	–	2400–20,000	12	0.022–0.054	4–16	1–4	30°–75°
Das et al. [134]	2020	400–800 W/m ²	0.01–0.02 kg/s/m ²	–	–	–	–	–	–
Bharadwaj et al. [135]	2017	–	–	4500–28,000	1.15	0.021–0.043	4–16	–	30°–75°
Prakash and Saini [136]	2019	–	–	2000–20,000	12	0.04	15–30	–	60°
Maithani et al. [137]	2020	1000 W/m ²	–	4500–16,500	–	–	–	–	–
Sethi et al. [138]	2012	0–1200 W/m ²	–	3600–18,000	11	0.021–0.036	10–20	–	45°–75°
Yadav et al. [139]	2013	0–1000 W/m ²	–	3600–18,100	11	0.015–0.03	12–24	–	45°–75°
Ghritlahre et al. [140]	2020	–	0.007–0.022 kg/s	–	–	0.0395	10	–	60°
Gill et al. [141]	2016	1000 W/m ²	–	2000–16,000	12	0.4	10	1	30°
Jain et al. [142]	2019	1000 W/m ²	–	3000–18,000	–	0.043	10	4	30°–75°
Kumar et al. [143]	2020	0–1200 W/m ²	–	5600–16,500	–	0.044	8	5	60°

with the smooth tube for different rib heights and Re, while the friction factor (f) is between the range of 1.46 and 1.93 when compared with a smooth tube. Andrade et al. [154] performed experiments to investigate the thermal and flow behaviour in all the three regimes inside helically corrugated tubes. The Re for the analysis has been varied from 429 to 6216. The tests are conducted in adiabatic as well as diabatic conditions with heat flux ranges between 5.5 and 21.1 kW/m². The results obtained for the HT from the investigation show that corrugated tubes are most effective in the transitional zone with maximum thermal transport followed by turbulent flow, while for laminar flow regime, corrugated tubes at low Re are not beneficial.

Li et al. [155] conducted experiments to investigate the thermal and flow characteristics of slush nitrogen turbulent flow in a helically corrugated tube. The results obtained for slush nitrogen are compared with results obtained for sub-cooled liquid nitrogen. A new correlation was proposed, which considers flow conditions as well as geometrical parameters for calculating friction factor (f) in a helically corrugated tube. Figure 9 shows the various corrugated ducts reviewed in this section. The discussed work is summarized in Table 8.

The corrugation on the surface of duct causes the flow separation which results in the shearing of boundary layer. This shearing of boundary layer causes intense mixing of fluid which led to higher heat transfer. A maximum heat

transfer enhancement of up to 230% is reported with corrugated duct. The flow regime is also an important factor in augmentation of heat transfer.

Dimpled duct

The dimpled tube enhances the HT by allowing better mixing of fluid inside the flow field. This mixing is possible because of the breaking of the boundary layer which allows initiation of secondary flow and hence augmenting the convective heat transfer [156, 157].

Xie et al. [158] conducted a numerical assessment to investigate the impact of dimpled geometries with the internal protrusion on the surface of the rectangular tube. The Re is used for the investigation varied from 7500 to 27,500. It was found that the internal protruded dimpled channel shows higher augmentation of HT with the low frictional penalty (f) when compared with a simple protruded channel. The structures also augment the thermal performance of the system when compared with the performance of the conventional dimpled channel. Li et al. [159] performed an experimental and numerical investigation on a dimpled tube for HT and pressure drop characteristics. Two working fluids, namely water and H₂O–glycol, are used for experiments with Re for water varied from 500 to 8000, while for H₂O–glycol Re varied between 150 and 2000. It was revealed that HT was augmented by 200% when compared with the smooth

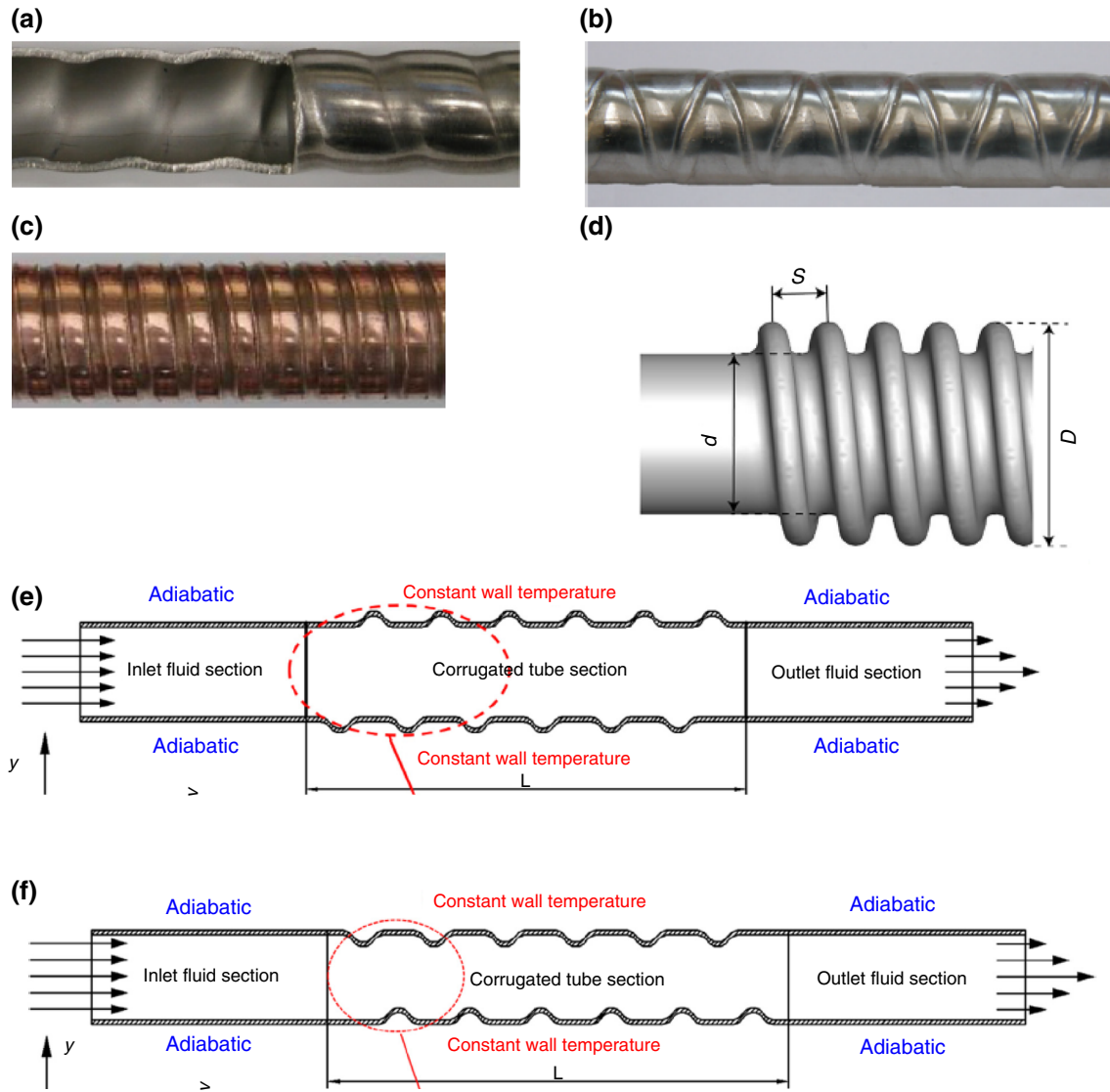


Fig. 9 Various kinds of corrugated ducts [149–153, 155]

tube. It was also found that HT is more than pressure drop which results in higher PEC. Another computational study by the same author [160] investigates single-phase flow in a dimpled tube for optimal thermal performance. The results obtained from the simulation study showed significant enhancement in HT performance. It was also observed that geometric parameters such as pitch, depth, and shape of dimples have a significant influence on thermo-hydraulics. Xie and co-workers [161–163] conducted a numerical investigation to study the thermal and flow characteristics in turbulent flow regime for various configurations of dimpled tubes. The results obtained from the investigations show that dimpled tubes performed much better when compared with plain tubes.

Wang et al. [164] performed experiments and reported the HT and flow behaviour in a novel ellipsoidal dimpled

tube. The data obtained from this investigation are compared with spherical dimpled tubes and smooth tube data. Water is taken as the working fluid in shell side flow at a constant flow rate, while air is drawn into the tube with a flow rate varied from 1 to 55 m³/h. Enhancement in HT and pressure drop was noticed for the dimpled tube when compared with the smooth duct/tube results. The critical Re for the transition was found to be 1000 for the ellipsoidal dimpled tube. Kumar et al. [165] conducted numerical as well as experimental investigations to compute the HT and pressure drop in a dimpled duct/tube. The Re for the investigation was taken between the range of 4000 and 28,000. Other parameters studied are streamwise spacing (x/d_d), spanwise spacing (y/d_d), and the ratio of dimpled depth and print diameter (eld_d). The results obtained after analysis show 3.18 times augmentation in heat transport and 2.87 times augmentation

Table 8 Summary of parameters used and important results for helically corrugated ducts

Authors and year of publication	Parameters used	Summary	Key results
Raimieri et al. [149], 2013	Reynolds No.—70 to 1200 Dean No.—12–290 Curvature ratio—0.031, 0.040, and 0.056 Working fluid—ethylene glycol	Influence of helically corrugated spirally twisted circular duct on the thermal and flow characteristics	Enhancement of HT of about 25 times was observed for helically twisted wall in comparison with plain channel, while pressure drop ranges between 1.5 and 2.5
Bozzoli et al. [150], 2020	Reynolds No.—50–14,000 Prandtl No.—5–150 Heat flux—1–11 kW/m ² Corrugation depth—0.6, 0.8, 1 mm Pitch—13 and 29 mm Working fluid—ethylene glycol	To evaluate the optimize geometry for maximum thermal transport	Enhancement in both HT and friction factor (f) was observed Optimal geometry for double-helix corrugation found to be Pitch, $l = 13$ mm, depth, $e = 0.8$ mm, and envelope dia., $D_{env} = 14$
Wang et al. [151], 2018	Reynolds No.—3800–43,800 Height-to-diameter ratio—0.05, 0.10, 0.15 Pitch-to-diameter ratio—0.5, 1.0, 1.5	Influence of various parameters on the thermal and flow characteristics in turbulent flow regime in outward corrugated tube	A great enhancement in HT was observed in turbulent flow regime with a maximum value of $Nu_{s,ave}/Nu_{s,ave}$ being 1.77 and PEC being 1.4
Wang et al. [152] 2018	Reynolds No.—10,020–40,060 Height-to-diameter ratio—0.03, 0.05, 0.08 Pitch-to-diameter ratio—1.0, 1.5, 2.0	Influence of various parameters on the thermal and flow characteristics in turbulent flow regime in inward corrugated tube	Enhancement in HT and pressure drop was noticed due to breaking and formation of hydrodynamic and thermal boundary layer. 123% to 232% of enhancement in HT rate
Pethkool et al. [153], 2011	Pitch-to-diameter ratio—0.18, 0.22 and 0.27 Rib height-to-diameter ratio—0.02, 0.04 and 0.06 Reynolds No.—5500 to 60,000	HT and pressure drop in turbulent flow regime in various helically corrugated circular tubes	Friction factor (f) is between the range of 1.46 and 1.93 when compared with smooth tube
Andrade et al. [154], 2019	Reynolds No.—429 to 6212 heat flux—5.5 kW/m ² to 21.1 kW/m ² Pitch—6 and 12 mm	To investigate the thermal and flow behaviour in all the three regimes inside helically corrugated tubes	Corrugated tubes are most effective in transitional zone with maximum thermal transport followed by turbulent flow
Li et al. [155], 2018	Pumping rate—9 L/s Inner diameter—10.2, 13.9 mm Reynolds No.—2000 to 17,000	To investigate the thermal and flow characteristics of slush nitrogen turbulent flow in helically corrugated tube	A new correlation was proposed which considers flow conditions as well as geometrical parameters for calculating friction factor (f) in helically corrugated tube

in thermo-hydraulic performance. Chen et al. [166] performed an experimental assessment to investigate the HT augmentation in the dimpled duct. Six dimpled tubes made of copper were used for the investigation. Water is taken as the working fluid with Re varied from 7500 to 52,000. It was found that augmentation in HT is ranged between 25 and 137% at a fixed value of Re , while at constant pumping power, augmentation in HT ranged between 15 and 84%. The studies related to this section are summarized in Table 9. Figure 10 shows the different geometries and arrangements of dimples on the duct.

Modified ducts with inserts

Du and Hong [167] performed experiments to investigate the influence of a corrugated tube (transverse ribbed tube) along with spaced helical tapes on thermo-hydraulic performance. The parameters studied are Re , pitch length ratio, and space ratio. The Re is varied from 5000 to 19,000, and air is taken as the working fluid. A maximum enhancement of 49% in HT was found with corrugated tube alone, while with tapes, it was further increased by 177%. Besides this, friction factor (f) was also increased for the corrugated tube by a maximum of 1.7 times, while along with spiral tapes, this increment was 15.31 times compared to the plane channel. Du et al. [168] experimentally compute the HT and flow behaviour in the corrugated tube fitted with a wire coil insert. Air is taken as the working fluid with Re between 6000 and 18,000. The results obtained from the investigation show enhancement in both HT and pressure drop.

Bhattacharyya et al. [22] conducted experiments to investigate the impact of tape inserts fitted inside a corrugated tube on the thermal and flow behaviour of the fluid. The parameters investigated are the pitch ratio, spring ratio, and Re . Air is taken as the working fluid for Reynolds number (Re) ranges between 10,000 and 50,000. The data were obtained for the plain channel, corrugated tube, and corrugated tube fitted with tape inserts. It was found that increasing the Re led to the enhancement of Nu in all the cases with the highest augmentation being noticed for corrugation pitch of 0.7 and spring ratio of 3.0, while the friction factor (f) decreases with an increase in the Re . Friction factor (f) was reported highest for the corrugated tube with tape inserts. Besides this, the thermo-hydraulic performance was also analysed by the authors and reported that it is independent of Re . Hasanpour et al. [169] experimentally reported the influence of different geometries of tape inserts fitted inside a corrugated channel on the thermal transport and flow behaviour. The various parameters investigated are twist ratio (3–7), hole diameter ratio (0.11–0.33), width and depth ratio (0.3–0.6), and Reynolds no. ($5000 \leq Re \leq 15,000$). Water is taken as the working fluid. The results obtained from the experiments reveal augmentation of both heat transport and

friction factor (f) when compared with plain corrugated tube, and the highest values are reported for modified twisted tapes. This is because modified twisted tapes add more turbulence to the flow field, which helps in the better fusion of fluid within the channel.

The application of artificial neural network in the prediction of thermal and flow behaviour inside a corrugated duct was investigated and reported that the predicted results for both HT and friction factor (f) are in very good agreement with experimental values [170]. A numerical study to investigate the influence of corrugation along with wire coil on the thermo-hydraulic behaviour in the turbulent regime ($Re = 5000–20,000$) was reported by Moghadam et al. [171]. The results obtained from the investigation show significant improvement in thermal performance. Saha [172] reported an experimental work on the thermal performance of axially corrugated square duct fitted with twisted tape insert with oblique teeth. The experiments were conducted in the laminar/viscous flow regime with oil that was taken as the working fluid. It was concluded that square duct with tape inserts performed better instead of using axial corrugation or taper inserts separately. Saha et al. [173] investigated the combined effect of axial corrugation in circular duct fitted with helical screw tape on the HT augmentation. A numerical study to investigate the impact of corrugated tube combined with tape insert on the thermal performance and economics of the waste heat recovery system was reported by Mokka-pati and Lin [174]. The results obtained from the investigation show more than 200% enhancement in HT rate when compared with the results obtained for the plain tube. Yang et al. [175] conducted a numerical investigation to study the impact of tape inserts and convex-shaped corrugation on the thermal and flow characteristics and reported augmentation in the rate of HT when compared with HT rate of the plain tube with tape insert. Thianpong et al. [176] conducted experiments to report the HT and friction factor (f) in a dimpled duct/tube fitted with twisted tape inserts. The range of Re is varied from 12,000 to 44,000. It was found that the thermal transport and friction factor (f) is maximum for dimpled duct/tube with insert when compared with the results of the dimpled tube or plain tube acting alone. Figure 11 shows the various modified ducts with inserts reviewed in this section. The above-discussed research works are summarized in Table 10.

Twisted tubes

Twisted elliptical tubes Yang et al. [177] experimentally and numerically analysed the convective HT characteristics of flow in twisted elliptical tubes in all flow regimes. The structural parameters of the tube-like aspect ratio and twist pitch were varied, and their effect on the HT was studied. The longitudinal vortex generated by the twisted tube

Table 9 Summary on dimpled ducts

Authors and year of publication	Parameters used	Summary	Key results
Xie et al. [158], 2013	Reynolds No.—7500 to 27,500 Heat flux—1000 W/m ² Pitch—50 mm	Impact of dimpled geometries with internal protrusion on the surface of a rectangular tube	Internal protruded dimpled channel shows higher augmentation of HT with low frictional penalty when compared with simple protruded channel
Li et al. [159], 2016	Re for water—500 to 8000 Re for ethylene glycol and water—150–2000 Pitch—10 mm	Experimental and numerical investigation on a dimpled tube for HT and pressure drop characteristics	HT was augmented by 200% when compared with smooth tube
Li et al. [160], 2016	Dia of dimple—5 mm Pitch—7, 10, 13 mm Depth, H—0.3–1.2 Diameter, d—4, 5, 7 mm	Computational study to investigate single-phase flow in dimpled tube for optimal thermal performance	Significant enhancement in HT performance
Xie et al. [161], 2018	Dimple shape—cone, sphere, ellipsoidal Reynolds No.—5000 to 30,000 Extruded depth, D—2–5 Pitch, P—20–40 Radius—2–5	Numerical investigation on enhanced dimpled tube	Enhanced dimpled tube allowed better mixing of fluid due to turbulence created by uneven structure of the duct, which results in the enhanced heat transfer
Xie et al. [162], 2018	Reynolds No.—5000–30,000 Dimple depth, D—1, 1.7, 2 mm Dimple pitch, P—16, 20, 28 mm Axis ratio, R—1, 2, 2.2 mm	Impact of ellipsoidal dimples on thermal transport and flow behaviour	Transverse and longitudinal dimples present on the surface of the duct helps in the augmentation of heat transfer
Xie et al. [163], 2019	Reynolds No.—5000 to 30,000 Depth, D—2, 3, 3.5, 4 mm Pitch—14, 15, 16, 19 mm Radius, R—3, 3.5, 4, 4.5 mm Flow rate—1 to 55 m ³ /h	Compared the impact of spherical dimples, ellipsoidal dimples and teary dimples on thermal and flow characteristics	Teary drop dimpled tube performed significantly better against spherical dimpled tube and ellipsoidal dimpled tube in terms of HT as well as pressure drop penalty
Wang et al. [164], 2010	Dimple height, h—1.5, 2 mm	Experiments to investigate the HT and flow behaviour in a novel ellipsoidal dimpled tube	Enhancement in HT and pressure drop compared to the smooth tube
Kumar et al. [165], 2017	Reynolds No.—4000 to 28,000 Dimple depth—1 mm x/d_d —15–3 y/d_d —15–35	Numerical and experimental investigation on the HT and pressure drop in a dimpled tube	The critical Re for the transition was found to be 1000 for ellipsoidal dimpled tube 3.18 times augmentation in heat transport and 2.87 times augmentation in thermo-hydraulic performance
Chen et al. [166], 2001	Reynolds No.—7500 to 52,000 Depth of dimple, e—0.5, 0.6, 0.7, 1.2, 1.3, 1.5 Dia of dimple—2, 3, 3.5, 4.5, 4.7, 5.5 Pitch—8, 10, 12, 14	HT augmentation in the copper dimpled tubes	Augmentation in HT is ranged between 25 and 137% at a fixed value of Re, while at constant pumping power, augmentation in HT ranged between 15 and 84%

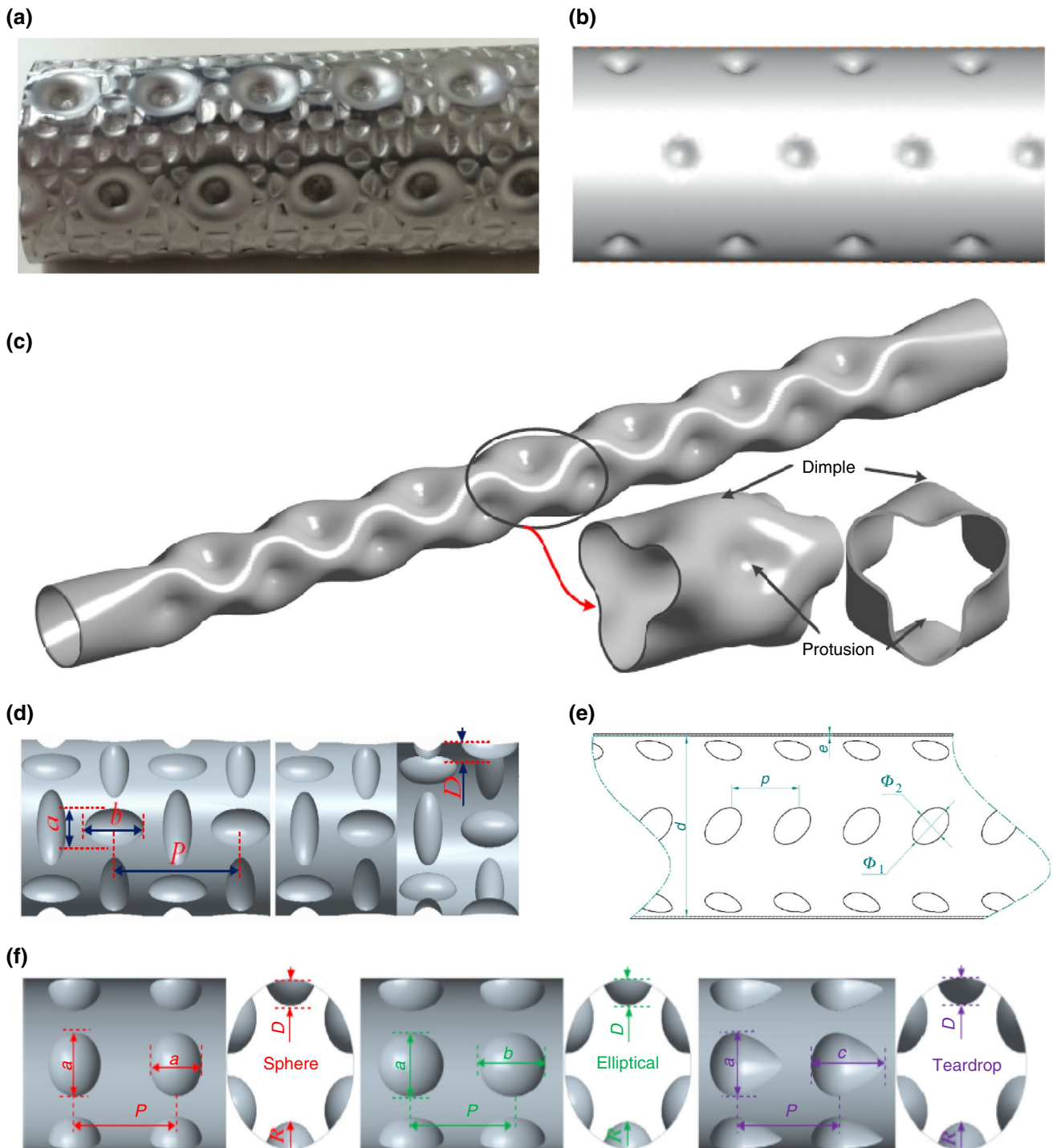


Fig. 10 Various kinds of dimpled tube [159–164]

wall improved the synergy between the velocity vector and temperature gradient, producing a smaller average synergy angle. This resulted in a higher Nusselt number. A larger aspect ratio and smaller twist pitch produced a higher Nusselt number and friction factor (f). Wu et al. [178] conducted

numerical simulations to understand the HTE of forced convection flow in a twisted elliptical tube in turbulent flow regime. They also found that the rotational motions caused by the twist of the tube aided HT performance. The tube with twist pitch $d = 96$ mm was found to have an increase

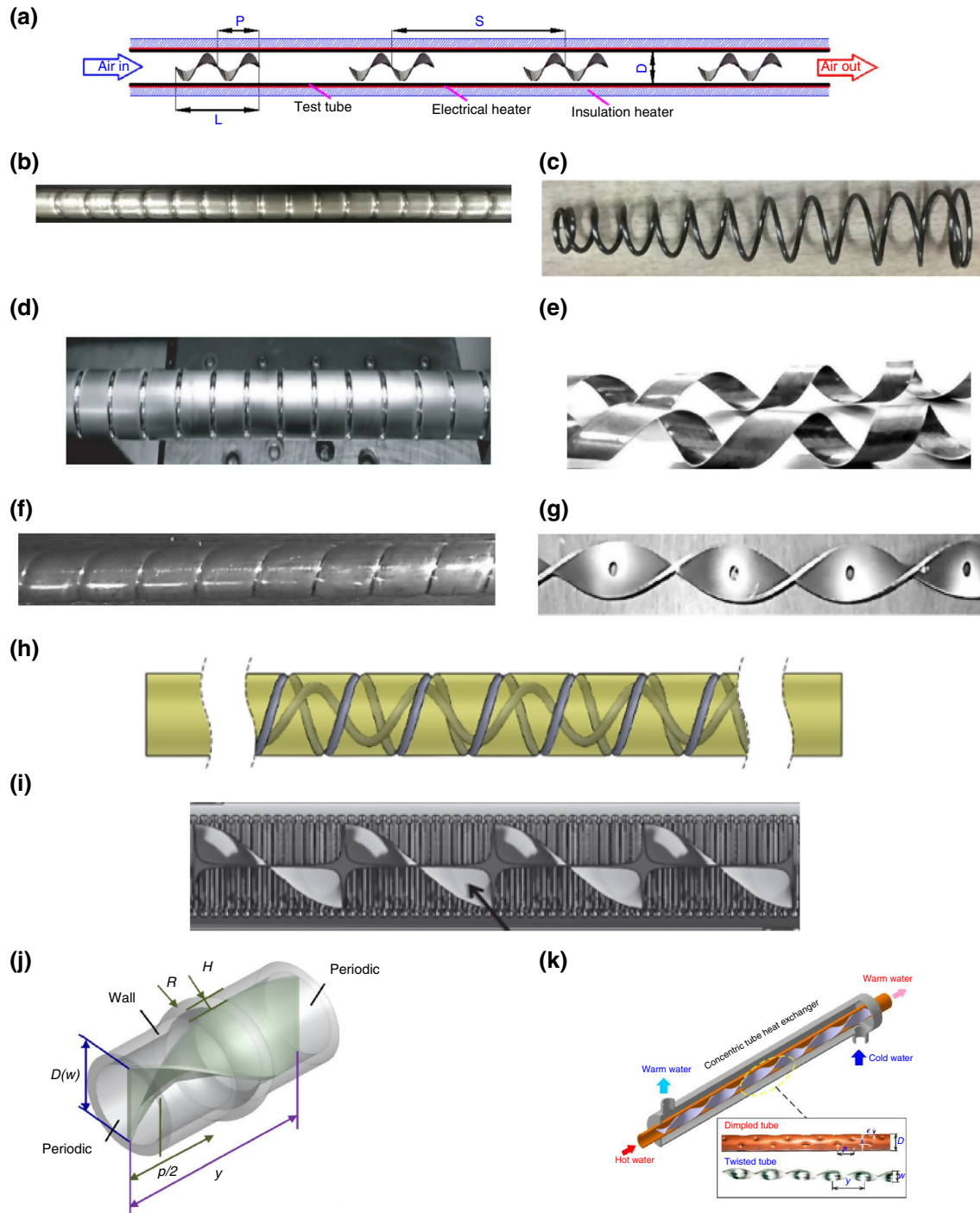


Fig. 11 Modified duct fitted with various turbulators [22, 167–169, 171, 174–176]

of 16–19% in Nusselt number and 58–60% in friction factor (f) in comparison with the plain tube. This was attributed to the reduction in entransy-based thermal resistance, which significantly improved heat transfer. The tube twist pitch of $d = 128$ mm was shown to have the best thermo-hydraulic performance.

Spiral twisted tube Dong et al. [179] experimentally studied the thermal characteristics of high viscosity thermal oil and water flow in a spirally twisted tube heat exchanger in a turbulent flow regime. They compared the performance of twisted spiral tube to that of ordinary tube exchangers and spiral groove tube exchangers. It was seen that the spirally twisted tube outperformed both ordinary and spiral groove

Table 10 Summary on modified duct with inserts

Authors and year of publication	Parameters used	Summary	Key results
Du and Hong [167], 2020	Tape length—60, 80, 100 mm Pitch length—30, 40, 50 mm Module distance —165, 206.3, 275, 412.5 mm $p/e=8.75$ to 5.625 $S/D=0.60, 1.55, 2.97, 5.34, 10.09$ $Re=6000$ to 18,000	Influence of corrugated tube (transverse ribbed tube) along with spaced helical tapes on thermo-hydraulic performance HT and flow behaviour in corrugated tube fitted with wire coil insert	A maximum enhancement of 49% in HT was found with corrugated tube alone, while with tapes it was further increased by 177% Enhancement in both HT and pressure drop
Bhattacharyya et al. [22], 2019	Reynolds No.—10,000 to 50,000 corrugation depth (d)—3.0 mm Pitch ratio, $y=0.7, 1.0$ Spring ratio, $s=3.0, 5.0, 7.0$ Twist ratios—3, 5 and 7	Impact of tape inserts fitted inside a corrugated tube	Increasing the Re led to enhancement of Nu in all the cases with the highest augmentation
Hasanpour et al. [169], 2016	hole diameter ratio 0.11, 0.33 width and depth ratio—0.3–0.6 $Re=5000–15,000$ $Re=3000–60,000$	Influence of different geometries of tape inserts fitted inside a corrugated channel on the thermal transport and flow behaviour The application of artificial neural network (ANN) in the prediction of thermal and flow behaviour inside a corrugated duct Influence of corrugation along with wire coil on the thermo-hydraulic behaviour in the turbulent regime	Augmentation of both heat transport and friction factor (f) when compared with plain corrugated tube and the highest values are reported for modified twisted tapes Predicted results for both HT and friction factor (f) are in very good agreement with experimental values significant improvement in thermal performance
Moghadam et al. [171], 2020	$Re=5000–20,000$ $P/d=2, 3, 4$ and 5 Roughness height, $e=0.5, 1, 2$ and 3 mm $Pr=175–538$ Twist ratio—2.5 Space ratio—2.5 Corrugation angles—30 deg and 60 deg $Re=40,000–77,000$	Experimental work on thermal performance of axially corrugated square duct fitted with twisted tape insert with oblique teeth	Square duct with tape inserts performed better instead of using axial corrugation or taper inserts separately
Yang et al. [175], 2016	Twisted ratio of $y/w=2.5$ $H=1$ mm $p=50$ mm $R=6$ mm $Re=3000$ to 10,000 $Re=12,000–44,000$ Tape width (w)—22 mm Tape pitch length ($y, 180^\circ$)—66, 110, and 154 mm Twist ratio (y/w)—3, 5, and 7 Dimpled outer tube diameter (D)—22.2 mm Dimpled pitch length (p)—15.5 and 22.2 mm Pitch ratio, $PR=p/D=0.7$ and 1.0	Impact of corrugated tube combined with tape insert Numerical investigation to study the impact of tape inserts and convex-shaped corrugation on thermal and flow behaviour HT and friction factor (f) in a dimpled tube fitted with twisted tape insert	200% enhancement in HT rate when compared with the results obtained for the plain tube Augmentation in rate of HT when compared with HT rate of plain tube with tape insert
Mokkapatni and Lin [174], 2014			
Thianpong et al. [176], 2009			

configurations and had an HTE index of 1.2–1.8 times the ordinary tube and 1.3–2.2 of the spiral groove configurations. The spirally twisted tube was especially suited for low Re flows and laminar flows, and this enhanced performance was again attributed to the flow rotation generated by the twisted tube. Tang et al. [180] experimentally and numerically tested the turbulent flow and HT characteristics of twisted tri-lobed tube (TTT) and twisted oval tube (TOT). The effect of various geometric parameters like cross section shape, twisted pitches, twist direction, and lobed numbers was studied. It was seen that at identical configuration TTT had an increase of 5.4% in Nusselt number and 8.4% in friction factor (f) over TOT. The enhanced performance was attributed to the helical flow and secondary flow induced by the twisted curved wall. The thermal performance was found to increase with the out-scribed circle diameter for TOT and various TTT. It was also found that the twisted tube with right–left rotation performed better than one with just right-hand rotation. Eiamsa-ard et al. [181] numerically studied the HTE of three-start spirally twisted tube with triple-channel twisted tape inserts. The tape width ratio and tube/tape arrangement (belly-to-belly and belly-to-neck) were varied. For a given tape width ratio, the belly-to-neck arrangement was found to outperform the other arrangement. This was attributed to stronger interaction between swirling flows and the inserted tapes, which reduced the friction factor (f). The twisted tube with a belly-to-neck arrangement with a tape width ratio of $w/D = 0.34$ produced the best thermal performance.

Twisted oval tubes Tan et al. [182] conducted a numerical and experimental study to understand the convective HTE of fluid flow in oval twisted tubes in a turbulent flow regime. The effect of the geometric parameters like the major and minor axis length has been studied. The Nusselt number and friction factor (f) increased with increasing axis ratio (a/b) and decreasing twist pitch length. From the numerical analysis, it was seen that the twisted wall produced a secondary swirling flow whose strength increases with increasing axis ratio. Through a field synergy analysis, it was determined that the increased HT was due to a reduction in the synergy angle. Cheng et al. [183] numerically studied the HTE of the twisted oval tube (TOT) in low Re flow. The effect of variation of geometric parameters (a/b) and twisted pitch length was studied. The transition Re of the flow was located to be at $Re = 500$. The TOT performed better than the smooth tube due to the effect of secondary flow and lessened field synergy angle. A maximum PEC of 1.7 was obtained for $a/b = 2.0$ and twisted pitch ratio of 0.33.

Li et al. [184] conducted experimental research on the airside HT characteristics of tube twisted oval bundle with staggered cross-flow layout in turbulent flow regime and reported that the performance of the oval twisted tube bundle was greater than the round tube bundle by 25.5–33.3%.

They further conducted a numerical parametric study of twisted oval tube having bundle in inline layout [185]. The effects of axis ratio (a/b), twist pitch length (S), transverse tube pitch (S_t), longitudinal tube pitch (S_l), and number of longitudinal rows (Z) were studied across all flow regimes. The Nusselt number and friction factor (f) were found to increase with increasing a/b , decreasing S , increasing S_t , and increasing S_l and is independent of Z .

Twisted square duct Bhadouriya et al. [186] performed a numerical and experimental study on the HTE of fluid flow in a twisted square duct in all flow regimes. The experiments were conducted by varying twist ratio, while the numerical simulation also varied the Prandtl number (Pr) of the fluid. It was seen that the twisted square duct performed significantly better than the normal square duct up to a Re of 9000 for all values of Prandtl number (Pr). Khoshvaght-Aliabadi et al. [187] conducted numerical studies on various configurations of twisted square channels (TSC) with working fluid as Al_2O_3 nanofluid in laminar flow regime. Different TSCs were created by varying the twist pitch along the tube in the following configurations: uniform, low to high (L–H), high to low (H–L), low to high to low (L–H–L), and high to low to high (H–L–H). The variation of twist pitch was seen to have a significant impact on HT performance, although all configurations had a PEC above unity for the domain of study. The L–H configuration had the best performance followed by H–L–H configuration for all Re.

Miscellaneous Sun et al. [188] performed an experimental study of the HT characteristics of nanofluid flow in built-in twisted belt external thread tubes in the turbulent flow regime. The nanofluids studied were Cu, Al, Al_2O_3 , Fe_2O_3 , multiwalled carbon, and graphite with a mass fraction of 0.1–0.6%. The pitch of the thread was also varied. Cu nanofluid performed the best among all nanofluids. The best performance was exhibited by Cu nanofluid with a mass concentration of 0.5% and pitch = 2 mm. Chen et al. [189] conducted a numerical study in the HTE of corn straw slurry from biogas plants in twisted hexagonal tubes in a turbulent flow regime. The mechanism of HTE was found to be the balanced radial mixing and the near-wall effect that leads to a high shear rate under considerable radial flow intensity. Yan et al. [190] experimentally investigated the performance of epoxy resin flows in a horizontal twisted tube in a laminar flow regime. The effect of short–long diameter ratios and twist ratios was studied. The horizontal twisted tube was found to significantly increase HT at the cost of the low-pressure drop. The best performance was observed for little lead, lower twist ratio, and big short–long diameter ratio. All the above studies are summarized in Table 11. The geometrical representation of various geometries of twisted ducts is shown in Fig. 12.

Wavy channels

Rush et al. [19] perform experiments to investigate the effect of the sinusoidal waviness of channel on the thermo-hydraulic behaviour. Three geometrical configurations of wavy channels were investigated. The results show augmentation of heat transfer due to waviness provided in the channel. This waviness allows enhanced mixing of fluid in the flow field at a high Reynolds number, which results in an increment of heat transfer. Configuration with $\phi = 180^\circ$ shows the best results even at very low Re, while other configurations perform well at higher Re. Ramgadia and Saha et al. [191] conducted a computational study of the turbulent flow and HT characteristics in the wavy walled duct. The wavy wall was described by the following function: $y = 2a \sin^2(\pi x/L)$. The flow was found to be highly 3D, but the flow along the downhill region was seen to laminar due to the deceleration of the flow. The strong 3D nature of the flow is fostered by the secondary flow, which helps in the mixing of the core fluid and near-wall fluid. The friction factor (f) was invariant with Re, but the Nusselt number increased significantly with Re. It was also observed the HTE provided by the wavy channel was similar to that of a square duct with inline transverse ribs. Yang et al. [192] performed a numerical optimization study on the HTE in a wavy channel using nanofluids in a laminar flow regime. The particle concentration and the geometrical parameters of the wavy channel (amplitude and wavy number) were varied. The Nusselt number and friction increased with an increase in amplitude and particle concentration. The results show that the nanofluid (Cu/water) used produced a thermal enhancement of 15–24% over the pure fluid. The optimal geometric configuration was also found using the integrated approach.

Mills et al. [193] investigated the HTE of laminar flow asymmetric wavy channels with sinusoidal walls using a computational simulation. The effects of amplitude, periodicity of waviness, and driving pressure on HTE were thoroughly studied. It was seen that for low Re flow, the flow was steady, and the major influencing factor was the amplitude. On the increase in Re, the flow transitioned to unsteady flow, which was now majorly influenced by the pressure drop instead of the amplitude. They also found that the small-amplitude wavy channels performed best under unsteady flow, resulting in a 50% improvement over the straight channel. Akbarzadeh et al. [194] numerically studied the entropy generation and thermo-hydraulic performance of a wavy channel with three corrugation profiles in a laminar flow regime. Sinusoidal, trapezoidal, and triangular were the corrugation shapes under consideration and reported that the trapezoidal channel had the highest Nusselt number and pressure drop as it had the largest recirculation region. Bhattacharyya et al. [195] numerically investigated the wavy channel for thermal and flow characteristics for viscous flow.

Water is used as a working fluid with Re between 100 and 2000. The investigation revealed enhancement in HT as well as pressure drop. The waviness of the channel allows disturbance in the flow field, which results in turbulence in the flow field, as a result of which HT increases. Various types of wavy channels used for investigations are shown in Fig. 13.

Thermal performance analysis

The performance of a thermal device can be calculated generally in terms of Nusselt number (Nu), Coburn's j -factor, heat transfer coefficient (HTC), friction factor (f) or pressure drop, thermal performance factor (TEF). Nusselt number (Nu), HTC, j -factor represented the augmentation in heat transfer rate while friction factor or pressure drop represents the enhancement in the flow resistance inside a channel. By calculating these factors one should easily understand the changes in the thermal performance due to the modifications employed. However, these terms do not provide clear picture of actual enhancement in thermal performance since both heat transfer and friction factor is increasing. Hence, to overcome this issue a term thermal performance factor is used. This is the ratio of augmentation of Nusselt number to the augmentation of friction factor. The ratio gives real enhancement in thermal performance at given pumping power.

The Dittus—Boelter equation [196] is written as

$$\text{Nu} = 0.023 \text{Re}^{0.8} \text{Pr}^{0.4} \quad (1)$$

The Gnielinski equation [197] is written as

$$\text{Nu} = \frac{\frac{f}{8}(\text{Re} - 1000)\text{Pr}}{1 + 12.7\frac{f}{8}^{1/2}(\text{Pr}^{2/3} - 1)} \quad (2)$$

The Thianpong equation [198] for Nusselt number is written as

$$\text{Nu} = 0.174 \text{Re}^{0.71} \text{Pr}^{0.4} \left(\frac{1}{D}\right)^{-0.18} \quad (3)$$

The Nusselt number correlation by Meyer et al. [199] can be written as

$$\text{Nu} = 0.013 \text{Re}^{0.867} \text{Pr}^{1/3} \quad (4)$$

There are several more correlations available in the open literature which are also used sometimes, but Eqs. 1–4 are used very frequently.

Similarly, several correlations are also available for calculating the friction factor. Most frequently used equation is the Darcy–Weisbach equation [200] for friction factor

Table 11 Summary of experimental investigation in twisted tubes

Author	Configuration	Flow regime	Parameters	Important results
Yang [177]	Twisted elliptical tube	All flow regimes	Aspect ratio Twist pitch	Longitudinal vortex generated by twisted tube decreased the synergy angle Nusselt number increased with higher aspect ratio and smaller twist pitch Showed the best performance at low Re
Dong [179]	Spiral twisted tube	Turbulent	High-viscosity oil and water flow	Performed better than ordinary tube and spiral groove configuration HTE attributed to flow rotation caused by the twisted tube walls
Tang [180]	Twisted tri-lobed tube (TTT) and twisted oval tube (TOT)	Turbulent	Cross section shape Twist pitch and direction	For identical set-ups, TTT performed better than TOT Thermal performance was found to increase without scribed circle diameter for both tubes (Fig. 54)
Tan [182]	Oval twisted tubes	Turbulent	Major and minor axis lengths (a,b) Twist Pitch	Nusselt number and friction factor (f) increased with increasing axis ratio (a/b)
Li [185]	Twisted oval bundle	Turbulent	Staggered cross-flow layout	The oval tube bundle had superior performance over the circular tube bundle
Bhadouriya [186]	Twisted square duct	All flow regimes	Twist ratio Number Prandtl	Twisted square duct outperformed the normal square duct up to Re of 9000 It also compared favourably with twisted elliptical duct and twisted tape inserts
Sun [188]	Nanofluid flow in built-in twisted belt external thread tubes	Turbulent	Nanofluid type and mass fraction Thread pitch	Cu nanofluid performed the best among the studied nanofluids Twisted belt external thread tube showed an increase of 50.32% in HT performance over a horizontal tube
Yan [190]	Epoxy resin flow in horizontal twisted tube	Laminar	Twist ratio Short-long Diameter ratio	Horizontal twisted tube provided a significant increase in thermal performance Lower twist ratio and higher short-long diameter ratio provided the best performance

$$f = \frac{16}{Re} \quad (5)$$

Another equation which is also used several times is the Blasius correlation [201]

$$f = 0.3125Re^{-0.25} \quad (6)$$

Other involves correlation of Petukhov [199]

$$f = (1.8\log Re - 1.5)^{-2} \quad (7)$$

Thermal performance factor is simple in understanding the real augmentation achieved by technique used for performance enhancement [22].

$$\eta = \frac{Nu/Nu_0}{(f/f_0)^{0.33}} \quad (8)$$

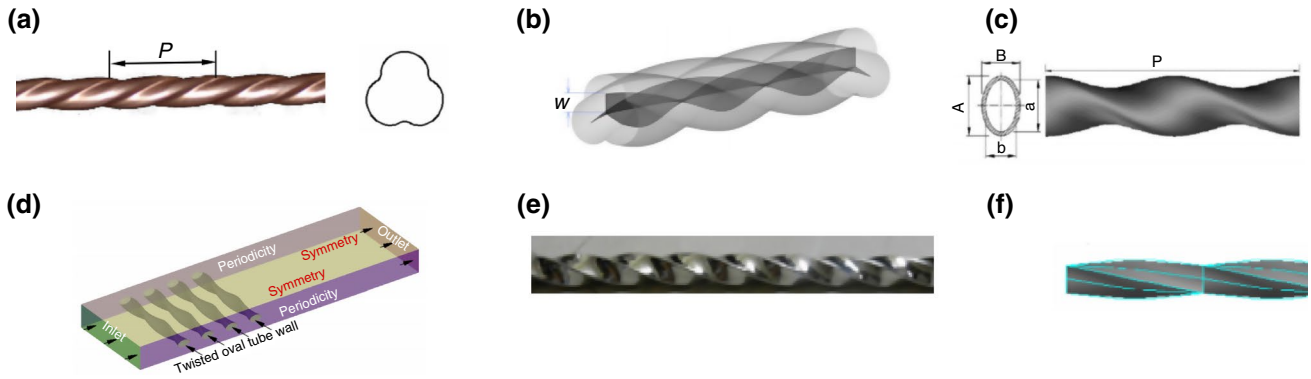


Fig. 12 Various twisted duct geometries [180–182, 184, 186, 187]

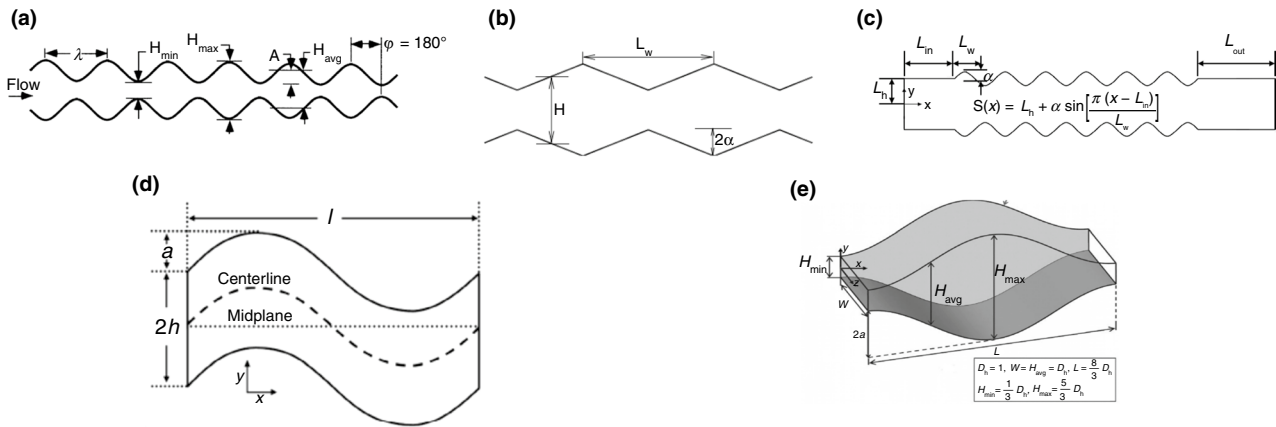


Fig. 13 Various kinds of wavy channels [19, 191–194]

Discussion

All the important studies related to passive techniques and parameters considered during the investigation are summarized in Table 12 presented a comparative study of various passive heat transfer techniques discussed in the present work. Considering the various passive techniques reviewed, it is found that it is difficult to compare them on the common ground. Still, an effort has been put by the authors to include all the possible comparison in Table 12. The use of inserts in the form of swirl devices, vortex generators, twisted tapes, etc., allowed better mixing of fluid due to the turbulence created in the flow field. Obstruction in the flow field in the form of such a device disturbed the boundary layer and allowed the formation of secondary flow in the flow field. This led to an enhanced heat transfer rate. These obstructions also enhance the frictional resistance, which led to increasing consumption of pumping power. Hence, the performance of such devices is measured in the form of TEF, which gives the comparison between HTE with respect to pressure drop. Figure 2 shows the comparison of thermal

performance factor for various twisted tape configurations illustrated in Sect. 3. It has been found that among various configuration of tape inserts, twisted tape insert with winglets performed best.

A separate comparison has been presented in for various duct modification techniques in Table 13. Duct modification is another way of HTE. By modifying the surface of ducts in the form of roughness, corrugations, dimples, protrusions, change in the cross section, waviness, etc., augments the heat transfer rate. However, studies are also reported with combinational methods in which corrugated duct along with nanofluids and/or tape inserts or swirl devices has been utilized. The presence of such modification promotes the vortices, rotation of fluid elements in the flow field. Besides this, modification on the duct surface also disturbs the boundary layer and promotes the secondary flow. These all effect together promotes thermal performance. It was also found that heat transfer enhancement is more prominent with the higher Re with lesser frictional losses. Most of the researches, as we discussed in this present paper, state that

Table 12 Comparison of various passive techniques along with parameters, correlations, and images

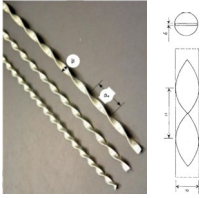
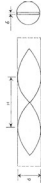
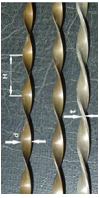
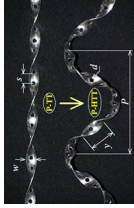

Author	Type of insert	Range of Reynolds number	Mass flow rate	Aspect ratio	Pitch ratio	Twist ratio	Volume fraction	Proposed correlations	Images
Lim et al. [56]	Twisted tapes	449–1371	–	–	–	2.5, 4 and 6	–	$Nu_m = 3.869Gz^{0.4002}y^{-0.185} \left(\frac{d}{h_w}\right)^{0.14}$	
Kumar and Prasad [57]	Twisted tapes	4000–21,000	–	–	–	–	–	$Nu_{tj} = 1.3 + \frac{2.88}{y}$	
Esmailzadeh et al. [72]	Twisted tapes	150–1600	–	–	–	3.21	0.5 and 1%	$Nu_{x*} = 4.36 + a(x*)^{-b} e^{(c*x*)} (0.001 + \varphi^d) \left(0.001 + \left(\frac{t}{d}\right)^f\right) x^*$ > 0.00468	
Azmi et al. [74]	Twisted tapes	–	–	–	–	5–25	0.5–4%	$\eta = aR \frac{e^b}{1 + \left(\frac{t}{d}\right)^c} (1 + \varphi^d)$ $\frac{f_{fr}}{f_{sl}} = 1.4 \left(0.001 + \frac{\varphi}{100}\right)^{0.05}$	–
Ibrahim[77]	Helical screw tape	5700–13,100	–	–	–	2.17, 3.33, 4.3, and 5	–	$Nu_{hf} = \frac{h_w D}{k_{eff}} = 0.073Re^{0.702}Pr_{hf}^{0.4} \left(1 + \frac{D}{H}\right)^{1.3}$ $Nu = 6.11Re^{0.199}(1+x)^{-0.064}Y^{-0.318}$ $f = 54.41Re^{-0.87}(1+x)^{-0.045}Y^{-0.146}$	–
Nanan et al. [78]	Twisted tapes	6000–20,000	–	–	–	1, 1.5 and 2	–	$Nu = 0.0355Re^{0.795}Pr^{0.4} \left(\frac{d}{w}\right)^{-0.068} \left(\frac{s}{w}\right)^{0.086}$	
Bhuiya et al. [79]	Twisted tapes	6950–50,050	–	–	–	1.95, 3.85, 5.92 and 7.75	–	$f = 1.915Re^{-0.299} \left(\frac{d}{w}\right)^{-0.068} \left(\frac{s}{w}\right)^{0.094}$ $\eta = 4.058Re^{-0.145} \left(\frac{d}{w}\right)^{-0.045} \left(\frac{s}{w}\right)^{0.054}$ $Nu = [-0.0007y^{0.3} + 0.0007y^{0.2} - 0.0385y + 0.4777] Re^{(0.0002y^3 - 0.0021y^2 + 0.0047y + 0.5894)} Pr^{0.33}$ $f = (-0.0009y^{0.3} - 0.1015y^{0.2} + 1.0842y + 8.685) Re^{(-0.0004y^3 + 0.0015y^2 - 0.0165y - 0.4722)}$	

Table 12 (continued)



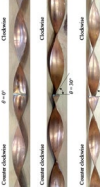
Author	Type of insert	Range of Reynolds number	Mass flow rate	Aspect ratio	Pitch ratio	Twist ratio	Volume fraction	Proposed correlations	Images
Eiamsa-Ard and Kiatkit-tipong [80]	Twisted tapes	5400–15,200				3	0.07–0.21%	$Nu = 0.103Re^{0.618}Pr^{0.4}(1+N)^{0.768}(1+\varphi)^{0.438}$ $f = 0.437Re^{-0.233}(1+N)^{1.25}(1+\varphi)^{0.268}$ $\eta = 3.597Re^{-0.178}(1+N)^{0.351}(1+\varphi)^{0.349}$ $Nu = 0.104Re^{0.618}Pr^{0.4}(1+N)^{0.789}(1+\varphi)^{0.439}$ $f = 0.468Re^{-0.234}(1+N)^{1.217}(1+\varphi)^{0.266}$ $\eta = 3.529Re^{-0.178}(1+N)^{0.384}(1+\varphi)^{0.349}$ $Nu = 0.096Re^{0.618}Pr^{0.4}(1+N)^{0.834}(1+\varphi)^{0.468}$ $f = 0.416Re^{-0.234}(1+N)^{1.221}(1+\varphi)^{0.262}$ $\eta = 3.401Re^{-0.178}(1+N)^{0.427}(1+\varphi)^{0.381}$ $Nu = \{0.0003y^3 - 0.0093y^2 + 0.0556y + 0.6194\}$ $Re\{-0.000004y^3 + 0.0002y^2 - 0.0001y + 0.546\}, Pr^{0.33}$ $f = \{0.0008y^3 - 0.0231y^2 - 0.1877y + 16.659\}$ $Re\{0.00004y^3 - 0.0012y^2 + 0.0108y - 0.5579\}$ $Re_c(x) = 1.46[Gr^*(x)]^{0.416}[\cos\theta]^{0.158}$	
Bhuiya et al. [81]	Twisted perforated tapes	7200–50,000						$Re_{qt}(x) = 19.4[Gr^*(x)]^{0.275}[\cos\theta]^{0.143}$ $j_L(x) = 6.52[Re(x)]^{-2.25}[Gr^*(x)]^{0.61}$ $j_R(x) = 2.37[Re(x)]^{-0.337}[Gr^*(x)]^{-0.168}[\cos\theta]^{-0.356}$ $j_T(x) = 1.57[Re(x)]^{-0.641}[\cos\theta]^{-0.102}$ $f_L = 10.6[Re_b]^{-0.849}[Gr_b^*]^{0.141}[\cos\theta]^{-0.176}$ $f_R = 5.77[Re_b]^{-0.252}[Gr_b^*]^{-0.0815}[\cos\theta]^{-0.214}$ $f_T = 11.6[Re_b]^{-0.517}[\cos\theta]^{-0.079}$	
Abolarin et al. [82]	Twisted tapes	300–11,404				5		$Re_{qt}(x) = 19.4[Gr^*(x)]^{0.275}[\cos\theta]^{0.143}$ $j_L(x) = 6.52[Re(x)]^{-2.25}[Gr^*(x)]^{0.61}$ $j_R(x) = 2.37[Re(x)]^{-0.337}[Gr^*(x)]^{-0.168}[\cos\theta]^{-0.356}$ $j_T(x) = 1.57[Re(x)]^{-0.641}[\cos\theta]^{-0.102}$ $f_L = 10.6[Re_b]^{-0.849}[Gr_b^*]^{0.141}[\cos\theta]^{-0.176}$ $f_R = 5.77[Re_b]^{-0.252}[Gr_b^*]^{-0.0815}[\cos\theta]^{-0.214}$ $f_T = 11.6[Re_b]^{-0.517}[\cos\theta]^{-0.079}$	

Table 12 (continued)



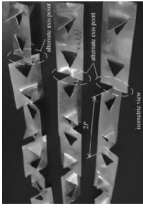
Author	Type of insert	Range of Reynolds number	Mass flow rate	Aspect ratio	Pitch ratio	Twist ratio	Volume fraction	Proposed correlations	Images
Murugesan et al. [83]	V-cut twisted tapes	2000–12,000	Cold water–0.166 kg/s Hot water–0.033 and 0.12 kg/s			2.0, 4.4 and 6.0		$Nu = 0.0296Re^{0.853}Pr^{0.33}\gamma^{-0.222}\left(1 + \left[\frac{d_c}{W}\right]\right)^{1.148}\left(1 + \left[\frac{w}{W}\right]\right)^{-0.751}$ $f = 8.632Re^{-0.615}\gamma^{-0.269}\left(1 + \left[\frac{d_c}{W}\right]\right)^{2.477}\left(1 + \left[\frac{w}{W}\right]\right)^{-1.914}$ $\eta = 1.392Re^{-0.01}\gamma^{-0.124}\left(1 + \left[\frac{d_c}{W}\right]\right)^{0.252}\left(1 + \left[\frac{w}{W}\right]\right)^{-0.058}$ $Nu_{PTT} = 0.027Re^{0.862}Pr^{0.33}\gamma^{-0.215}$	
Murugesan et al. [84]	Square-cut twisted tape	2000–12,000	Cold water–0.166 kg/s Hot water–0.033 and 0.12 kg/s			2.0, 4.4 and 6.0		$f_{PTT} = 2.642Re^{-0.474}\gamma^{-0.302}$ $Nu_{STT} = 0.027Re^{0.826}Pr^{0.33}\gamma^{-0.228}$ $f_{STT} = 2.642Re^{-0.579}\gamma^{-0.259}$ $Nu = 0.101Re^{0.733}Pr^{0.45}e_p^{-0.265}e_w^{0.287}$	
Eiamsa-ard and Promvongse [87]	Alternate axis tapes	4000–20,000			0.75–1.25			$f = 0.8988Re^{-0.094}e_p^{-0.516}e_w^{0.655}$ $\eta = 2.48Re^{-0.096}e_p^{-0.086}e_w^{0.064}$ $Nu = 0.112Re^{0.731}Pr^{0.4}e_p^{-0.283}e_w^{0.316}$ $f = 1.55Re^{-0.138}e_p^{-0.635}e_w^{0.759}$ $\eta = 2.666Re^{-0.099}e_p^{-0.078}e_w^{0.087}$ $Nu = 0.128Re^{0.723}Pr^{0.4}e_p^{-0.188}e_w^{0.318}$ $f = 1.09Re^{-0.098}e_p^{-0.198}e_w^{0.547}$ $\eta = 3.02Re^{-0.011}e_p^{-0.198}e_w^{0.135}$ $Nu = 0.139Re^{0.723}Pr^{0.4}e_p^{-0.198}e_w^{0.339}$ $f = 1.68Re^{-0.127}e_p^{-0.198}e_w^{0.636}$ $\eta = 2.98Re^{-0.107}e_p^{-0.198}e_w^{0.111}$	

Table 12 (continued)

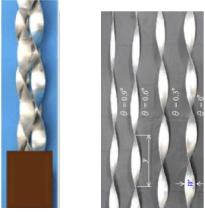






Author	Type of insert	Range of Reynolds number	Mass flow rate	Aspect ratio	Pitch ratio	Twist ratio	Volume fraction	Proposed correlations	Images
Lin et al. [88]	Twisted tapes	50–600				3.0–6.0		$Nu_m = 4.3543Re^{0.2245} \left(\frac{\alpha}{180}\right)^{0.2428} \left(\frac{S}{D}\right)^{-0.2219}$ $f = 47.0429Re^{-0.8528} \left(\frac{\alpha}{180}\right)^{0.2764} \left(\frac{S}{D}\right)^{-0.2018}$ $Nu = 0.2516Re^{0.6976} Pr^{0.4} R_p^{-0.1547} R_B^{0.1494}$ $f = 7.8086Re^{-0.2860} R_p^{-0.2648} R_B^{0.4171}$ $Nu = 0.076Re^{0.75} Pr^{0.4} \left(\frac{y}{W}\right)^{-0.39} (1 + \theta)^{-0.1}$ $f = 16.559Re^{-0.49} \left(\frac{y}{W}\right)^{-0.51} (1 + \theta)^{-0.53}$ $\eta = 1.871Re^{-0.04} \left(\frac{y}{W}\right)^{-0.22} (1 + \theta)^{0.08}$ $Nu = 0.198Re^{0.618} Pr^{0.4} \gamma \left(\frac{l}{L}\right)^{-0.0677} \left(\frac{SW}{W}\right)^{-0.0422}$ $f = 2.927Re^{-0.3857} \left(\frac{l}{L}\right)^{-0.1} \left(\frac{SW}{W}\right)^{-0.0148}$ $TPF = 1.636Re^{-0.0486} \left(\frac{l}{L}\right)^{-0.035} \left(\frac{SW}{W}\right)^{-0.0373}$ $Nu_{SRTTs} = 0.12634Re^{0.6469} Pr^{0.3421} Y^{-0.0923}$ $f_{SRTTs} = 11.6228Re^{-0.5112} Y^{-0.1919}$ $Nu = 0.3415Re^{0.591} \rho_{Pr}^{0.32} (0.9058c^3 + 0.5439c^2 - 1.345c + 1.271)$	
Promvonge [90]	V-finned twisted tapes	4000–30,000			4–16	4			
Piriyarungrod et al. [91]	Twisted tapes	6000–20,000			3.5–4.0				
Mushatet et al. [92]	Twisted tapes	10,000–40,000							
Zhang et al. [93]	Twisted tapes	12,000–45,000				2.2, 3, 4, and 6			
He et al. [94]	Twisted tapes	5600–18,000							
Reddy and Rao [96]	Helical coil inserts	4000–15,000			1 and 2.5		0.0004–0.02%	$f = 9.348Re^{-0.3959} (5.53c^3 + 2.578c^2 - 7.307c + 3.499)$ $Nu_{Reg} = 0.007523Re^{0.8} Pr^{0.5} \gamma (1 + f)^{7.6} \left(1 + \frac{P}{d}\right)^{0.037}$ $f_{Reg} = 0.3250Re^{-0.2377} (1 + f)^{2.723} \left(1 + \frac{P}{d}\right)^{0.041}$	

Table 12 (continued)

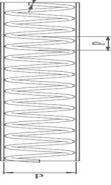
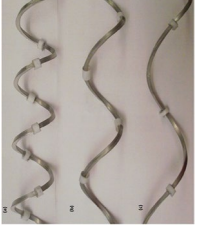
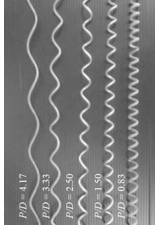
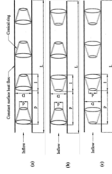
Author	Type of insert	Range of Reynolds number	Mass flow rate	Aspect ratio	Pitch ratio	Twist ratio	Volume fraction	Proposed correlations	Images
San et al. [97]	Coiled wire inserts	3718–17,157			1.304–2.319			$Nu = 0.00585(Re)^{0.51+6.16(\epsilon/d)-23.15(\epsilon/d)^2} [(e/d)^2 - 0.0042]^{-0.24} (p/d)^{-0.22}$ $Nu = 2.55(Re)^{0.57} (e/d)^{-0.17}(p/d)^{0.65} (p/d)^{-1.13}$ $f = 36.16Re^{-0.36}(e/d)[\ln(p/d)]^{-0.52}$ $Nu = 1.087Re^{0.569} \left(\frac{p}{d}\right)^{-0.330} \left(\frac{s}{d}\right)^{-0.152} Pr^{0.4}$	
Keklikcioglu and Ozceyhan [98]	Coiled wire inserts	3429–26,663			1–3			$f = 6.423Re^{-0.301} \left(\frac{p}{d}\right)^{-0.587} \left(\frac{s}{d}\right)^{-0.106}$ $Nu_{reg} = 1.65 \times 10^{-4} \left(1 + \frac{p}{100}\right)^{8.58} Re^{0.705} Pr^{2.64} \left(\frac{p}{D_c}\right)^{-0.411}$	
Abdul et al. [99]	Wire coil insert	2300–12,000			0.83–4.17		0.5–3.0%	$f_{reg} = 4.16 \left(1 + \frac{p}{100}\right)^{3.31} Re^{-0.269} \left(1 + \frac{p}{D_c}\right)^{-1.17}$ $Nu = 0.467Re^{0.636} Pr^{0.324} \left(\frac{p}{d}\right)^{-0.358} \left(\frac{\epsilon}{d}\right)^{0.448} \left(\frac{H_m}{H_m}\right)^{-0.14}$ $f = 198.7Re^{-0.708} \left(\frac{p}{d}\right)^{-0.943} \left(\frac{\epsilon}{d}\right)^{0.362} \left(\frac{H_m}{H_m}\right)^{0.58}$ $Nu = 0.1144Re^{0.6635} Pr^{0.4} \gamma (d/D)^{-1.128} (PR)^{-0.3214}$	
Saeednia et al. [100]	Coiled wire inserted	10–120	0.01–0.059 kg/s		1.79, 2.14 and 2.50		0.07, 0.15 and 0.3%	$f = 1.888Re^{-0.265} \gamma (d/D)^{-4.458} (PR)^{-0.784}$ $Nu = 0.3678Re^{0.544} Pr^{0.4} \gamma (d/D)^{-1.284} (PR)^{-0.3524}$ $f = 1.778Re^{-0.218} \gamma (d/D)^{-4.387} (PR)^{-0.8177}$ $Nu = 1.185Re^{0.472} Pr^{0.4} \gamma (d/D)^{-1.188} (PR)^{-0.4550}$ $f = 15.225Re^{-0.3935} (d/D)^{-4.425} (PR)^{-0.7335}$	
Ibrahim et al. [102]	Conical rings turbulators	6000–25,000			2, 3, and 4				

Table 12 (continued)

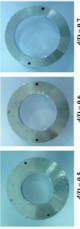
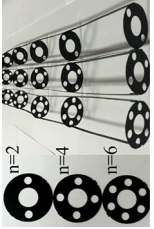
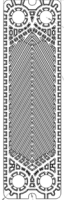
Author	Type of insert	Range of Reynolds number	Mass flow rate	Aspect ratio	Pitch ratio	Twist ratio	Volume fraction	Proposed correlations	Images
Kongkaitpaiboon et al. [103]	Circular ring turbulator	4000–20,000			6, 8 and 12			$Nu = 0.354Re^{0.697}Pr^{0.4}DR^{-0.555}PR^{-0.598}$	
Acir et al. [105]	Circular ring turbulators	3000–7500			2, 2.8, 3.5			$f = 0.715Re^{-0.081}DR^{-4.775}PR^{-0.846}$ $\eta = 5.315Re^{-0.078}DR^{1.031}PR^{-0.317}$ $Nu = 0.391Re^{0.637}\eta(PR)^{-0.461}(N)^{-0.208}$	
Nilpueng and Keawkam-rop [125]	Surface roughness	1200–3500						$f = 116.5Re^{-0.676}PR^{-0.321}N^{-0.432}$ $\eta = 86.282Re^{-0.443}PR^{-0.335}N^{-0.022}$ $Nu = 0.343Re^{0.604}\eta Pr^{0.33}\left(\frac{e}{D_H}\right)^{0.133}(\varepsilon/30)^{-1.327}$ $f = 1.98Re^{-0.237}\eta(e/D_H)^{0.168}(\varepsilon/30)^{-0.903}$	

Table 13 Comparison table for modified ducts

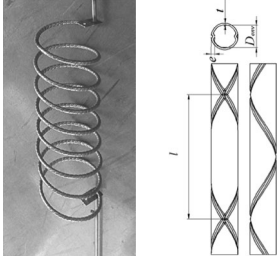

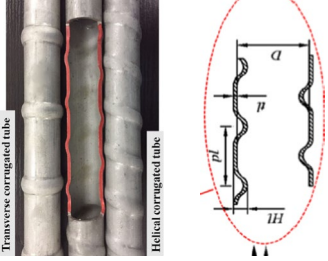
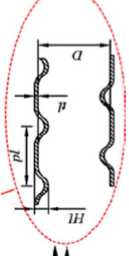

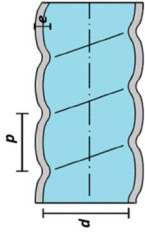
Authors	Type of modifications	Reynolds range	Other parameters	Correlations	Images
Raimieri et al. [149]	Corrugated helical duct	70–1200	Dean number—12–290 Curvature ratio—0.031, 0.040, and 0.056	For smooth duct $Nu = 1.168 \cdot De^{0.47} \cdot Pr^{0.16}$	
Bozzoli et al. [150]	Cross-helix corrugation	50–14,000	Prandtl number—5–150	For corrugated duct $Nu = 0.0191 \cdot De^{1.36} \cdot Pr^{0.2}$ For $Re < 600$ $Nu = 0.097 \cdot Re^{0.65} \cdot Pr^{0.4}$	
Wang et al. [151]	Outward corrugation	3800–43,800	Corrugation depth—0.6, 0.8, 1 mm Pitch—13 and 29 mm Height-to-diameter ratio—0.05, 0.10, 0.15	For $600 < Re < 14,000$ $Nu = 0.082 \cdot Re^{0.75} \cdot Pr^{0.4}$	
Wang et al. [152]	Inward corrugation	10,020–40,060	Pitch-to-diameter ratio—0.5, 1.0, 1.5 Height-to-diameter ratio—0.03, 0.05, 0.08	—	
Pethkool et al. [153]	Helically corrugated channel	5500–60,000	Pitch-to-diameter ratio—1.0, 1.5, 2.0 Pitch-to-diameter ratio—0.18, 0.22 and 0.27	$Nu = 1.579 Re^{0.639} Pr^{0.3} \left(\frac{e}{D_H}\right)^{0.46} \left(\frac{P}{D_H}\right)^{0.35}$	
Andrade et al. [154]	Corrugated duct	429–6212	Rib height-to-diameter ratio—0.02, 0.04 and 0.06 Pitch—6 and 12 mm	$f = 1.15 Re^{-0.239} \left(\frac{e}{D_H}\right)^{0.179} \left(\frac{P}{D_H}\right)^{0.164}$ $\eta = 39.419 Re^{-0.161} (e/D_H)^{0.375} (P/D_H)^{0.283}$	

Table 13 (continued)

Authors	Type of modifications	Reynolds range	Other parameters	Correlations	Images
Li et al. [155]	Helicallly corrugated pipes	20,000–175,000	Pumping rate—9 L/s	For 20,000 ≤ Re ≤ 175,000	
Xie et al. [158]	Internal protruded dimples	7500–27,500	Inner diameter—10.2, 13.9 mm Pitch—50 mm	$f = 108.575.12 Re^{0.29}$	
Li et al. [159]	Dimples	500–8000 for water	Pitch—10 mm	$Nu = 0.033Re^{0.82}Pr^{0.4}$	
Li et al. [160]	Dimples	150–2000 for Glycol–water 2300–15,000	Dia of dimple—5 mm Pitch—7, 10, 13 mm	$f = 5.3176Re^{-0.614}$ (500 < Re < 1300) $f = 0.0003Re^{0.7033}$ (1300 < Re < 3000) $f = 0.3486Re^{-0.18}$ (3000 < Re < 8000)	
Xie et al. [161]	Dimples and protrusions	5000–30,000	Depth, H—0.3–1.2 m Diameter, d—4, 5, 7 m Dimple shape—cone, sphere, ellipsoidal Extruded depth, D—2–5	—	
			Pitch, P—20 to 40 Radius—2 to 5		



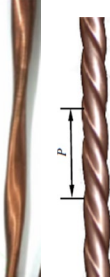
Table 13 (continued)

Authors	Type of modifications	Reynolds range	Other parameters	Correlations	Images
Xie et al. [162]	Cross-ellipsoidal dimples	5000–30,000	Dimple depth, $D=1, 1.7, 2$ mm	–	
Xie et al. [163]	Dimples	5000–30,000	Dimple pitch, $P=16, 20, 28$ mm	–	
			Axis ratio, $R=1, 2, 2.2$ mm		
			Depth, $D=2, 3, 3.5, 4$ mm		
Wang et al. [164]	Dimples	–	Pitch—14, 15, 16, 19 mm	$Nu_{a, Tube 2} = 0.671Re^{0.348}Pr^{\frac{1}{3}} (1500 < Re < 2000)$ $Nu_{a, Tube 2} = 0.098Re^{0.655}Pr^{\frac{1}{3}} (2000 < Re < 60,000)$ $Nu_{a, Tube 3} = 0.245Re^{0.571}Pr^{\frac{1}{3}} (1500 < Re < 60,000)$ $f_{a, Tube 2} = \frac{1}{(2.772Re^{0.293}-11.127)} (1500 < Re < 2000)$ $f_{a, Tube 2} = 0.432Re^{-0.221} (2000 < Re < 60,000)$ $f_{a, Tube 3} = 0.326Re^{-0.227} (1500 < Re < 60,000)$	  
			Radius, $R=3, 3.5, 4, 4.5$ mm		
			Flow rate—1 to 55 m ³ /h		
Wang et al. [164]	Dimples	–	Dimple height, $h=1.5, 2$ mm	–	

Table 13 (continued)

Authors	Type of modifications	Reynolds range	Other parameters	Correlations	Images
Kumar et al. [165]	Dimples	4000–28,000	Dimple depth—1 mm	-	
Du and Hong et al. [167]	Traverse ribs	5000–19,000	x/d_f —15–35 y/d_f —15–35 Pitch length ratios (P/D)—1.034, 1.379 and 1.724 spaced distance ratios (S/D)—5.690, 7.114, 9.483 and 14.224	$Nu = 0.0412Re^{0.86224}(P/D)^{-0.11395}(S/D)^{-0.17507}Pr^{0.4}$ $f = 39.17661Re^{-0.39561}(P/D)^{-1.07246}(S/D)^{-0.37832}$	
Du et al. [168]	Traverse corrugation	6000–18,000	p/e —8.75 to 5.625 S/D —0.60, 1.55, 2.97, 5.34, 10.09	For TCT $Nu = 0.0054Re^{0.98433}Pr^{0.4}$ $f = 0.83108Re^{-0.29443}$	
Hasanpour et al. [169]	Helical corrugation	5000–15,000	Twist ratios—3, 5, and 7; hole diameter ratio—0.11, 0.33; width and depth ratio—0.3 to 0.6	For DWC $Nu = 0.00968Re^{0.96541} \frac{S^{-0.04802}}{D} e^{-0.0006(\ln^2 \frac{S}{D})^2} e^{-0.00459(\ln^2 \frac{S}{D})^3} Pr^{0.4}$ $f = 4.98538Re^{-0.29227} S^{-0.13009} e^{-0.16155(\ln^2 \frac{S}{D})^2} e^{0.0312(\ln^2 \frac{S}{D})^3}$	
Moghaddam et al. [171]	Corrugated tube	5000–20,000	P/d —2, 3, 4, and 5 Roughness height, e —0.5, 1, 2, and 3 mm	For CWC $Nu = 0.00855Re^{0.97153}Pr^{0.4}$ $f = 4.1171Re^{-0.28596}$	
Yang et al. [175]	Corrugated tube	3000–10,000	Twisted ratio of y/w —42.5. $H = 1$ mm, $p = 50$ mm, $R = 6$ mm	For DCWC $Nu = 0.00928Re^{0.96644}Pr^{0.4}$ $f = 4.31743Re^{-0.29011}$	

Table 13 (continued)

Authors	Type of modifications	Reynolds range	Other parameters	Correlations	Images
Thianpong et al. [176]	Dimpled tube	12,000–44,000	Tape width (w)—22 mm	$Nu = 0.04Re^{0.76} (PR)^{-0.59} Pr^{0.3}$ $f = 2.69Re^{-0.35} (PR)^{-0.29}$ $Nu = 0.014Re^{0.9} (PR)^{-0.93} (y/w)^{-0.12} Pr^{0.3}$ $f = 9.1Re^{-0.37} (PR)^{-0.11} (y/w)^{-0.2}$	
Yang et al. [177]	Twisted elliptical tubes	600–55,000	Tape pitch length (y, 180°)—66, 110, and 154 mm Twist ratio (y/w)—3, 5, and 7 Dimpled outer tube diameter, (D)—22.2 mm Dimpled pitch length (p)—15.5 and 22.2 mm Pitch ratio, PR = p/D 0.7 and 1.0 Twist pitch, S (mm)—104, 152, 192	$Nu = 0.3496Re^{0.615} Pr^{\frac{1}{3}} \left(\frac{A_1}{B_1}\right)^{0.490} \left(\frac{S}{d_c}\right)^{-0.394}$ $f = 1.529Re^{-0.350} \left(\frac{A_1}{B_1}\right)^{1.686} \left(\frac{S}{d_c}\right)^{-0.366}$	
Tang et al. [180]	Twisted spiral tube	8000–21,000	Aspect ratio—1.49, 1.60, 1.76, 1.90, 2015	—	

heat transfer with respect to pressure loss is more beneficial in turbulent flow regime with higher Re .

Future direction

The literature review has identified several fields of interest that may be helpful for further study. The following can be the key points for future research work:

1. All of the researches discussed in the paper were focussed in laminar and turbulent flow regime, specifically avoiding the transitional flow regime. It is important to investigate the thermal transfer and flow behaviour in the transitional flow regime.
2. The literature reviewed in the present paper utilized single-passive techniques or a combination of two or more passive techniques, but none of them explored active and passive techniques altogether. This will become a future point of research.
3. A very few authors reported on entropy generation or irreversibility concept. This will provide the future direction for research, especially for the case of the modified duct.
4. Developing heat transfer fluid for special applications on heat transfer enhancement.

Conclusions

In this review paper, an effort has been made to review the recent development in the field of HTE i.e. active and passive techniques. A comprehensive work has been carried out to evaluate the performance of various augmentation methods in a tabular form, and a comparison is also made to estimate the best configuration in terms of thermal performance. Based upon the study, the following conclusions are drawn:

1. Using heat transfer augmentation techniques is quite advantageous in terms of heat transfer enhancement but it leads to increase in pumping power.
2. Heat transfer as well as friction factor depends upon working flow regimes, viz. laminar, transitional, and turbulent, and it helps in the estimation of the improvement in thermal performance.
3. An active technique also shows a significant enhancement in the performance of heat exchangers.
4. Use of passive augmentation techniques, i.e. vortex generators, artificial roughness, etc., changes flow pattern significantly that helps in the heat transfer augmentation. Understanding of fluid flow behaviour is very essential

and helps in the cause of the heat transfer augmentation that will further help in using compound techniques.

5. Duct geometry, viz. corrugated duct, square channel, twisted tubes, etc., plays a significant role in the thermo-hydraulic behaviour.
6. Altering the duct's surface using ribs, dimples, roughness, etc., shows the thermal performance enhancement of more than 200% when the results were compared with the plain channel. The modified duct may be combined with any other passive augmentation technique which will further lead to performance enhancement.

References

1. Pantzali MN, Kanaris AG, Antoniadis KD, Mouza AA, Paras SV. Effect of nanofluids on the performance of a miniature plate heat exchanger with modulated surface. *Int J Heat Fluid Flow*. 2009;30:691–9. <https://doi.org/10.1016/j.ijheatfluidflow.2009.02.005>.
2. Panchamgam SS, Chatterjee A, Plawsky JL, Wayner PC. Comprehensive experimental and theoretical study of fluid flow and heat transfer in a microscopic evaporating meniscus in a miniature heat exchanger. *Int J Heat Mass Transf*. 2008;51:5368–79. <https://doi.org/10.1016/j.ijheatmasstransfer.2008.03.023>.
3. Fazeli SA, Hosseini Hashemi SM, Zirakzadeh H, Ashjaee M. Experimental and numerical investigation of heat transfer in a miniature heat sink utilizing silica nanofluid. *Superlattices Microstruct*. 2012;51:247–64. <https://doi.org/10.1016/j.spmi.2011.11.017>.
4. Bahiraei M, Naghibzadeh SM, Jamshidmofid M. Efficacy of an eco-friendly nanofluid in a miniature heat exchanger regarding to arrangement of silver nanoparticles. *Energy Convers Manag*. 2017;144:224–34. <https://doi.org/10.1016/j.enconman.2017.04.076>.
5. Ozden A. Sizing and selection of heat exchanger at defined saving e investment ratio. *Appl Thermal Eng*. 2011;31(5):727–34. <https://doi.org/10.1016/j.applthermaleng.2010.10.013>.
6. Aghayari R, Maddah H, Pourkiaei SM, Ahmadi MH, Chen L, Ghazvini M. Theoretical and experimental studies of heat transfer in a double-pipe heat exchanger equipped with twisted tape and nanofluid. *Eur Phys J Plus*. 2020;135:252. <https://doi.org/10.1140/epjp/s13360-020-00252-8>.
7. Ahmadi MH, Ghazvini M, Sadeghzadeh M, Alhuyi Nazari M, Kumar R, Naeimi A, et al. Solar power technology for electricity generation: a critical review. *Energy Sci Eng*. 2018;6:340–61. <https://doi.org/10.1002/ese3.239>.
8. Pourkiaei SM, Ahmadi MH, Sadeghzadeh M, Moosavi S, Pourfayaz F, Chen L, et al. Thermoelectric cooler and thermoelectric generator devices: a review of present and potential applications, modeling and materials. *Energy*. 2019;186: 115849. <https://doi.org/10.1016/j.energy.2019.07.179>.
9. Mahesh J, Diksha RA, Amol B, Mayura M. Review on enhancement of heat transfer by active method. *Int J Curr Eng Technol*. 2016;6:221–5.
10. Wang CC. Heat transfer and friction characteristics of typical wavy fin-and-tube heat exchangers. *Expr Thermal Fluid Sci*. 1997;1777:174–86.
11. Bergles AE. Heat transfer and pressure drop correlations for the rectangular offset strip fin compact heat exchanger. *Expr Thermal Fluid Sci*. 1995;1777:171–80.

12. Joen CT, Jacobi A, De PM. Flow visualisation in inclined louvered fins. *Exp Therm Fluid Sci.* 2009;33:664–74. <https://doi.org/10.1016/j.expthermflusci.2009.01.003>.
13. Lyman AC, Stephan RA, Thole KA, Zhang LW, Memory SB. Scaling of heat transfer coefficients along louvered fins. *Exp Therm Fluid Sci.* 2002;26:547–63. [https://doi.org/10.1016/S0894-1777\(02\)00163-2](https://doi.org/10.1016/S0894-1777(02)00163-2).
14. Jabardo JMS. Experimental study of the air side performance of louver and wave fin-and-tube coils. *Exp Therm Fluid Sci.* 2006;30:621–31. <https://doi.org/10.1016/j.expthermflusci.2006.01.001>.
15. Cuevas C, Makaïre D, Dardenne L, Ngendakumana P. Thermo-hydraulic characterization of a louvered fin and flat tube heat exchanger. *Exp Therm Fluid Sci.* 2011;35:154–64. <https://doi.org/10.1016/j.expthermflusci.2010.08.015>.
16. DeJong NC, Jacobi AM. Flow, heat transfer, and pressure drop in the near-wall region of louvered-fin arrays. *Exp Therm Fluid Sci.* 2003;27:237–50. [https://doi.org/10.1016/S0894-1777\(02\)00224-8](https://doi.org/10.1016/S0894-1777(02)00224-8).
17. Oviedo-Tolentino F, Romero-Méndez R, Hernández-Guerrero A, Girón-Palomares B. Use of diverging or converging arrangement of plates for the control of chaotic mixing in symmetric sinusoidal plate channels. *Exp Therm Fluid Sci.* 2009;33:208–14. <https://doi.org/10.1016/j.expthermflusci.2008.08.002>.
18. Regele A, Kottke V. Taylor-goertler vortices. *Exp Therm Fluid Sci.* 1995;1777:270–5.
19. Rush TA, Newell TA, Jacobi AM. An experimental study of flow and heat transfer in sinusoidal wavy passages. *Int J Heat Mass Transf.* 1999;42:1541–53. [https://doi.org/10.1016/S0017-9310\(98\)00264-6](https://doi.org/10.1016/S0017-9310(98)00264-6).
20. Sarmadian A, Shafaei M, Mashouf H, Mohseni SG. Condensation heat transfer and pressure drop characteristics of R-600a in horizontal smooth and helically dimpled tubes. *Exp Therm Fluid Sci.* 2017;86:54–62. <https://doi.org/10.1016/j.expthermflusci.2017.04.001>.
21. Bhattacharyya S, Saha S, Saha SK. Laminar flow heat transfer enhancement in a circular tube having integral transverse rib roughness and fitted with centre-cleared twisted-tape. *Exp Therm Fluid Sci.* 2013;44:727–35. <https://doi.org/10.1016/j.expthermflusci.2012.09.016>.
22. Bhattacharyya S, Benim AC, Chattopadhyay H, Banerjee A. Experimental investigation of heat transfer performance of corrugated tube with spring tape inserts. *Exp Heat Transf.* 2019;32:411–25. <https://doi.org/10.1080/08916152.2018.1531955>.
23. Bhattacharyya S. Fluid flow and heat transfer in a heat exchanger channel with short-length twisted tape turbulator inserts. *Iran J Sci Technol - Trans Mech Eng.* 2020;44:217–27. <https://doi.org/10.1007/s40997-018-0251-0>.
24. Bhattacharyya S, Chattopadhyay H, Bandyopadhyay S. Numerical study on heat transfer enhancement through a circular duct fitted with centre-trimmed twisted tape. *Int J Heat Technol.* 2016;34:401–6. <https://doi.org/10.18280/ijht.340308>.
25. Bhattacharyya S, Chattopadhyay H, Haldar A. Design of twisted tape turbulator at different entrance angle for heat transfer enhancement in a solar heater. *Beni-Suef Univ J Basic Appl Sci.* 2018;7:118–26. <https://doi.org/10.1016/j.bjbas.2017.08.003>.
26. Lu H, Xu M, Gong L, Duan X, Chai JC. Effects of surface roughness in microchannel with passive heat transfer enhancement structures. *Int J Heat Mass Transf.* 2020;148: 119070. <https://doi.org/10.1016/j.ijheatmasstransfer.2019.119070>.
27. Wagner S, Shishkina O. Heat flux enhancement by regular surface roughness in turbulent thermal convection. *J Fluid Mech.* 2015;763:109–35. <https://doi.org/10.1017/jfm.2014.665>.
28. Zhang Q, Wang LB, Zhang YH. The mechanism of heat transfer enhancement using longitudinal vortex generators in a laminar channel flow with uniform wall temperature. *Int J Therm Sci.* 2017;117:26–43. <https://doi.org/10.1016/j.ijthermalsci.2017.03.003>.
29. Ramanathan S, Thansekhar MR, Kanna PR, Gunnasegaran P. A new method of acquiring prerequisites of recirculation and vortex flow in sudden expansion solar water collector using vortex generator to augment heat transfer. *Int J Therm Sci.* 2020;153: 106346. <https://doi.org/10.1016/j.ijthermalsci.2020.106346>.
30. da Silva FAS, Dezan DJ, Pantaleão AV, Salviano LO. Longitudinal vortex generator applied to heat transfer enhancement of a flat plate solar water heater. *Appl Therm Eng.* 2019;158: 113790. <https://doi.org/10.1016/j.applthermaleng.2019.113790>.
31. Naphon P, Wiriyasart S. Pulsating flow and magnetic field effects on the convective heat transfer of TiO₂-water nanofluids in helically corrugated tube. *Int J Heat Mass Transf.* 2018;125:1054–60. <https://doi.org/10.1016/j.ijheatmasstransfer.2018.05.015>.
32. Jafari M, Farhadi M, Sedighi K. Convection heat transfer of SWCNT-nanofluid in a corrugated channel under pulsating velocity profile. *Int Commun Heat Mass Transf.* 2015;67:137–46. <https://doi.org/10.1016/j.icheatmasstransfer.2015.07.008>.
33. Zimparov V. Enhancement of heat transfer by a combination of a single-start spirally corrugated tubes with a twisted tape. *Exp Therm Fluid Sci.* 2002;25:535–46. [https://doi.org/10.1016/S0894-1777\(01\)00112-1](https://doi.org/10.1016/S0894-1777(01)00112-1).
34. Léal L, Miscevic M, Lavieille P, Amokrane M, Pigache F, Topin F, et al. An overview of heat transfer enhancement methods and new perspectives: focus on active methods using electroactive materials. *Int J Heat Mass Transf.* 2013;61:505–24. <https://doi.org/10.1016/j.ijheatmasstransfer.2013.01.083>.
35. Sheikholeslami M, Chamkha AJ. Electrohydrodynamic free convection heat transfer of a nanofluid in a semi-annulus enclosure with a sinusoidal wall. *Numer Heat Transf Part A Appl.* 2016;69:781–93. <https://doi.org/10.1080/10407782.2015.1090819>.
36. Sathiyamoorthy M, Chamkha A. Effect of magnetic field on natural convection flow in a liquid gallium filled square cavity for linearly heated side wall(s). *Int J Therm Sci.* 2010;49:1856–65. <https://doi.org/10.1016/j.ijthermalsci.2010.04.014>.
37. Chamkha AJ, Mohamed RA, Ahmed SE. Unsteady MHD natural convection from a heated vertical porous plate in a micropolar fluid with Joule heating, chemical reaction and radiation effects. *Meccanica.* 2011;46:399–411. <https://doi.org/10.1007/s11012-010-9321-0>.
38. Chamkha AJ, Aly AM. MHD free convection flow of a nanofluid past a vertical plate in the presence of heat generation or absorption effects. *Chem Eng Commun.* 2011;198:425–41. <https://doi.org/10.1080/00986445.2010.520232>.
39. Dhanalakshmi NP, Nagarajan R, Sivagaminathan N, Prasad BVSS. Acoustic enhancement of heat transfer in furnace tubes. *Chem Eng Process Process Intensif.* 2012;59:36–42. <https://doi.org/10.1016/j.cep.2012.05.001>.
40. Staats WL, Brisson JG. Active heat transfer enhancement in air cooled heat sinks using integrated centrifugal fans. *Int J Heat Mass Transf.* 2015;82:189–205. <https://doi.org/10.1016/j.ijheatmasstransfer.2014.10.075>.
41. Shakouri Pour M, Esmailzadeh E. Experimental investigation of convective heat transfer enhancement from 3D-shape heat sources by EHD actuator in duct flow. *Exp Therm Fluid Sci.* 2011;35:1383–91. <https://doi.org/10.1016/j.expthermflusci.2011.05.006>.
42. Diao YH, Guo L, Liu Y, Zhao YH, Wang S. Electric field effect on the bubble behavior and enhanced heat-transfer characteristic of a surface with rectangular microgrooves. *Int J Heat Mass Transf.* 2014;78:371–9. <https://doi.org/10.1016/j.ijheatmasstransfer.2014.07.004>.

43. Moganlou FS, Khorrani AS, Esmaeilzadeh E, Aminfar H. Experimental study on electrohydrodynamically induced heat transfer enhancement in a minichannel. *Exp Therm Fluid Sci.* 2014;59:24–31. <https://doi.org/10.1016/j.expthermflusci.2014.07.019>.
44. Nasirivatan S, Kasaean A, Ghalamchi M, Ghalamchi M. Performance optimization of solar chimney power plant using electric/corona wind. *J Electrostat.* 2015;78:22–30. <https://doi.org/10.1016/j.elstat.2015.09.007>.
45. Ang KM, Yeo LY, Friend JR, Hung YM, Tan MK. Acoustically enhanced heat transport. *Rev Sci Instrum.* 2016;87:1–8. <https://doi.org/10.1063/1.4939757>.
46. Izadpanah E, Babaie Rabiee M, Sadeghi H, Talebi S. Effect of rotating and oscillating blade on the heat transfer enhancement of non-Newtonian fluid flow in a channel. *Appl Therm Eng.* 2017;113:1277–82. <https://doi.org/10.1016/j.applthermaleng.2016.11.124>.
47. Bezaatpour M, Goharkhah M. Convective heat transfer enhancement in a double pipe mini heat exchanger by magnetic field induced swirling flow. *Appl Therm Eng.* 2020;167: 114801. <https://doi.org/10.1016/j.applthermaleng.2019.114801>.
48. Ramadhan AA, Kapur N, Summers JL, Thompson HM. Numerical development of EHD cooling systems for laptop applications. *Appl Therm Eng.* 2018;139:144–56. <https://doi.org/10.1016/j.applthermaleng.2018.04.119>.
49. Bao SR, Zhang RP, Zhang YF, Tang Y, Zhang JH, Qiu LM. Enhancing the convective heat transfer in liquid oxygen using alternating magnetic fields. *Appl Therm Eng.* 2016;100:125–32. <https://doi.org/10.1016/j.applthermaleng.2016.01.088>.
50. Wang TH, Peng M, Wang XD, Yan WM. Investigation of heat transfer enhancement by electrohydrodynamics in a double-wall-heated channel. *Int J Heat Mass Transf.* 2017;113:373–83. <https://doi.org/10.1016/j.ijheatmasstransfer.2017.05.079>.
51. Alam T, Kim MH. A comprehensive review on single phase heat transfer enhancement techniques in heat exchanger applications. *Renew Sustain Energy Rev.* 2018;81:813–39. <https://doi.org/10.1016/j.rser.2017.08.060>.
52. Varun GMO, Nautiyal H, Khurana S, Shukla MK. Heat transfer augmentation using twisted tape inserts: a review. *Renew Sustain Energy Rev.* 2016;63:193–225. <https://doi.org/10.1016/j.rser.2016.04.051>.
53. Sheikholeslami M, Gorji-Bandpy M, Ganji DD. Review of heat transfer enhancement methods: focus on passive methods using swirl flow devices. *Renew Sustain Energy Rev.* 2015;49:444–69. <https://doi.org/10.1016/j.rser.2015.04.113>.
54. Zheng N, Yan F, Zhang K, Zhou T, Sun Z. A review on single-phase convective heat transfer enhancement based on multi-longitudinal vortices in heat exchanger tubes. *Appl Therm Eng.* 2020;164: 114475. <https://doi.org/10.1016/j.applthermaleng.2019.114475>.
55. Ahmadi MH, Mirlohi A, Alhuyi Nazari M, Ghasempour R. A review of thermal conductivity of various nanofluids. *J Mol Liq.* 2018;265:181–8. <https://doi.org/10.1016/j.molliq.2018.05.124>.
56. Lim KY, Hung YM, Tan BT. Performance evaluation of twisted-tape insert induced swirl flow in a laminar thermally developing heat exchanger. *Appl Therm Eng.* 2017;121:652–61. <https://doi.org/10.1016/j.applthermaleng.2017.04.134>.
57. Kumar A, Prasad BN. Investigation of twisted tape inserted solar water heaters - Heat transfer, friction factor and thermal performance results. *Renew Energy.* 2000;19:379–98. [https://doi.org/10.1016/S0960-1481\(99\)00061-0](https://doi.org/10.1016/S0960-1481(99)00061-0).
58. Ramadhan Al-Obaidi A, Chaer I. Study of the flow characteristics, pressure drop and augmentation of heat performance in a horizontal pipe with and without twisted tape inserts. *Case Stud Therm Eng.* 2021;25: 100964. <https://doi.org/10.1016/j.csite.2021.100964>.
59. Al-Obaidi AR. Analysis of the flow field, thermal performance, and heat transfer augmentation in circular tube using different dimple geometrical configurations with internal twisted-tape insert. *Heat Transf.* 2020;49:4153–72. <https://doi.org/10.1002/htj.21821>.
60. Al-Obaidi AR. Investigation of the flow, pressure drop characteristics, and augmentation of heat performance in a 3D flow pipe based on different inserts of twisted tape configurations. *Heat Transf.* 2021;50:5049–79. <https://doi.org/10.1002/htj.22115>.
61. Al-Obaidi AR, Sharif A. Investigation of the three-dimensional structure, pressure drop, and heat transfer characteristics of the thermohydraulic flow in a circular pipe with different twisted-tape geometrical configurations. *J Therm Anal Calorim.* 2021;143:3533–58. <https://doi.org/10.1007/s10973-019-09244-y>.
62. Sharifpur M, Solomon AB, Ottermann TL, Meyer JP. Optimum concentration of nanofluids for heat transfer enhancement under cavity flow natural convection with TiO₂ – Water. *Int Commun Heat Mass Transf.* 2018;98:297–303. <https://doi.org/10.1016/j.icheatmasstransfer.2018.09.010>.
63. Giwa SO, Sharifpur M, Goodarzi M, Alsulami H, Meyer JP. Influence of base fluid, temperature, and concentration on the thermophysical properties of hybrid nanofluids of alumina–ferrofluid: experimental data, modeling through enhanced ANN, ANFIS, and curve fitting. *J Therm Anal Calorim.* 2020. <https://doi.org/10.1007/s10973-020-09372-w>.
64. Giwa SO, Sharifpur M, Meyer JP. Effects of uniform magnetic induction on heat transfer performance of aqueous hybrid ferrofluid in a rectangular cavity. *Appl Therm Eng.* 2020;170: 115004. <https://doi.org/10.1016/j.applthermaleng.2020.115004>.
65. Mahdavi M, Garbadeen I, Sharifpur M, Ahmadi MH, Meyer JP. Study of particle migration and deposition in mixed convective pipe flow of nanofluids at different inclination angles. *J Therm Anal Calorim.* 2019;135:1563–75. <https://doi.org/10.1007/s10973-018-7720-y>.
66. Osman S, Sharifpur M, Meyer JP. Experimental investigation of convection heat transfer in the transition flow regime of aluminium oxide-water nanofluids in a rectangular channel. *Int J Heat Mass Transf.* 2019;133:895–902. <https://doi.org/10.1016/j.ijheatmasstransfer.2018.12.169>.
67. Mahdavi M, Sharifpur M, Meyer JP. Implementation of diffusion and electrostatic forces to produce a new slip velocity in the multiphase approach to nanofluids. *Powder Technol.* 2017. <https://doi.org/10.1016/j.powtec.2016.11.032>.
68. Ramezanizadeh M, Alhuyi Nazari M, Ahmadi MH, Wing CK. Experimental and numerical analysis of a nanofluidic thermosiphon heat exchanger. *Eng Appl Comput Fluid Mech.* 2019;13:40–7. <https://doi.org/10.1080/19942060.2018.1518272>.
69. Ahmadi MH, Ghazvini M, Maddah H, Kahani M, Pourfarhang S, Pourfarhang A, et al. Prediction of the pressure drop for CuO/(Ethylene glycol-water) nanofluid flows in the car radiator by means of Artificial Neural Networks analysis integrated with genetic algorithm. *Phys A Stat Mech Its Appl.* 2020;546: 124008. <https://doi.org/10.1016/j.physa.2019.124008>.
70. Sadeghzadeh M, Ahmadi MH, Kahani M, Sakhaeinia H, Chaji H, Chen L. Smart modeling by using artificial intelligent techniques on thermal performance of flat-plate solar collector using nanofluid. *Energy Sci Eng.* 2019;7:1649–58. <https://doi.org/10.1002/ese3.381>.
71. Ramezanizadeh M, Ahmadi MH, Nazari MA, Sadeghzadeh M, Chen L. A review on the utilized machine learning approaches for modeling the dynamic viscosity of nanofluids. *Renew Sustain Energy Rev.* 2019;114: 109345. <https://doi.org/10.1016/j.rser.2019.109345>.
72. Esmaeilzadeh E, Almohammadi H, Nokhosteen A, Motezaker A, Omrani AN. Study on heat transfer and friction factor characteristics of γ -Al₂O₃/water through circular tube with twisted tape

- inserts with different thicknesses. *Int J Therm Sci.* 2014;82:72–83. <https://doi.org/10.1016/j.ijthermalsci.2014.03.005>.
73. He W, Toghraie D, Lotfipour A, Pourfattah F, Karimpour A, Afrand M. Effect of twisted-tape inserts and nanofluid on flow field and heat transfer characteristics in a tube. *Int Commun Heat Mass Transf.* 2020. <https://doi.org/10.1016/j.icheatmasstransfer.2019.104440>.
 74. Azmi WH, Sharma KV, Sarma PK, Mamat R, Anuar S, Syam SL. Numerical validation of experimental heat transfer coefficient with SiO₂ nanofluid flowing in a tube with twisted tape inserts. *Appl Therm Eng.* 2014;73:296–306. <https://doi.org/10.1016/j.applthermaleng.2014.07.060>.
 75. Sundar LS, Singh MK, Punnaiah V, Sousa ACM. Experimental investigation of Al₂O₃/water nanofluids on the effectiveness of solar flat-plate collectors with and without twisted tape inserts. *Renew Energy.* 2018;119:820–33. <https://doi.org/10.1016/j.renene.2017.10.056>.
 76. Eiamsa-ard S, Promvong P. Enhancement of heat transfer in a tube with regularly-spaced helical tape swirl generators. *Sol Energy.* 2005;78:483–94. <https://doi.org/10.1016/j.solener.2004.09.021>.
 77. Ibrahim EZ. Augmentation of laminar flow and heat transfer in flat tubes by means of helical screw-tape inserts. *Energy Convers Manag.* 2011;52:250–7. <https://doi.org/10.1016/j.enconman.2010.06.065>.
 78. Nanan K, Thianpong C, Promvong P, Eiamsa-ard S. Investigation of heat transfer enhancement by perforated helical twisted-tapes. *Int Commun Heat Mass Transf.* 2014;52:106–12. <https://doi.org/10.1016/j.icheatmasstransfer.2014.01.018>.
 79. Bhuiya MMK, Sayem ASM, Islam M, Chowdhury MSU, Shahabuddin M. Performance assessment in a heat exchanger tube fitted with double counter twisted tape inserts. *Int Commun Heat Mass Transf.* 2014;50:25–33. <https://doi.org/10.1016/j.icheatmasstransfer.2013.11.005>.
 80. Eiamsa-ard S, Kiatkittipong K. Heat transfer enhancement by multiple twisted tape inserts and TiO₂/water nanofluid. *Appl Therm Eng.* 2014;70:896–924. <https://doi.org/10.1016/j.applthermaleng.2014.05.062>.
 81. Bhuiya MMK, Azad AK, Chowdhury MSU, Saha M. Heat transfer augmentation in a circular tube with perforated double counter twisted tape inserts. *Int Commun Heat Mass Transf.* 2016;74:18–26. <https://doi.org/10.1016/j.icheatmasstransfer.2016.03.001>.
 82. Abolarin SM, Everts M, Meyer JP. Heat transfer and pressure drop characteristics of alternating clockwise and counter clockwise twisted tape inserts in the transitional flow regime. *Int J Heat Mass Transf.* 2019;133:203–17. <https://doi.org/10.1016/j.ijheatmasstransfer.2018.12.107>.
 83. Murugesan P, Mayilsamy K, Suresh S, Srinivasan PSS. Heat transfer and pressure drop characteristics in a circular tube fitted with and without V-cut twisted tape insert. *Int Commun Heat Mass Transf.* 2011;38:329–34. <https://doi.org/10.1016/j.icheatmasstransfer.2010.11.010>.
 84. Murugesan P, Mayilsamy K, Suresh S. Turbulent heat transfer and pressure drop in tube fitted with square-cut twisted tape. *Chinese J Chem Eng.* 2010;18:609–17. [https://doi.org/10.1016/S1004-9541\(10\)60264-9](https://doi.org/10.1016/S1004-9541(10)60264-9).
 85. Abed AM, Sh Majdi H, Hussein Z, Fadhil D, Abdulkadhim A. Numerical analysis of flow and heat transfer enhancement in a horizontal pipe with P-TT and V-Cut twisted tape. *Case Stud Therm Eng.* 2018;12:749–58. <https://doi.org/10.1016/j.csite.2018.10.004>.
 86. Chu WX, Tsai CA, Lee BH, Cheng KY, Wang CC. Experimental investigation on heat transfer enhancement with twisted tape having various V-cut configurations. *Appl Therm Eng.* 2020;172:115148. <https://doi.org/10.1016/j.applthermaleng.2020.115148>.
 87. Eiamsa-ard S, Promvong P. Influence of double-sided delta-wing tape insert with alternate-axes on flow and heat transfer characteristics in a heat exchanger tube. *Chinese J Chem Eng.* 2011;19:410–23. [https://doi.org/10.1016/S1004-9541\(11\)60001-3](https://doi.org/10.1016/S1004-9541(11)60001-3).
 88. Lin ZM, Wang LB, Lin M, Dang W, Zhang YH. Numerical study of the laminar flow and heat transfer characteristics in a tube inserting a twisted tape having parallelogram winglet vortex generators. *Appl Therm Eng.* 2017;115:644–58. <https://doi.org/10.1016/j.applthermaleng.2016.12.142>.
 89. Promvong P, Suwannapan S, Pimsarn M, Thianpong C. Experimental study on heat transfer in square duct with combined twisted-tape and winglet vortex generators. *Int Commun Heat Mass Transf.* 2014;59:158–65. <https://doi.org/10.1016/j.icheatmasstransfer.2014.10.005>.
 90. Promvong P. Thermal performance in square-duct heat exchanger with quadruple V-finned twisted tapes. *Appl Therm Eng.* 2015;91:298–307. <https://doi.org/10.1016/j.applthermaleng.2015.08.047>.
 91. Piriyaarungrod N, Eiamsa-ard S, Thianpong C, Pimsarn M, Nanan K. Heat transfer enhancement by tapered twisted tape inserts. *Chem Eng Process Process Intensif.* 2015;96:62–71. <https://doi.org/10.1016/j.ccep.2015.08.002>.
 92. Mushatet KS, Rishak QA, Fagr MH. Experimental and numerical investigation of swirling turbulent flow and heat transfer due to insertion of twisted tapes of new models in a heated tube. *Appl Therm Eng.* 2020;171:115070. <https://doi.org/10.1016/j.applthermaleng.2020.115070>.
 93. Zhang S, Lu L, Dong C, Cha SH. Performance evaluation of a double-pipe heat exchanger fitted with self-rotating twisted tapes. *Appl Therm Eng.* 2019;158:113770. <https://doi.org/10.1016/j.applthermaleng.2019.113770>.
 94. He Y, Liu L, Li P, Ma L. Experimental study on heat transfer enhancement characteristics of tube with cross hollow twisted tape inserts. *Appl Therm Eng.* 2018;131:743–9. <https://doi.org/10.1016/j.applthermaleng.2017.12.029>.
 95. Sharifi K, Sabeti M, Rafiei M, Mohammadi AH, Shirazi L. Computational fluid dynamics (CFD) technique to study the effects of helical wire inserts on heat transfer and pressure drop in a double pipe heat exchanger. *Appl Therm Eng.* 2018;128:898–910. <https://doi.org/10.1016/j.applthermaleng.2017.08.146>.
 96. Chandra Sekhara Reddy M, Vasudeva Rao V. Experimental investigation of heat transfer coefficient and friction factor of ethylene glycol water based TiO₂ nanofluid in double pipe heat exchanger with and without helical coil inserts. *Int Commun Heat Mass Transf.* 2014;50:68–76. <https://doi.org/10.1016/j.icheatmasstransfer.2013.11.002>.
 97. San JY, Huang WC, Chen CA. Experimental investigation on heat transfer and fluid friction correlations for circular tubes with coiled-wire inserts. *Int Commun Heat Mass Transf.* 2015;65:8–14. <https://doi.org/10.1016/j.icheatmasstransfer.2015.04.008>.
 98. Keklikcioglu O, Ozceyhan V. Experimental investigation on heat transfer enhancement of a tube with coiled-wire inserts installed with a separation from the tube wall. *Int Commun Heat Mass Transf.* 2016;78:88–94. <https://doi.org/10.1016/j.icheatmasstransfer.2016.08.024>.
 99. Abdul Hamid K, Azmi WH, Mamat R, Sharma KV. Heat transfer performance of TiO₂-SiO₂ nanofluids in a tube with wire coil inserts. *Appl Therm Eng.* 2019;152:275–86. <https://doi.org/10.1016/j.applthermaleng.2019.02.083>.
 100. Saeedinia M, Akhavan-Behabadi MA, Nasr M. Experimental study on heat transfer and pressure drop of nanofluid flow in a horizontal coiled wire inserted tube under constant heat flux. *Exp Therm Fluid Sci.* 2012;36:158–68. <https://doi.org/10.1016/j.expthermflusci.2011.09.009>.

101. Anvari AR, Javaherdeh K, Emami-Meibodi M, Rashidi AM. Numerical and experimental investigation of heat transfer behavior in a round tube with the special conical ring inserts. *Energy Convers Manag.* 2014;88:214–7. <https://doi.org/10.1016/j.enconman.2014.08.030>.
102. Ibrahim MM, Essa MA, Mostafa NH. A computational study of heat transfer analysis for a circular tube with conical ring turbulators. *Int J Therm Sci.* 2019;137:138–60. <https://doi.org/10.1016/j.ijthermalsci.2018.10.028>.
103. Kongkai-paiboon V, Nanan K, Eiamsa-ard S. Experimental investigation of convective heat transfer and pressure loss in a round tube fitted with circular-ring turbulators. *Int Commun Heat Mass Transf.* 2010;37:568–74. <https://doi.org/10.1016/j.icheatmasstransfer.2009.12.016>.
104. Sheikholeslami M, Gorji-Bandpy M, Ganji DD. Experimental study on turbulent flow and heat transfer in an air to water heat exchanger using perforated circular-ring. *Exp Therm Fluid Sci.* 2016;70:185–95. <https://doi.org/10.1016/j.expthermflusci.2015.09.002>.
105. Acir A, Ata I, Canli ME. Investigation of effect of the circular ring turbulators on heat transfer augmentation and fluid flow characteristic of solar air heater. *Exp Therm Fluid Sci.* 2016;77:45–54. <https://doi.org/10.1016/j.expthermflusci.2016.04.012>.
106. Fiebig M, Kallweit P, Mitra N, Tiggelbeck S. Heat transfer enhancement and drag by longitudinal vortex generators in channel flow. *Exp Therm Fluid Sci.* 1991;4:103–14. [https://doi.org/10.1016/0894-1777\(91\)90024-L](https://doi.org/10.1016/0894-1777(91)90024-L).
107. Fiebig M. Embedded vortices in internal flow: heat transfer and pressure loss enhancement. *Int J Heat Fluid Flow.* 1995;16:376–88. [https://doi.org/10.1016/0142-727X\(95\)00043-P](https://doi.org/10.1016/0142-727X(95)00043-P).
108. Gentry MC, Jacobi AM. Heat transfer enhancement by delta-wing vortex generators on a flat plate: vortex interactions with the boundary layer. *Exp Therm Fluid Sci.* 1997;14:231–42. [https://doi.org/10.1016/S0894-1777\(96\)00067-2](https://doi.org/10.1016/S0894-1777(96)00067-2).
109. Xu Y, Islam MD, Kharoua N. Experimental study of thermal performance and flow behaviour with winglet vortex generators in a circular tube. *Appl Therm Eng.* 2018;135:257–68. <https://doi.org/10.1016/j.applthermaleng.2018.01.112>.
110. Wu JM, Tao WQ. Numerical study on laminar convection heat transfer in a rectangular channel with longitudinal vortex generator. part a: verification of field synergy principle. *Int J Heat Mass Transf.* 2008;51:1179–91. <https://doi.org/10.1016/j.ijheatmasstransfer.2007.03.032>.
111. Wu JM, Tao WQ. Numerical study on laminar convection heat transfer in a channel with longitudinal vortex generator. part b: parametric study of major influence factors. *Int J Heat Mass Transf.* 2008;51:3683–92. <https://doi.org/10.1016/j.ijheatmasstransfer.2007.03.031>.
112. Sinha A, Ashoke Raman K, Chattopadhyay H, Biswas G. Effects of different orientations of winglet arrays on the performance of plate-fin heat exchangers. *Int J Heat Mass Transf.* 2013;57:202–14. <https://doi.org/10.1016/j.ijheatmasstransfer.2012.10.034>.
113. Lemouedda A, Breuer M, Franz E, Botsch T, Delgado A. Optimization of the angle of attack of delta-winglet vortex generators in a plate-fin-and-tube heat exchanger. *Int J Heat Mass Transf.* 2010;53:5386–99. <https://doi.org/10.1016/j.ijheatmasstransfer.2010.07.017>.
114. Oneissi M, Habchi C, Russeil S, Bougeard D, Lemenand T. Novel design of delta winglet pair vortex generator for heat transfer enhancement. *Int J Therm Sci.* 2016;109:1–9. <https://doi.org/10.1016/j.ijthermalsci.2016.05.025>.
115. Min C, Qi C, Wang E, Tian L, Qin Y. Numerical investigation of turbulent flow and heat transfer in a channel with novel longitudinal vortex generators. *Int J Heat Mass Transf.* 2012;55:7268–77. <https://doi.org/10.1016/j.ijheatmasstransfer.2012.07.055>.
116. Gupta A, Roy A, Gupta S, Gupta M. Numerical investigation towards implementation of punched winglet as vortex generator for performance improvement of a fin-and-tube heat exchanger. *Int J Heat Mass Transf.* 2020;149: 119171. <https://doi.org/10.1016/j.ijheatmasstransfer.2019.119171>.
117. Ahmed HE, Mohammed HA, Yusoff MZ. Heat transfer enhancement of laminar nanofluids flow in a triangular duct using vortex generator. *Superlattices Microstruct.* 2012;52:398–415. <https://doi.org/10.1016/j.spmi.2012.05.023>.
118. Xu Z, Han Z, Wang J, Liu Z. The characteristics of heat transfer and flow resistance in a rectangular channel with vortex generators. *Int J Heat Mass Transf.* 2018;116:61–72. <https://doi.org/10.1016/j.ijheatmasstransfer.2017.08.083>.
119. Ali S, Habchi C, Menanteau S, Lemenand T, Harion JL. Three-dimensional numerical study of heat transfer and mixing enhancement in a circular pipe using self-sustained oscillating flexible vorticity generators. *Chem Eng Sci.* 2017;162:152–74. <https://doi.org/10.1016/j.ces.2016.12.039>.
120. Zhou G, Ye Q. Experimental investigations of thermal and flow characteristics of curved trapezoidal winglet type vortex generators. *Appl Therm Eng.* 2012;37:241–8. <https://doi.org/10.1016/j.applthermaleng.2011.11.024>.
121. Zhou G, Feng Z. Experimental investigations of heat transfer enhancement by plane and curved winglet type vortex generators with punched holes. *Int J Therm Sci.* 2014;78:26–35. <https://doi.org/10.1016/j.ijthermalsci.2013.11.010>.
122. Chamoli S, Lu R, Yu P. Thermal characteristic of a turbulent flow through a circular tube fitted with perforated vortex generator inserts. *Appl Therm Eng.* 2017;121:1117–34. <https://doi.org/10.1016/j.applthermaleng.2017.03.145>.
123. Promvong P, Skullong S. Thermo-hydraulic performance in heat exchanger tube with V-shaped winglet vortex generator. *Appl Therm Eng.* 2020;164: 114424. <https://doi.org/10.1016/j.applthermaleng.2019.114424>.
124. Katoh K, Choi KS, Azuma T. Heat-transfer enhancement and pressure loss by surface roughness in turbulent channel flows. *Int J Heat Mass Transf.* 2000;43:4009–17. [https://doi.org/10.1016/S0017-9310\(00\)00033-8](https://doi.org/10.1016/S0017-9310(00)00033-8).
125. Nilpueng K, Keawkamrop T, Ahn HS, Wongwises S. Effect of chevron angle and surface roughness on thermal performance of single-phase water flow inside a plate heat exchanger. *Int Commun Heat Mass Transf.* 2018;91:201–9. <https://doi.org/10.1016/j.icheatmasstransfer.2017.12.009>.
126. Alammar AA, Al-Mousawi FN, Al-Dadah RK, Mahmoud SM, Hood R. Enhancing thermal performance of a two-phase closed thermosyphon with an internal surface roughness. *J Clean Prod.* 2018;185:128–36. <https://doi.org/10.1016/j.jclepro.2018.03.020>.
127. Sagar P, Teotia P, Sahlot AD, Thakur HC. Heat transfer analysis and optimization of engine fins of varying surface roughness. *Mater Today Proc.* 2017;4:8565–70. <https://doi.org/10.1016/j.matpr.2017.07.203>.
128. Zhang YZ, Sun C, Bao Y, Zhou Q. How surface roughness reduces heat transport for small roughness heights in turbulent Rayleigh-Bénard convection. *J Fluid Mech.* 2018. <https://doi.org/10.1017/jfm.2017.786>.
129. Ting K, Mozumder AK, Das PK. Effect of surface roughness on heat transfer and entropy generation of mixed convection in nanofluid. *Phys Fluids.* 2019. <https://doi.org/10.1063/1.5111104>.
130. Patil PM, Shashikant A, Hiremath PS. Influence of liquid hydrogen and nitrogen on MHD triple diffusive mixed convection nanoliquid flow in presence of surface roughness. *Int J Hydrogen Energy.* 2018;43:20101–17. <https://doi.org/10.1016/j.ijhydene.2018.09.033>.
131. Patil PM, Kulkarni M, Hiremath PS. Effects of surface roughness on mixed convective nanofluid flow past an exponentially

- stretching permeable surface. *Chinese J Phys.* 2020;64:203–18. <https://doi.org/10.1016/j.cjph.2019.12.006>.
132. Patil PM, Doddagoudar SH, Hiremath PS, Momoniati E. Influence of applied magnetic field on mixed convective nanofluid flow past an exponentially stretching surface with roughness. *J Brazilian Soc Mech Sci Eng.* 2019;41:1–11. <https://doi.org/10.1007/s40430-019-2065-4>.
 133. Kumar K, Prajapati DR, Samir S. Heat transfer and friction factor correlations development for solar air heater duct artificially roughened with ‘S’ shape ribs. *Exp Therm Fluid Sci.* 2017;82:249–61. <https://doi.org/10.1016/j.expthermflusc.2016.11.012>.
 134. Das B, Mondol JD, Debnath S, Pugsley A, Smyth M, Zacharopoulos A. Effect of the absorber surface roughness on the performance of a solar air collector: an experimental investigation. *Renew Energy.* 2020;152:567–78. <https://doi.org/10.1016/j.renene.2020.01.056>.
 135. Bharadwaj G, Varun KR, Sharma A. Heat transfer augmentation and flow characteristics in ribbed triangular duct solar air heater an experimental analysis. *Int J Green Energy.* 2017;14:587–98. <https://doi.org/10.1080/15435075.2017.1307751>.
 136. Prakash C, Saini RP. Heat transfer and friction in rectangular solar air heater duct having spherical and inclined rib protrusions as roughness on absorber plate. *Exp Heat Transf.* 2019;32:469–87. <https://doi.org/10.1080/08916152.2018.1543367>.
 137. Maitihani R, Kumar A, Gholamali Zadeh P, Safaei MR, Gholamalizadeh E. Empirical correlations development for heat transfer and friction factor of a solar rectangular air passage with spherical-shaped turbulence promoters. *J Therm Anal Calorim.* 2020;139:1195–212. <https://doi.org/10.1007/s10973-019-08551-8>.
 138. Sethi M, Varun TNS. Correlations for solar air heater duct with dimpled shape roughness elements on absorber plate. *Sol Energy.* 2012;86:2852–61. <https://doi.org/10.1016/j.solener.2012.06.024>.
 139. Yadav S, Kaushal M, Siddhartha V. Nusselt number and friction factor correlations for solar air heater duct having protrusions as roughness elements on absorber plate. *Exp Therm Fluid Sci.* 2013;44:34–41. <https://doi.org/10.1016/j.expthermflusc.2012.05.011>.
 140. Ghritlahre HK, Sahu PK, Chand S. Thermal performance and heat transfer analysis of arc shaped roughened solar air heater – an experimental study. *Sol Energy.* 2020;199:173–82. <https://doi.org/10.1016/j.solener.2020.01.068>.
 141. Gill RS, Hans VS, Saini JS, Singh S. Investigation on performance enhancement due to staggered piece in a broken arc rib roughened solar air heater duct. *Renew Energy.* 2017;104:148–62. <https://doi.org/10.1016/j.renene.2016.12.002>.
 142. Jain SK, Das AG, Misra R. Experimental investigation of thermo-hydraulic performance of the solar air heater having arc-shaped ribs with multiple gaps. *J Therm Sci Eng Appl.* 2020;12:1–10. <https://doi.org/10.1115/1.4044427>.
 143. Kumar R, Goel V, Kumar M. Effect of providing gap in multiple-arc rib-roughened solar air heater - part 1. *J Mech Sci Technol.* 2020;34:2619–25. <https://doi.org/10.1007/s12206-020-0535-3>.
 144. Al-Obaidi AR, Alhamid J. Numerical investigation of fluid flow, characteristics of thermal performance and enhancement of heat transfer of corrugated pipes with various configurations. *J Phys Conf Ser.* 2021. <https://doi.org/10.1088/1742-6596/1733/1/012004>.
 145. Alhamid J, Al-Obaidi RA. Flow pattern investigation and thermo-hydraulic performance enhancement in three-dimensional circular pipe under varying corrugation configurations. *J Phys Conf Ser.* 2021. <https://doi.org/10.1088/1742-6596/1845/1/012061>.
 146. Al-Obaidi AR. Investigation of fluid field analysis, characteristics of pressure drop and improvement of heat transfer in three-dimensional circular corrugated pipes. *J Energy Storage.* 2019;26: 101012. <https://doi.org/10.1016/j.est.2019.101012>.
 147. Al-Obaidi AR. Investigation on effects of varying geometrical configurations on thermal hydraulics flow in a 3D corrugated pipe. *Int J Therm Sci.* 2022;171: 107237. <https://doi.org/10.1016/j.ijthermalsci.2021.107237>.
 148. Al-Obaidi AR, Alhamid J. Investigation of flow pattern, thermo-hydraulic performance and heat transfer improvement in 3D corrugated circular pipe under varying structure configuration parameters with development different correlations. *Int Commun Heat Mass Transf.* 2021;126: 105394. <https://doi.org/10.1016/j.icheatmasstransfer.2021.105394>.
 149. Rainieri S, Bozzoli F, Cattani L, Pagliarini G. Compound convective heat transfer enhancement in helically coiled wall corrugated tubes. *Int J Heat Mass Transf.* 2013;59:353–62. <https://doi.org/10.1016/j.ijheatmasstransfer.2012.12.037>.
 150. Bozzoli F, Cattani L, Rainieri S. Cross-helix corrugation: the optimal geometry for effective food thermal processing. *Int J Heat Mass Transf.* 2020;147: 118874. <https://doi.org/10.1016/j.ijheatmasstransfer.2019.118874>.
 151. Wang W, Zhang Y, Li B, Li Y. Numerical investigation of tube-side fully developed turbulent flow and heat transfer in outward corrugated tubes. *Int J Heat Mass Transf.* 2018;116:115–26. <https://doi.org/10.1016/j.ijheatmasstransfer.2017.09.003>.
 152. Wang W, Zhang Y, Li Y, Han H, Li B. Numerical study on fully-developed turbulent flow and heat transfer in inward corrugated tubes with double-objective optimization. *Int J Heat Mass Transf.* 2018;120:782–92. <https://doi.org/10.1016/j.ijheatmasstransfer.2017.12.079>.
 153. Pethkool S, Eiamsa-ard S, Kwankaomeng S, Promvong P. Turbulent heat transfer enhancement in a heat exchanger using helically corrugated tube. *Int Commun Heat Mass Transf.* 2011;38:340–7. <https://doi.org/10.1016/j.icheatmasstransfer.2010.11.014>.
 154. Andrade F, Moita AS, Nikulin A, Moreira ALN, Santos H. Experimental investigation on heat transfer and pressure drop of internal flow in corrugated tubes. *Int J Heat Mass Transf.* 2019;140:940–55. <https://doi.org/10.1016/j.ijheatmasstransfer.2019.06.025>.
 155. Li Y, Wu S, Jin T. Experimental investigation on pressure drop and friction factor of slush nitrogen turbulent flow in helically corrugated pipes. *Cryogenics (Guildf).* 2018;94:56–61. <https://doi.org/10.1016/j.cryogenics.2018.07.007>.
 156. Al-Obaidi AR. Study the influence of concavity shapes on augmentation of heat-transfer performance, pressure field, and fluid pattern in three-dimensional pipe. *Heat Transf.* 2021;50:4354–81. <https://doi.org/10.1002/htj.22079>.
 157. Alhamid J, Al-Obaidi AR. Effect of concavity configuration parameters on hydrodynamic and thermal performance in 3D circular pipe using Al₂O₃ nanofluid based on CFD simulation. *J Phys Conf Ser.* 2021;1845:012060. <https://doi.org/10.1088/1742-6596/1845/1/012060>.
 158. Xie G, Liu J, Ligrani PM, Zhang W. Numerical analysis of flow structure and heat transfer characteristics in square channels with different internal-protruded dimple geometrics. *Int J Heat Mass Transf.* 2013;67:81–97. <https://doi.org/10.1016/j.ijheatmasstransfer.2013.07.094>.
 159. Li M, Khan TS, Al-Hajri E, Ayub ZH. Single phase heat transfer and pressure drop analysis of a dimpled enhanced tube. *Appl Therm Eng.* 2016;101:38–46. <https://doi.org/10.1016/j.applthermaleng.2016.03.042>.
 160. Li M, Khan TS, Al-Hajri E, Ayub ZH. Geometric optimization for thermal-hydraulic performance of dimpled enhanced tubes for single phase flow. *Appl Therm Eng.* 2016;103:639–50. <https://doi.org/10.1016/j.applthermaleng.2016.04.141>.

161. Xie S, Liang Z, Zhang L, Wang Y, Ding H, Zhang J. Numerical investigation on heat transfer performance and flow characteristics in enhanced tube with dimples and protrusions. *Int J Heat Mass Transf.* 2018;122:602–13. <https://doi.org/10.1016/j.ijheatmasstransfer.2018.01.106>.
162. Xie S, Liang Z, Zhang L, Wang Y. A numerical study on heat transfer enhancement and flow structure in enhanced tube with cross ellipsoidal dimples. *Int J Heat Mass Transf.* 2018;125:434–44. <https://doi.org/10.1016/j.ijheatmasstransfer.2018.04.106>.
163. Xie S, Liang Z, Zhang J, Zhang L, Wang Y, Ding H. Numerical investigation on flow and heat transfer in dimpled tube with tear-drop dimples. *Int J Heat Mass Transf.* 2019;131:713–23. <https://doi.org/10.1016/j.ijheatmasstransfer.2018.11.112>.
164. Wang Y, He YL, Lei YG, Zhang J. Heat transfer and hydrodynamics analysis of a novel dimpled tube. *Exp Therm Fluid Sci.* 2010;34:1273–81. <https://doi.org/10.1016/j.expthermflusci.2010.05.008>.
165. Kumar A, Maithani R, Suri ARS. Numerical and experimental investigation of enhancement of heat transfer in dimpled rib heat exchanger tube. *Heat Mass Transf Und Stoffuebertragung.* 2017;53:3501–16. <https://doi.org/10.1007/s00231-017-2080-x>.
166. Chen J, Müller-Steinhagen H, Duffy GG. Heat transfer enhancement in dimpled tubes. *Appl Therm Eng.* 2001;21:535–47. [https://doi.org/10.1016/S1359-4311\(00\)00067-3](https://doi.org/10.1016/S1359-4311(00)00067-3).
167. Du J, Hong Y. Experimental investigation on thermal-hydraulic characteristics in a traverse rib tube fitted with regularly spaced helical tapes. *Int J Heat Mass Transf.* 2020;154:119726. <https://doi.org/10.1016/j.ijheatmasstransfer.2020.119726>.
168. Du J, Hong Y, Wang S, Ye WB, Huang SM. Experimental thermal and flow characteristics in a traverse corrugated tube fitted with regularly spaced modified wire coils. *Int J Therm Sci.* 2018;133:330–40. <https://doi.org/10.1016/j.ijthermalsci.2018.05.032>.
169. Hasanpour A, Farhadi M, Sedighi K. Experimental heat transfer and pressure drop study on typical, perforated, V-cut and U-cut twisted tapes in a helically corrugated heat exchanger. *Int Commun Heat Mass Transf.* 2016;71:126–36. <https://doi.org/10.1016/j.icheatmasstransfer.2015.12.032>.
170. Nasr MRJ, Khalaj AH. Heat transfer coefficient and friction factor prediction of corrugated tubes combined with twisted tape inserts using artificial neural network. *Heat Transf Eng.* 2010;31:59–69. <https://doi.org/10.1080/01457630903263440>.
171. Kazemi Moghadam H, Mousavi Ajarostaghi SS, Poncet S. Extensive numerical analysis of the thermal performance of a corrugated tube with coiled wire. *J Therm Anal Calorim.* 2020;140:1469–81. <https://doi.org/10.1007/s10973-019-08876-4>.
172. Saha SK. Thermohydraulics of laminar flow through rectangular and square ducts with axial corrugation roughness and twisted tapes with oblique teeth. *J Heat Transfer.* 2010;132:1–12. <https://doi.org/10.1115/1.4001313>.
173. Saha SK, Swain BN, Dayanidhi GL. Friction and thermal characteristics of laminar flow of viscous oil through a circular tube having axial corrugations and fitted with helical screw-tape inserts. *J Fluids Eng Trans ASME.* 2012;134:1–9. <https://doi.org/10.1115/1.4006669>.
174. Mokkalapati V, Sen LC. Numerical study of an exhaust heat recovery system using corrugated tube heat exchanger with twisted tape inserts. *Int Commun Heat Mass Transf.* 2014;57:53–64. <https://doi.org/10.1016/j.icheatmasstransfer.2014.07.002>.
175. Yang L, Han H, Li Y, Li X. A numerical study of the flow and heat transfer characteristics of outward convex corrugated tubes with twisted-tape inserts. *J Heat Transfer.* 2016;138:1–8. <https://doi.org/10.1115/1.4031171>.
176. Thianpong C, Eiamsa-ard P, Wongcharee K, Eiamsa-ard S. Compound heat transfer enhancement of a dimpled tube with a twisted tape swirl generator. *Int Commun Heat Mass Transf.* 2009;36:698–704. <https://doi.org/10.1016/j.icheatmasstransfer.2009.03.026>.
177. Yang S, Zhang L, Xu H. Experimental study on convective heat transfer and flow resistance characteristics of water flow in twisted elliptical tubes. *Appl Therm Eng.* 2011;31:2981–91. <https://doi.org/10.1016/j.applthermaleng.2011.05.030>.
178. Wu CC, Chen CK, Yang YT, Huang KH. Numerical simulation of turbulent flow forced convection in a twisted elliptical tube. *Int J Therm Sci.* 2018;132:199–208. <https://doi.org/10.1016/j.ijthermalsci.2018.05.028>.
179. Dong X, Jin X, Li P, Bi Q, Gui M, Wang T. Experimental research on heat transfer and flow resistance properties in spiral twisted tube heat exchanger. *Appl Therm Eng.* 2020;176:115397. <https://doi.org/10.1016/j.applthermaleng.2020.115397>.
180. Tang X, Dai X, Zhu D. Experimental and numerical investigation of convective heat transfer and fluid flow in twisted spiral tube. *Int J Heat Mass Transf.* 2015;90:523–41. <https://doi.org/10.1016/j.ijheatmasstransfer.2015.06.068>.
181. Eiamsa-ard S, Promthaisong P, Thianpong C, Pimsarn M, Chuwattanakul V. Influence of three-start spirally twisted tube combined with triple-channel twisted tape insert on heat transfer enhancement. *Chem Eng Process Process Intensif.* 2016;102:117–29. <https://doi.org/10.1016/j.cep.2016.01.012>.
182. Tan XH, Zhu DS, Zhou GY, Zeng LD. Experimental and numerical study of convective heat transfer and fluid flow in twisted oval tubes. *Int J Heat Mass Transf.* 2012;55:4701–10. <https://doi.org/10.1016/j.ijheatmasstransfer.2012.04.030>.
183. Cheng J, Qian Z, Wang Q. Analysis of heat transfer and flow resistance of twisted oval tube in low Reynolds number flow. *Int J Heat Mass Transf.* 2017;109:761–77. <https://doi.org/10.1016/j.ijheatmasstransfer.2017.02.061>.
184. Li X, Zhu D, Yin Y, Liu S, Mo X. Experimental study on Heat transfer and pressure drop of twisted oval tube bundle in cross flow. *Exp Therm Fluid Sci.* 2018. <https://doi.org/10.1016/j.expthermflusci.2018.07.030>.
185. Li X, Zhu D, Yin Y, Tu A, Liu S. International journal of heat and mass transfer parametric study on heat transfer and pressure drop of twisted oval tube bundle with in line layout. *Int J Heat Mass Transf.* 2019;135:860–72. <https://doi.org/10.1016/j.ijheatmasstransfer.2019.02.031>.
186. Bhadouriya R, Agrawal A, Prabhu SV. International journal of heat and mass transfer experimental and numerical study of fluid flow and heat transfer in a twisted square duct. *Heat Mass Transf.* 2015;82:143–58. <https://doi.org/10.1016/j.ijheatmasstransfer.2014.11.054>.
187. Khoshvaght-aliabadi M, Arani-lahtari Z. Proposing new configurations for twisted square channel (TSC): nanofluid as working fluid. *Appl Therm Eng.* 2016;108:709–19. <https://doi.org/10.1016/j.applthermaleng.2016.07.173>.
188. Sun B, Yang A, Yang D. International Journal of Heat and Mass Transfer Experimental study on the heat transfer and flow characteristics of nanofluids in the built-in twisted belt external thread tubes. *Int J Heat Mass Transf.* 2017;107:712–22. <https://doi.org/10.1016/j.ijheatmasstransfer.2016.11.084>.
189. Chen J, Hai Z, Lu X, Wang C, Ji X. Heat-transfer enhancement for corn straw slurry from biogas plants by twisted hexagonal tubes. *Appl Energy.* 2020;262:114554. <https://doi.org/10.1016/j.apenergy.2020.114554>.
190. Wanbo Y, Xuenong G, Wendong X, Cong D, Zigeng L, Zhengguo Z. Heat transfer performance of epoxy resin flows in a horizontal twisted tube. *Appl Therm Eng.* 2017. <https://doi.org/10.1016/j.applthermaleng.2017.08.013>.
191. Ramgadiga AG, Saha AK. Three-dimensional numerical study of turbulent flow and heat transfer in a wavy-walled duct. *Int J Heat Mass Transf.* 2013;67:98–117. <https://doi.org/10.1016/j.ijheatmasstransfer.2013.07.081>.

192. Yang YT, Wang YH, Tseng PK. Numerical optimization of heat transfer enhancement in a wavy channel using nanofluids. *Int Commun Heat Mass Transf.* 2014;51:9–17. <https://doi.org/10.1016/j.icheatmasstransfer.2013.12.002>.
193. Mills ZG, Warey A, Alexeev A. Heat transfer enhancement and thermal-hydraulic performance in laminar flows through asymmetric wavy walled channels. *Int J Heat Mass Transf.* 2016;97:450–60. <https://doi.org/10.1016/j.ijheatmasstransfer.2016.02.013>.
194. Akbarzadeh M, Rashidi S, Esfahani JA. Influences of corrugation profiles on entropy generation, heat transfer, pressure drop, and performance in a wavy channel. *Appl Therm Eng.* 2017;116:278–91. <https://doi.org/10.1016/j.applthermaleng.2017.01.076>.
195. Bhattacharyya S, Chattopadhyay H, Swami A, Uddin MK. Convective heat transfer enhancement and entropy generation of laminar flow of water through a wavy channel. *Int J Heat Technol.* 2016;34:727–33. <https://doi.org/10.18280/ijht.340425>.
196. Dittus FW, Boelter LMK. Heat transfer in automobile radiators of the tubular type. *Int Commun Heat Mass Transf.* 1985;12:3–22. [https://doi.org/10.1016/0735-1933\(85\)90003-X](https://doi.org/10.1016/0735-1933(85)90003-X).
197. Salam B, Biswas S, Saha S, Bhuiya MMK. Heat transfer enhancement in a tube using rectangular-cut twisted tape insert. *Procedia Eng.* 2013;56:96–103. <https://doi.org/10.1016/j.proeng.2013.03.094>.
198. Thianponga C, Eiamsa-arda P, Promvongea P, Eiamsa-ardb S. Effect of perforated twisted-tapes with parallel wings on heat transfer enhancement in a heat exchanger tube. *Energy Procedia.* 2012;14:1117–23. <https://doi.org/10.1016/j.egypro.2011.12.1064>.
199. Meyer JP, Everts M, Coetzee N, Grote K, Steyn M. Heat transfer coefficients of laminar, transitional, quasi-turbulent and turbulent flow in circular tubes. *Int Commun Heat Mass Transf.* 2019;105:84–106. <https://doi.org/10.1016/j.icheatmasstransfer.2019.03.016>.
200. White FM. *Fluid Mechanics seventh edition* by Frank M. White. Power 2011.
201. Blasius H. Das Aehnlichkeitsgesetz bei Reibungsvorgängen in Flüssigkeiten. *Mitteilungen über Forschungsarbeiten auf dem Gebiete des Ingenieurwesens*, 1913, p. 1–41. doi: <https://doi.org/10.1007/978-3-662->